IMPROVEMENT OF CONVERSION EFFICIENCY OF DYE-SENSITIZED SOLAR CELL WITH OPTIMIZED TITANIUM OXIDE LAYERS BY INCORPORATION OF GOLD NANOPARTICLES

LIU CHIN CHIN

MASTER OF ENGINEERING SCIENCE

LEE KONG CHIAN FACULTY OF ENGINEERING AND SCIENCE
UNIVERSITI TUNKU ABDUL RAHMAN
April 2018

IMPROVEMENT OF CONVERSION EFFICIENCY OF DYE-SENSITIZED SOLAR CELL WITH OPTIMIZED TITANIUM OXIDE LAYERS BY INCORPORATION OF GOLD NANOPARTICLES

By

LIU CHIN CHIN

A dissertation submitted to the Department of Mechanical and Material Engineering,
Lee Kong Chian Faculty of Engineering and Science,
Universiti Tunku Abdul Rahman,
in partial fulfilment of the requirements for the degree of
Master of Engineering Science
April 2018

ABSTRACT

IMPROVEMENT OF CONVERSION EFFICIENCY OF DYE-SENSITIZED SOLAR CELL WITH OPTIMIZED TITANIUM OXIDE LAYERS BY INCORPORATION OF GOLD NANOPARTICLES

Liu Chin Chin

Dye-Sensitized Solar Cell (DSSC) is a photochemical solar device that converts light energy to electricity. Unlike other solar devices, DSSC is made from low cost materials and its fabrication process is relatively simple. However, the power conversion efficiency of DSSC is low compared to the silicon-based solar cell available in the market. Numerous studies were done to improve the power conversion efficiency, η of DSSC with deposition of noble metal (e.g. gold / silver) on titanium oxide, TiO_2 layer. However, there is limited study on the performance of multi-layer TiO_2 DSSC with gold nanoparticles. Therefore, this study aims to investigate the effect of gold nanoparticles on the performance of DSSC with optimized TiO_2 layers.

Firstly, three series of TiO_2 powders with average sizes of 15 nm, 30 nm and 150 nm were fabricated by hydrothermal process and sol-gel method. Secondly, in each series, a number DSSC samples were constructed with TiO_2 layers of similar thickness, N719 dye, iodide / triiodide electrolyte and platinum counter electrode. Samples with the optimum performance within each series were chosen for further study with the addition of gold nanoparticles. Lastly, DSSC with different combination of TiO_2-Au layers were fabricated in the search for the ideal combination that provides the highest light conversion efficiency. The ideal combination was found to be of 15 nm + 30 nm and its power conversion efficiency has improved by ~28% compared to those samples without gold addition.

ACKNOWLEDGEMENTS

First of all, I would like to express my appreciation to my supervisors, Dr. Liang Meng Suan and Dr. Khaw Chwin Chieh for their invaluable advices, guidance and their enormous patience throughout the development of the research.

Next, I would like to thank all the laboratory officers that help me from time to time during the research. This work could not be completed without their assistance. The whole project really brought me together to appreciate the true value of responsibility and friendship.

Lastly, I would like to thank my family for their support and encouragement throughout my study. I am grateful to everyone who had contributed to the successful completion of this project.

APPROVAL SHEET

This dissertation/thesis entitled **"**Improvement of Conversion Efficiency of Dye-Sensitized Solar Cell with Optimized Titanium Oxide Layers by Incorporation of Gold Nanoparticles**"** was prepared by LIU CHIN CHIN and submitted as partial fulfilment of the requirements for the degree of Master of Engineering Science at Universiti Tunku Abdul Rahman.

Approved by:

_____

(Dr. Liang Meng Suan) Date:……..
Associate Professor/Supervisor
Department of Mechanical and Material Engineering
Lee Kong Chian Faculty of Engineering and Science
Universiti Tunku Abdul Rahman

_____

(Dr. Khaw Chwin Chieh) Date:……..
Assistant Professor/Co-supervisor
Department of Mechanical and Material Engineering
Lee Kong Chian Faculty of Engineering and Science
Universiti Tunku Abdul Rahman

LEE KONG CHIAN FACULTY OF ENGINEERING AND SCIENCE

UNIVERSITI TUNKU ABDUL RAHMAN

Date: 13 / April / 2018

SUBMISSION OF DISSERTATION

It is hereby certified that Liu Chin Chin (ID No: 1303476) has completed this dissertation entitled "Improvement of of Conversion Efficiency of Dye-Sensitized Solar Cell with Optimized Titanium Oxide Layers by Incorporation of Gold Nanoparticles" under the supervision of Dr. Liang Meng Suan from the Department of Mechanical and Material Engineering, Lee Kong Chian Faculty of Engineering and Science, and Dr. Khaw Chwin Chieh from the Department of Mechanical and Material Engineering, Lee Kong Chian Faculty of Engineering and Science.

I understand that University will upload softcopy of my dissertation in pdf format into UTAR Institutional Repository, which may be made accessible to UTAR community and public.

Yours truly,

_____

(*Liu Chin Chin*)

DECLARATION

I hereby declare that the dissertation is based on my original work except for quotations and citations which have been duly acknowledged. I also declare that it has not been previously or concurrently submitted for any other degree at UTAR or other institutions.

Name _____

Date _____

TABLE OF CONTENTS

LIST OF TABLES

LIST OF FIGURES

LIST OF SYMBOLS / ABBREVIATIONS

k_B	Boltzmann constant
Cd	Cadmium
CdTe	Cadmium Telluride
q	Charge
$HAuCl_4$	Chloroauric acid
N719	cis–di(thiocyanato)–N,N'–bis(2,2'–bipyridyl–4–carboxylic acid–4'–tetrabutylammonium carboxylate)–ruthenium(II)
CIGS	Copper Indium Gallium Selenide
Cu_2S/CdS	Copper sulphide / cadmium sulphide
J_{max}	Current at maximum power, mA/cm^2
I_{dark}	Dark current
DSSC	Dye-sensitised solar cell
EDX	Energy-dispersive x-ray spectroscopy
FE-SEM	Field-emission scanning electron microscope
FF	Fill factor
FTO	Fluorine-doped tin oxide
Au	Gold
Au@MTNs	Gold nanoparticles inlaid mesoporous titania nanoparticles
Au-DSSC	Gold-incorporated DSSC
Au@MTNs	Gold-mesoporous titania nanoparticles
ITO	Indium-doped tin oxide
ITO-PEN	Indium-doped tin oxide coated polyethyleneaphtalate
Φ	Intensity of the incident light, W/m^2
I^-/I_3^-	Iodide / triiodide
LSPR	Localized surface plasmon resonance
P_{max}	Maximum power

MP-TiO_2	Mesoporous titanium oxide
MLCT	Metal-to-ligand charge transfer
V_{oc}	Open circuit voltage, V
I_{photo}	Photocurrent
I-V	Photocurrent-voltage
Pt	Platinum
P123	Poly(ethylene glycol)-poly(propylene glycol)-poly(ethylene glycol) triblock copolymer
PVP	Polyvinylpyrrolidone
η	Power conversion efficiency. %
J_{sc}	Short circuit current density, mA/cm^2
Ag	Silver
$NaBH_4$	Sodium borohydride
NaOH	Sodium hydroxide
SPP	Surface plasmon polarity
SPR	Surface plasmon resonance
T	Temperature, °C
SnO_2	Tin (II) oxide
Ti^{4+}	Titanium (IV) ionic
TTIP	Titanium isopropoxide
TiO_2	Titanium oxide
TiO_2 DSSC	Titanium oxide dye-sensitized solar cell
TiO_2-Au	Titanium oxide-gold
TiO_2-Au DSSC	Titanium oxide-gold dye-sensitized solar cell
TCO	Transparent conducting oxide
TEA	Triethanolamine
V_{max}	Voltage at maximum power, V
XRD	X-ray diffractometer
ZnO	Zinc oxide

LIST OF APPENDICES

CHAPTER 1

INTRODUCTION

1.1 Background

Solar energy is a pollution-free, sustainable and renewable energy source. Solar cell is a device that converts solar energy into electric power and its operation doesn't emit harmful gasses that contribute to global warming and there are abundant of uncaptured sunlight available.

The photovoltaic effect was discovered by a French scientist, Alexandre-Edmond Becquerel in 1839. He encountered that voltage was generated when the light reacted with the metal electrodes in an electrolyte. The first solar cell was fabricated by an American, Charles Fritts in 1883. The cell was constructed by coating the semiconductor selenium with an ultra-thin layer of gold, Au to form the junctions with the efficiency of 1%. A breakthrough in solar cell development occurred in the 1940s and 1950s when the method for synthesising highly pure single crystal silicon was discovered. This led to the first practical silicon solar cell being built at Bell Telephone Laboratories in 1954 with efficient of 4%.

Solar cell technology is divided into three generations. The first generation solar cell is single junction P-N solar cell developed by Gerald Pearson, Darryl Chapin and Calvin Fuller. It was the first commercial solar cell that was able to convert solar energy into electricity that are sufficient to power daily household electrical appliances. Today, this solar cell possesses an

efficiency of about 25% (Green et al., 2017) and accounted most of the solar cell market. However, the manufacturing cost for this solar cell remains high due to the high energy needed for silicon purification process.

The second generation solar cell is thin film solar cell. It was invented in 1965. The first thin film solar cell with efficiency greater than 10% was developed by The Institute of Energy Conversion at University of Delware in 1980 using copper sulphide / cadmium sulphide, Cu_2S/CdS technology. The application of materials such as Cadmium Telluride, CdTe and Copper Indium Gallium Selenide, CIGS in this solar cell by other researchers (Ferekides et al., 2004; Wu, 2004; Nakada, 2012; Ray and Mallick, 2013; Movla, 2014; Romeo et al., 2014; Banerjee et al., 2016) was intended to improve its energy conversion efficiency. However, the cell performance was still much lower compared to the first generation solar cell. Moreover, the environmental concern on the toxicity of cadmium, Cd brought about the downward trend on the development of the second generation solar cell in recent years.

The third generation solar cell includes organic solar cell, perovskite solar cell, quantum-dot solar cell and dye-sensitized solar cell (DSSC). Among these, the DSCC is the most developed 3rd generation solar cell. This solar cell was invented in Switzerland by Micheal Grätzel and Brian O' Regan at the École Polytechnique Féderale de Lausanne in 1991. This solar cell employed nanostructure technology and its operation mimics the process plant used to convert sunlight into energy. The development of this type of solar cell enables the manufacturers to counteract the high production cost of first generation solar cell and reduce the environmental impact due to the usage of cadmium in second generation solar cell.

1.2 Dye-Sensitized Solar Cell

DSSC also known as Grätzel cell is named after its inventor, Micheal Grätzel. Figure 1.1 shows the configuration of a DSSC. Its technology is reviewed as

artificial photosynthesis where dye molecules coated on semiconductor oxide are used to absorb sunlight and the charge separation is accomplished by kinetic competition that leads to photovoltaic generation. Currently, DSSC has achieved the highest efficiency of about 13% (Mathew et al., 2014).

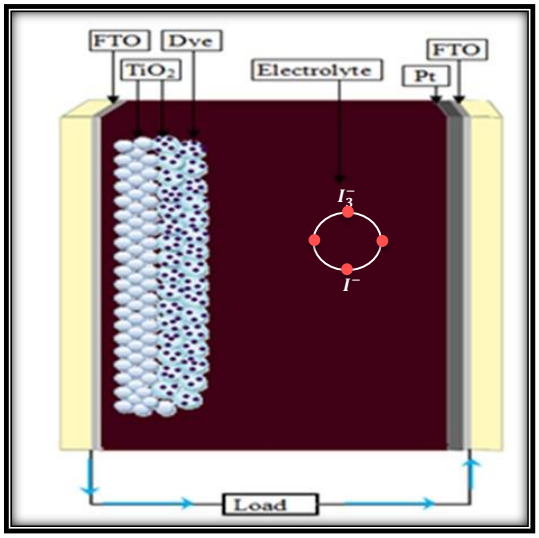

Figure 1.1: Configuration of Dye-Sensitized Solar Cell (DSSC)

1.2.1 Dye-Sensitized Solar Cell Structure

A basic DSSC consists of transparent conducting oxide (TCO) coated glass, semiconductor oxide film, sensitizing dye, electrolyte and counter electrode.

The TCO glass substrate is a conductive glass used in DSSC. The glass has low sheet resistance, high transparency and capability to inhibit impurities such as water and oxygen from entering the DSSC. Besides, the TCO glass surface should have good mechanical and electrical contact with the semiconductor oxide layer. The common TCO glasses used in DSSC are fluorine-doped tin oxide (FTO) coated glass and indium-doped tin oxide (ITO) coated glass. The sheet resistance of ITO is lower than FTO. However, FTO coated glass is preferable due to its thermal stability during the photoelectrode sintering process at 500 °C. Sima et al. (2010) reported that the resistivity value of ITO coated glass increased with thermal treatment while the resistivity value

of FTO coated glass remained unchanged. In addition, the ITO electrical properties can be degraded in the presence of oxygen at ~500 °C. Besides the abovementioned glass substrates, other substrates in DSSC are plastic foil, metal sheet and conductive plastics such as indium-doped tin oxide coated polyethyleneaphtalate, ITO-PEN.

The semiconductor oxide layer such as titanium oxide, TiO_2, zinc oxide, ZnO and tin (II) oxide, SnO_2 serves as photoanode for dye loading, transporter of excited electrons from dye to external circuit. Thus, semiconductor with a large surface area and excellent charge transport properties will be an ideal photoanode. It is one of the important factors affecting the solar cell performance. The most extensively used semiconductor oxide is titanium oxide, TiO_2 due to its economical, abundant, non-toxic, biocompatible, good energetic properties and chemical stability under light irradiation.

The sensitizing dye is the photoactive element of the DSSC. It is used to absorb light for photo-to-electron conversion. It plays a key role in the DSSC light absorption efficiency and overall power conversion efficiency. The ideal dye should have a wide range of solar spectrum coverage as the solar spectrum has high photo-flux in between 400 nm and 800 nm, high extinction coefficient throughout the absorption band in order to harvest most of the light with minimum dye and long dye excited state lifetime for efficient electron injection. Besides, the dye should bind strongly to the semiconductor oxide surface. The most widely used dye is ruthenium organometallic complexes. The Ruthenium complex dye such as cis–di(thiocyanato)–*N,N'*– bis(2,2'–bipyridyl–4–carboxylic acid–4'–tetrabutylammonium carboxylate)–ruthenium(II), commonly known as N719, has absorption throughout the visible spectrum capturing most of the sunlight and higher open-circuit voltage.

The electrolyte contains redox couple in an organic solvent. It serves to collect electrons at the counter electrode and regenerate oxidized dye molecules. The dye regeneration is essential in avoiding oxidized dye molecules from reduction via recombination. Two ways of recombination are TiO_2 electrons

combine with oxidized dye molecules or with acceptors in the electrolyte. The most commonly used redox couple is iodide / triiodide, I^-/I_3^- redox couple due to its slow interception of electrons at TiO_2 surface which reduces recombination losses.

The counter electrode is prepared by coating a thin layer of metal such as platinum, Pt on the FTO coated glass. It serves to supply electrons to the electrolyte that regenerates oxidized dye molecules. Platinum catalyst is most widely used due to its high catalytic activity towards I^-/I_3^- redox reaction.

Sometimes, metal nanoparticles such as gold or silver are coated on the semiconductor oxide layer to enhance the DSSC performance. The role of metal nanoparticles serves as co-catalyst in facilitating electron discharge at the interfaces.

1.2.2 Operation Principle

The operation principle of a dye-sensitized solar cell is shown in Figure 1.2. When light enters the cell through the FTO coated glass, the light will interact with sensitizing dye, *D* coated on the semiconductor oxide surface causing it to switch to an excited state, *D**.

$$D + photon \rightarrow D^* \tag{1.1}$$

*D** is metastable and would soon resume to its ground state, *D*. Before this change of states takes place, an electron is injected into the conduction band by the excited dye. A carrier is created in the semiconductor layer and diffuses to the photo-electrode and then becoming available to the external circuit.

The dye molecule becomes oxidized by injecting an electron into a neighbouring region. A hole is created and must be regenerated. Redox

electrolyte containing iodide / triiodide couple serves to reduce the dye and acquires a hole. The oxidized dye receives electron from the iodide ion which in turn gets oxidized to triiodide, I_3^- in the process. The cycle is closed by the reduction of triiodide ion at counter electrode. The triiodide ion gets reduce back to iodide by combining with the electron that coming back to the cell via external circuit. This cycle is repeated to produce electrical power.

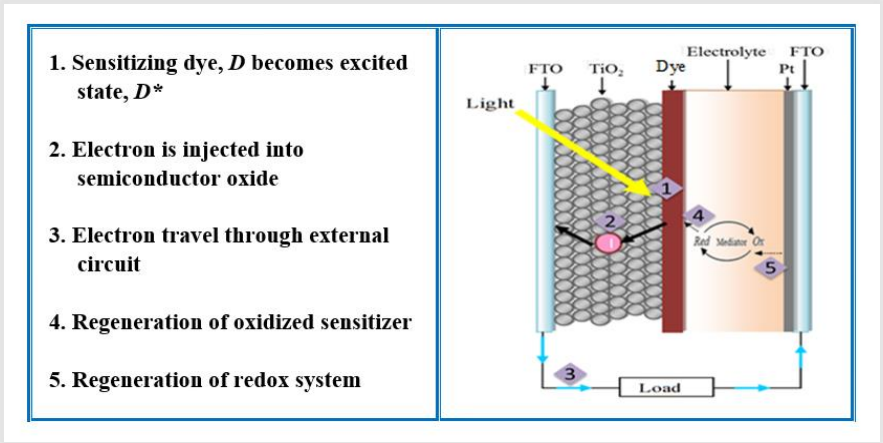

Figure 1.2: Operation Principle of Dye-Sensitized Solar Cell

1.2.3 Advantages and Disadvantages of DSSC

Dye-sensitized solar cell as the third generation solar offers an efficient and cost effective alternative energy supply technology for the future. It is a promising technology for power generation due to its simple and energy-efficient manufacturing. DSSC is made from low cost material and does not require elaborate apparatus and clean-room facility to manufacture. Therefore, its production cost is much lower compared to conventional silicon-based solar cell. Furthermore, the materials used for this solar cell are less prone to environmental pollution and contamination.

The DSSC has a large degree of freedom in design. It can be produced in a wide variety of colour depending on the type of dye employed. The DSSC

exhibits some transparency thus it is suitable to incorporate in a wide variety of end-user products like lamp, sunglasses and radio. Besides, this solar cell can be operated even under low light condition making it a suitable choice for indoor applications such as window panels, doors and particularly suitable for practical use on cloudy day.

However, the major hindrances of this solar technology are reliability and durability. DSSC has the lowest power conversion efficient amongst the solar cell available in the market. In addition, most of the DSSCs contain liquid electrolyte which has poor long-term stability and must be carefully sealed. Liquid electrolyte is prone to leakage and evaporation thus eventually degrades the solar cell performance over time.

1.3 Project Motivation

Dye-sensitized solar cell can be considered as an alternative choice to replace silicon-based solar cell as it is made from economical materials and can be produced without elaborate apparatus. In addition, DSSC operating principle mimics the photosynthesis reaction of green plants. It separates the function of light absorption from the photo-electron transport. The dye provides photoelectrons generation while the semiconductor oxide serves as charge transportation. However, the conversion efficiency performance of DSSC is relatively low compared to silicon-based solar cell (~ 25%) (Green et al., 2017). Recently, several approaches to boost the performance of DSSC were developed, particularly by coupling titanium oxide, TiO_2 with noble metal such as gold, Au and silver, Ag. At the moment, the highest achieved efficiency for gold-incorporated dye-sensitized solar cell (Au-DSSC) is about 10% in laboratory scale (Choi, Chen and Kamat, 2012).

Previous studies by other researchers were mainly focused on the effect of gold nanoparticles on DSSC with TiO_2 layer of the same particle size. The conversion efficiency obtained by those studies was approximately 6%. (Muduli

et al., 2012) However, to date, little systematic thought has been given to the question of how gold nanoparticles might be used advantageously in DSSC with multi-layer TiO_2 of different particle sizes. The photovoltaic efficiency enhancement of DSSC by combining different TiO_2 particle sizes is well development. Most of the studies report that the prformance of multi-layer structure (combination of different TiO_2 particle sizes) is superior to the double-layer single particle size structure. Hence, in this study, the effect of gold nanoparticles incorporated in optimized TiO_2 layers of three particle sizes (~ 15 nm, 30 nm and 150 nm) are studied in pursuit of DSSC with better performance. Three series of TiO_2 powder with the abovementioned particle sizes were chemically synthesised by hydrothermal process and sol-gel method and then converted to TiO_2 films by conventional doctor blade technique for DSSC fabrication. The performance of the fabricated DSSC was studied in the search for sample with optimum performance in each series. Next, the three samples with optimized TiO_2 layers were selected for further characterisation. Lastly, various combination of titanium oxide-gold, TiO_2-Au layers were fabricated and the conversion efficiency of those Au-doped DSSC were analysed to identify the sample with the highest light conversion efficiency.

1.4 Aim and Objectives

The aim of this study is to improve the power conversion efficiency of dye-sensitized solar cell with gold nanoparticles.

The objectives are as below:

1. To synthesise TiO_2 powder by hydrothermal and sol-gel methods.
2. To characterise DSSC fabricated with multi-layer TiO_2.
3. To improve the performance of DSSC with the addition of gold nanoparticles on the optimized TiO_2 layers.

1.5 Thesis outline

Chapter 1 describes the dye-sensitized solar cell background, aim, objectives and a brief review of this study.

Chapter 2 gives the literature review on topics related to this study. Existing literature on the fabrication of semiconductor oxide powder and dye-sensitized solar cell are reported.

Chapter 3 describes the experimental methods and procedures applied in the research. It includes semiconductor oxide powder fabrication and DSSC preparation, assembly and characterize by x-ray diffractometer (XRD), field-emission scanning electron microscope (FE-SEM), UV-visible spectroscopy, energy-dispersive x-ray spectroscopy (EDX) and I-V measurement.

Chapter 4 presents the result and discussion of the study. This chapter is divided into two sections. The first section presents the results and discussion on the TiO_2 nanoparticles dye-sensitized solar cell performance. Three series of TiO_2 powders were synthesised; series A and series B served as active layer and were fabricated using hydrothermal process while series C fabricated using sol-gel method was used as scattering layer. Series A were fabricated by varying triethanolamine, TEA volume to produce TiO_2 nanoparticles with large surface area that favours dye absorption, whilst, series B and series C were produced by varying titanium isopropoxide, TTIP volume with the former producing TiO_2 powders with larger particle size that possessed haze effect and sufficient dye absorption and the latter producing TiO_2 powders that facilitate light scattering effect. The TiO_2 DSSC efficiency for series A, series B and series C were reported. Second section of the chapter presents the results and discussion on the performance of DSSC with different combination of TiO_2-Au layers (series D).

Chapter 5 concludes this study along with suggestions for further work.

CHAPTER 2

LITERATURE REVIEW

2.1 Introduction

Dye-sensitized solar cell provides an efficient and economical source of energy. Basically, a DSSC consists of nanocrystalline active layer, sensitizing dye, electrolyte and platinum counter electrode. Titanium Oxide, TiO_2 is the most widely employed metal oxide in DSSC due to its inexpensive, ease of handling and high photovoltaic. The DSSC power conversion efficiency is affected by the properties of the nanocrystalline titanium oxide layer. Several methods were developed to synthesise nanocrystalline titanium oxide, TiO_2. Among those methods, hydrothermal process and sol-gel method are the most common and popular fabrication methods. Gold nanoparticles were added to the nanocrystalline titanium oxide, TiO_2 layer to improve the DSSC performance. The conversion efficiency of DSSC is affected by its electrical properties, for example, short circuit current density, J_{sc}, and fil factor, *FF*.

2.2 Fabrication of Titanium Oxide Nanoparticles Powder

Hydrothermal and sol-gel synthesis of TiO_2 nanoparticles powder has attracted much interest due to its broad applications. The TiO_2 powder size and crystalline phase are greatly influenced by the fabrication process and parameters such as heat treatment temperature and duration, concentration of precursor and

surfactant and the solvent composition. Oguri et al. (1988) reported that the fabrication method influences the properties of synthesised TiO_2 powder. The study demonstrated that a homogeneous spherical anatase TiO_2 powder was successfully fabricated by hydrothermal method.

2.2.1 Fabrication of TiO_2 Powder by Hydrothermal Process

Hydrothermal synthesis is the chemical reaction that occurred under the concurrent application of heat and pressure to produce a highly crystalline structure at low temperature (Yang et al., 2000; Byrappa and Yoshimura, 2001). The internal pressure is greatly controlled by the treatment temperature and the volume of solution in the autoclave. Hydrothermal reaction is broadly employed in ceramics industry to produce small particles (Chen and Mao, 2007).

Reyes-Coronado et al. (2008) stated that the benefit of hydrothermal synthesis is that the average nanoparticle size can be regulated by altering the hydrothermal duration and temperature. The crystallite size of prepared titanium oxide powder increased as the hydrothermal treatment time and temperature increased. The width of XRD peak of the prepared anatase TiO_2 powder reduced with longer treatment time indicated that the crystallite size is increased. The study also revealed that synthesising bigger nanoparticles was possible by increasing the hydrothermal treatment temperature as it improved the particle coarsening rate. In addition, Yang et al. (2000) reported that the treatment temperature has a big impact on TiO_2 powder particle size and agglomeration. The particle size is increased and agglomeration is reduced as the temperature was raised.

Chae et al. (2003) studied the effect of precursor and solvent composition toward the particle size of TiO_2 powder. The study found that the particle size was essentially depended on the concentration of titanium isopropoxide, TTIP and the ethanol-to-water ratio in the solvent system. Anatase TiO_2 powder in the range of 7 nm – 25 nm was produced by altering

the TTIP and the composition of solvent system. Small particles were obtained under ethanol-rich solvent system and the particle size increased as the ethanol to water ratio was higher.

Titanium oxide powder with average particle size of ~ 20 nm and narrow size distribution was fabricated by Chang et al. (2012). The TiO_2 powders was produced by hydrothermal reaction of titanium isopropoxide, TTIP with triethanolamine, TEA in an ethanol-water solution. The TEA acts as capping agent controlling the nanoparticle size distribution of anatase TiO_2 powder.

2.2.2 Fabrication of TiO_2 Powder by Sol-Gel Method

Sol-gel process is a process based mainly on the formation of a colloidal suspension or sol and the gelation process to transform the sol into a semisolid colloidal suspension or gel. Sol is formed from the hydrolysis and polymerisation of metal alkoxides (Chen and Mao, 2007). The control of hydrolysis was important in order to have a homogenous marco-molecular oxide network (Wu et al., 2002). The advantages of sol-gel method include low processing temperature and equipment cost, ability to fabricate homogenous material and ease of controlling the material composition (Abdel-Azim et al., 2014). Similarly, the properties and crystallinity of sol-gel prepared TiO_2 power was affected by the precursor and solvent composition, the type and concentration of surfactant, and the hydrolysis, gelation and calcination process (Bischoff and Anderson, 1995; Wu et al., 2002; Mahshid et al., 2007).

Wu et al. (2002) reported that the final properties and crystallization of the TiO_2 powder is influenced by the concentration of precursor. Besides, the water to precursor ratio had a great impact on the characteristics and morphology of the sol (Ding et al., 1995; Vorkapic and Matsoukas, 1998; Yu et al., 2016). Ding et al. demonstrated that the volume of water had a great effect on the rate of hydrolysis and the initial compound formation of sol which consequently influenced the reaction of secondary polymerization. The study

reported that TiO_2 powder with larger particle size was obtained as the volume of water increased. Yu et al. (2016) justified that the titanium-alkoxide to water ratio was an important factor during the sol-gel reaction. The study showed that lower ratio was able to produce powder of monodispersed TiO_2 sphere with smaller diameter. However, the reaction was hard to control under an excessive water-rich condition due to rapid hydrolysis of titanium-alkoxide.

The properties of sol-gel fabricated TiO_2 powder was strongly influenced by the calcination temperature. The calcination temperature was critical as the purpose of calcination process is to enhance the crystallinity of titanium oxide powder. When the temperature was low, the synthesised powder may contain left-over organic molecules that caused inadequate TiO_2 crystallization. However, aggregation and phase transformation occurred when the temperature was too high (Wu et al., 2002; You et al., 2014). Mahshid et al. (2007) reported that the crystallite size of produced anatase TiO_2 powder has enlarged as the calcination temperature increased since the growth rate was increased. You et al (2014) research team successfully synthesized TiO_2 powder with particle size of 20 nm – 65 nm by controlling the calcination temperature.

Surfactant is added to TiO_2 powder fabrication with the intention of improving the morphology and dispersion of the final product. It serves as a stabilizer and dispersing agent to reduce particle agglomeration. Sometimes, certain surfactant was utilized to control the crystallites shape of the powder by regulating the crystallographic faces growth rate (Jun et al., 2003). The quantity, group and relative molar mass of surfactant have an incredible effect on the shape, purity, dispersion characteristics, particle size, pore size and size distribution of the synthesised powder.

The particle size of synthesised powder is affected by the type and quantity of the surfactant. Chai et al (2006) reported that the particle size of TiO_2 powder was reduced by adding anion surfactant or by increasing the surfactant volume. Jang et al. (2016) demonstrated the effect of three types of surfactant toward the powder particle size. The TiO_2 powder with average particle size of 155 nm, 105 nm and 380 nm were obtained by using

polyvinylpyrrolidone, PVP (Mw: ~55000), Triton X-100 and poly(ethylene glycol)-poly(propylene glycol)-poly(ethylene glycol) triblock copolymer, P123 (Mn: 5800) as surfactant.

Huang et al. (2014) reported that too much or too little surfactant produce TiO_2 powder with wide particle size distribution. Small amount of surfactant was not adequate to cover the particles causing aggregation, whilst too much surfactant increased the viscosity of solution leading to higher surface tension and difficulty in controlling the morphology of the final product. In addition, Liao and Liao (2007) discovered that the shape of TiO_2 nanoparticle can be altered with the aid of surfactants. They found that the use of sodium dodecyl benzene sulfonate produced uniform spherical TiO_2 nanoparticles of 250 nm in diameter and sodium dodecyl sulfate resulted in cubic nanoparticles of 150 nm – 300 nm in length.

2.3 Titanium Oxide Layer on Dye-sensitized Solar Cell Performance

Titanium oxide, TiO_2 properties become one of the essential factors affecting the DSSC performance as it absorbs large amount of sensitizing dye that provides electrons. The efficiency of DSSC is affected by the morphology and structure of TiO_2 layer. Moreover, the degree of haze and film thickness of TiO_2 layer has an effect on cell efficiency.

2.3.1 TiO_2 Properties on DSSC Performance

The photovoltaic conversion of DSSC is strongly influenced by the nature and properties of titanium oxide nanoparticles. The TiO_2 nanoparticles properties affect the degree of dye absorption, the transmittance of light intensity, the degree of haze and the rate of electron recombination and diffusion which in turn determines the electrical properties of a DSSC. A good dispersion and

highly crystalline TiO_2 layer is essential for a good photoanode. Benk et al. (2003) study revealed that better crystallinity leads to higher electron injection rate from the excited dye to TiO_2 nanoparticles thereby improved the short circuit current density, J_{sc} of the DSSC.

Besides, the surface area and potential of the titanium oxide determined the dye loading capacity thus controlling the amount of photo-generated electron (Lee and Yang, 2011). Jeng et al. (2013a) study illustrated that the power conversion efficiency of DSSC with ~ 10 nm TiO_2 nanoparticles was higher than the DSSC with ~ 200 nm TiO_2 nanoparticles for the same oxide layer thickness. The large surface area of the small nanoparticles improved the amount dye absorbed on the TiO_2 layer, thus enhanced the photocurrent of the solar cell leading to higher DSSC efficiency. However, the electron recombination rate was increased as the amount of dye that can be absorbed increased and small particles cannot support a space for charge separation caused lower DSSC efficiency. (Hagfeldt and Graetzel, 1995)

In addition, Wang et al. (2004) reported that light absorption in the red region was low due to the low absorption of N719 in longer wavelength. Besides, the transparent TiO_2 nano-layer has no light scattering effect causing light loss due to back scattering, therefore diminished the performance of DSSC.

On the other hand, several studies found that by incorporating large TiO_2 nanoparticles or submicro TiO_2 particles might improve the conversion efficiency of DSSC even though dye loading capacity was reduced as the surface area of large TiO_2 nanoparticles were lower (Grätzel, 2005; Chiba et al., 2006; Lee and Yang, 2011; Jeng et al., 2013b; Gong et al., 2017). Large or submicro TiO_2 particles are capable of overcoming the light loss due to back scattering and low light absorption in the red region. The study exposed that the electron injection capacity was improved as the TiO_2 nanoparticles size increased (Nakade et al., 2003). Zhu et al. (2012) study also discovered that the electron diffusion coefficient has deteriorated as the average TiO_2 nanoparticles size was decreased due to the reduced average pore size. The study found that TiO_2 microspheres with an average size of 400 nm showed the most effective

electron transport properties due to pore properties that are suitable for electrolyte diffusion.

Moreover, the transparency of TiO_2 film is influenced by adding large TiO_2 nanoparticles. Studies confirmed that the degree of haze affects the photocurrent density of DSSC which in turn influences the solar cell power conversion efficiency. Chiba et al. (2006) reported that the degree of haze was controlled by adding submicron TiO_2 particle size of 400 nm to the photoanode. It was defined as the proportion of diffused light transmittance to total light transmittance measured at wavelength of 800 nm by an integral sphere. The study discovered that the power conversion efficiency, η of 11.1% and short circuit current density, J_{sc} of 21 mA/cm^2 was achieved when employing TiO_2 photoanode with haze degree of 76%. The absorption in the infrared region was greatly improved as the degree of haze increased from 3% to 76%. Similarly, Grätzel (2005) reviewed that the light harvesting efficiency of DSSC in red or near-infrared region was enhanced with the addition of 200 nm – 400 nm anatase TiO_2 particles either mixed in the oxide layer or deposited as an overlayer above the smaller particles layer.

Wang et al (2004) study found that the photovoltaic performance rose by ~ 10% when large TiO_2 particles were mixed with the nanoparticles matrix. The DSSC efficiency enhancement is ascribed from the light scattering effect of large TiO_2 particles. Besides, Zhu et al (2012) revealed that microsphere TiO_2 was assumed as bifunction materials that enhanced the scattering effect as well as retaining adequate dye absorption. The dye-sensitized solar cell conversion efficiency was increased by 40% as the microsphere TiO_2 was employed.

2.3.2 TiO_2 Film Thickness on DSSC Performance

The variation in thickness of the nanocrystalline titanium oxide, TiO_2 layer is a critical feature in optimizing the photovoltaic performances of dye-sensitized solar cell. The TiO_2 layer thickness can be measured using a surface profiler. In general, thick and porous oxide film improves dye loading capacity and light harvesting efficiency of photoanode (Maldonado-Valdivia et al., 2013).

Shin et al. (2010) study demonstrated that the performance of DSSC was enhanced when the TiO_2 layer thickness was increased from 3 μm to 20 μm even though the open circuit voltage, V_{oc} was about the same for all thickness. The photovoltaic efficiency enhancement is attributed to the increased short current density, J_{sc} as the dye loading capacity was increased when the thickness of TiO_2 layer was increased. It was also proven by the increse in light absorption in the range from 400 nm to 750 nm indicated that more dye molecules were absorbed on the increased surface of TiO_2 as the thickness of TiO_2 layer was increased. However, the study discovered that power conversion efficiency was dropped as much as 32% as TiO_2 film thickness was increased to 26 μm. The lower DSSC performance was caused by higher electron recombination and lower charge collection efficiency as the photo-generated electron travelling distance was increased as the TiO_2 layer thickness was increased (Chander et al., 2014). Moreover, thick film tends to reduce the transmittance of light as well as the incident light absorbed by the sensitizer. Additionally, the electron travelling hindrance was notably higher in thick oxide layer (Jeng et al., 2013a). It was also discovered that the incident light intensity strongly affects the electron travelling. The electron travelling was faster when light intensities were greater (Cao et al., 1996; Dloczik et al., 1997).

Ito et al. (2008) study concluded that the optimum thickness was 12 μm to 14 μm for a DSSC of 20 nm sized particulate film with the addition of adhered anti-reflection film. Ngamsinlapasathian et al. (2005) reported that the solar cell performance dropped dramatically when the oxide layer thickness exceeded the optimum thickness. The cell performance has diminished as the short current

density, J_{sc} was dropped. Thick oxide film tends to crack due to shrinkage. The shrinkage was attributed to the decomposition and evaporation of organic substances and the change in volume due to crystallization induced significant stress in the film (Kajihara and Yao, 2000).

The power conversion efficiency of a DSSC is improved by deposited double-layer TiO_2 film. The double-layer DSSC was synthesised by coating a TiO_2 scattering layer on top of the active TiO_2 layer. The active TiO_2 layer promotes better dye loading capacity whereas the scattering layer imposes light scattering effect. In Ngamsinlapasathian et al. (2005) study, the double-layer DSSC achieved efficiency of 12.6% with the TiO_2 film thickness of 17 μm. The double-layer DSSC showed an improvement of 75% compared to single layered DSSC. The study applied mesoporous titanium oxide, MP-TiO_2 as the first oxide layer followed by MP-TiO_2 + P25 as second oxide layer and reported that the big P25 particles in second layer act as scattering agent which improves the solar cell light harvesting efficiency while the first transparent MP-TiO_2 layer promotes better dye loading.

In addition, the photovoltaic performance showed 30% enhancement when 450 nm monodispersed TiO_2 sphere was applied as scattering layer on the double-layer DSSC (Yu et al., 2011). Barbe et al. (1997) justified that the photovoltaic efficiency enhancement by scattering is depends on the ability of TiO_2 nanoparticles to scatter the light. The scattering of light improves the path length of the photon within the DSSC leading to higher probability to react with sensitizing dye and introduces an electron into the oxide layer. This was particularly important for red light absorption where ruthenium-based dye was not so significant.

2.4 Effect of Gold Nanoparticles on Dye-sensitized Solar Cell Performance

The recent efforts to enhance the conversion efficiency of DSSC by adding noble metal has drawn significant attention due to it promising path to boost the light absorption in the active layer and the photocurrent generation of the solar cell. Among all the noble metal, gold nanoparticles are the most commonly utilized to improve the DSSC performance due to their surface plasmon resonance (SPR) can be tuned in the visible zone of the electromagnetic spectrum (Chander et al., 2014). The characteristic of Au-DSSC is affected by the properties of Au nanoparticles on the TiO_2 layer.

The primary role of gold in DSSC is to receive electrons from the photo-excited TiO_2 with the intention of reducing recombination rate (Wood et al., 2001). The interfacial charge transfer process and stability of interfaces have a big impact on the ability of semiconductor-metal nanocomposite to sustain charge separation. Muduli et al. (2012) study demonstrated that the charge transfer resistance at oxide-dye-electrolyte interface was reduced by 23% with the addition of gold, Au. Besides, the open circuit voltage, V_{oc} was increased by ~ 6% and fill factor, *FF* was improved by ~ 9% when chloroauric acid, $HAuCl_4$ was added to TiO_2 powder synthesis indicated that the electron-hole recombination rate of the cell was decreased.

Previous studies have shown that deposition of Au nanoparticles on TiO_2 particles enhance the photocatalytic electron transfer processes leading to improvement in photocurrent density, therefore better power conversion efficiency (Subramanian et al., 2001). The short circuit current density, J_{sc} shown 60% improvement when the surface plasmon nanoparticles were coated on the oxide layer of the solar cell. The photovoltaic performance improvement was attributed to the plasmon induced charge transfer from Au nanoparticles to titanium oxide layer (Lin et al., 2012).

The plasmonic characteristic of noble metal such as the localized surface plasmon resonance (LSPR) absorption intensity, the plasmon bandwidth and

stability of Au nanoparticles greatly influences the light harvesting efficiency of the cell (Qi et al., 1999; Xie et al., 2006; Kawawaki et al., 2013; Dang et al., 2013). In addition, Chen et al. (2015) reported that the increment of DSSC photovoltaic performance was correlated to the improvement of light harvesting due to the LSPR effect of gold nanoparticles. The study demonstrated that the absorption in the visible region was improved significantly when the amount of gold in TiO_2 layer was increased. In addition, a strong light reflectance was arisen due to the light scattering effect at the interfaces between the gold-mesoporous titania nanoparticles, Au@MTNs. The photocurrent density, *Jsc* and light conversion efficiency, η were improved by 25% and 14% respectively when Au nanoparticles were incorporated.

In general, incorporating noble metal nanoparticles to increase the light harvesting efficiency of sensitizer without increasing the TiO_2 layer thickness has been extensively studied. The plasmonic effect arises as gold nanoparticles interact with the incident light at the visible region. Moreover, the study illustrated that gold-incorporated DSSC achieved enhancement of 25% in short circuit current density, *Jsc* and 40% in conversion efficiency of DSSC (Al-Azawi et al., 2016). Besides, Chander et al. (2014) revealed that the size and concentration of gold, Au nanoparticles have a synergy effect on the improvement of photocurrent generation and overall conversion efficiency of DSSC. The optimum DSSC enhancement was achieved by utilising Au nanoparticle in the size range of 15 nm – 40 nm and the concentration of 0.1 wt% – 0.25 wt%. The photocurrent and conversion efficiency enhancement were ascribed from the plasmonic effect of gold in the DSSC which was the increased near-field excitation of the sensitizer.

Lai et al. (2008) study showed that the gold nanoparticles acts as a Schottky barrier that formed in the interface between gold and oxide layer, consequently improved the electron injection efficiency of the cell. Su et al. (2007) discovered that the DSSC showed an improvement of 116% in short circuit current density and 265% in overall conversion efficiency when gold nanoparticle layer was employed in the water-based DSSC.

In particular, the enhancement of Au-DSSC is achieved through excitation of localized surface plasmon resonance of gold nanoparticles, coupling of incident light to propagating surface plasmon polarity (SPP) and scattering of incident light by gold nanoparticle. Studies revealed that these three light trapping methods able to reduce the oxide film thickness while the light harvesting efficiency remains unaffected.

CHAPTER 3

METHODOLOGY

3.1 Introduction

This chapter describes the experimental procedures involved in this study. It covers semiconductor oxide powder fabrication, semiconductor oxide pastes fabrication and dye-sensitized solar cell assembly and characterization techniques.

Figure 3.1 shows the research flow involved in this study. Two categories of semiconductor oxide powder were fabricated which were titanium oxide, TiO_2 nanoparticles and titanium oxide-gold, TiO_2-Au nanocomposite powder. The TiO_2 nanoparticles powders were converted into pastes and deposited on the FTO coated glass by doctor blade technique. The samples were then subjected to sintering process, dye absorption and assembly. The performance of assembled DSSC of various TiO_2 layers was then analysed by I-V tester. The TiO_2 DSSC with optimum performance was selected as the baseline for the study. Gold nanoparticles were added to the optimized TiO_2 layers in order to study the effect of gold nanoparticles on DSSC performance.

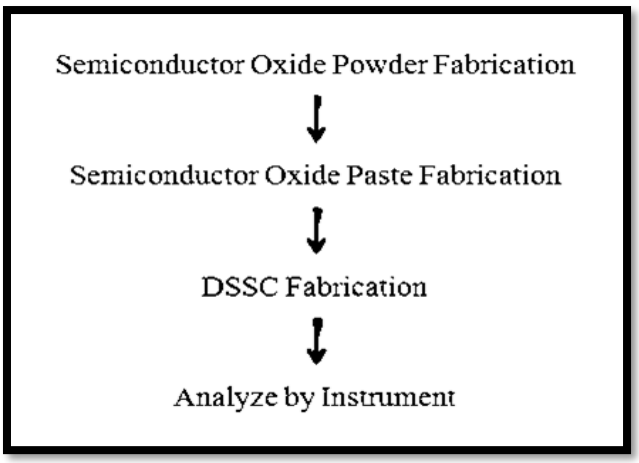

Figure 3.1: Schematic Representation of Research Flow

3.2 Fabrication of Semiconductor Oxide Powder

Three series of TiO_2 nanoparticles powders (series A, series B and series C) were synthesised. Then a series of TiO_2-Au nanocomposite powders (series D) were fabricated. All the oxide powders were fabricated by hydrothermal process and sol-gel method.

3.2.1 Fabrication of Titanium Oxide Nanoparticles Powder

Series A and series B TiO_2 powders serve as active layer and were synthesized by hydrothermal process. Series A powders were fabricated by varying TEA volume to produce TiO_2 nanoparticles with large surface area that favours dye absorption, whilst series B powders were produced by varying TTIP volume to produce TiO_2 powders with larger particle size that possessed haze effect and sufficient dye loading capacity. Series C powders serve as scattering layer and were fabricated using sol-gel method by varying TTIP volume.

3.2.1.1 Materials

Series A and series B TiO_2 powders were synthesised using titanium isopropoxide (TTIP), triethanolamine (TEA), deionized water and ethanol by hydrothermal process. Series C TiO_2 powders were synthesised using TTIP, polyvinylpyrrolidone (PVP), deionized water and ethanol by sol-gel method.

3.2.1.2 Synthesis of TiO_2 Powder by Hydrothermal Process

Series A TiO_2 powders were prepared by mixing 11.2 ml of TTIP with various TEA volume to produce titanium (IV) ionic, Ti^{4+} solution. Then the Ti^{4+} solution was added dropwise to a solution of deionized water:ethanol (1:14) mixture and stirred at room temperature for 24 hours. The mixture was then heated at 180 °C for 24 hours in a Teflon-lined autoclave. The obtained slurry was centrifuged and washed several times with ethanol. The slurry was dried at 60 °C for overnight. The dried slurry was then ground in a mortar and sintered at 450 °C for 2 hours. The volume of TEA was altered to study the effect of surfactant on DSSC performance.

Series B TiO_2 powders were prepared following the procedure shown in Figure 3.2 with the amount of TEA was fixed to 5 ml and the volume of TTIP was varied to study the effect of precursor on DSSC performance. Figure 3.2 shows the fabrication scheme of TiO_2 powder by hydrothermal process.

Figure 3.2: Fabrication Scheme of TiO_2 Powder by Hydrothermal Process

3.2.1.3 Synthesis of TiO_2 Powder by Sol-Gel Method

Series C TiO_2 powders were prepared by mixing various volume of titanium TTIP with PVP (1g:10g of 10% solution in absolute ethanol). Then the solution was added dropwise to a solution of deionized water:ethanol (5:3) mixture. The mixture was stirred overnight to form gel and dried at 60 °C. The dried slurry was then ground in a mortar and sintered at 450 °C for 2 hours. The fabrication scheme of TiO_2 powder by sol-gel method is shown in Figure 3.3.

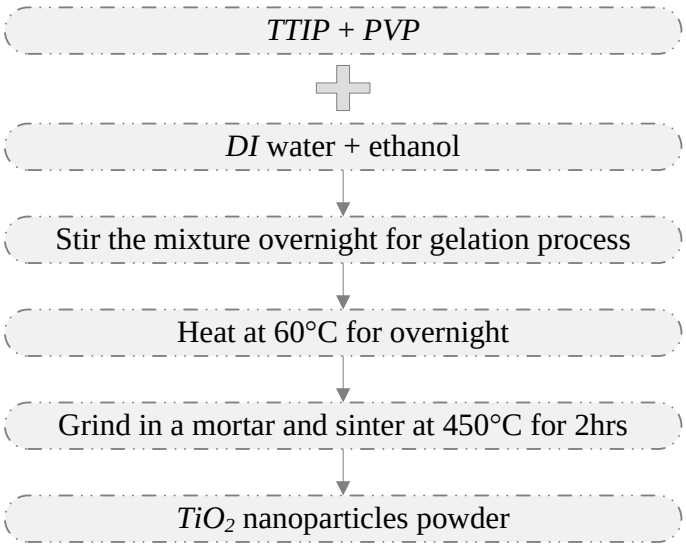

Figure 3.3: Fabrication Scheme of TiO_2 Powder by Sol-Gel Method

3.2.2 Synthesis of Titanium Oxide-Gold Nanocomposite Powder

Gold nanoparticles were added during TiO_2 powder synthesis to produce TiO_2-Au nanocomposite powder in order to reduce the synthesis process and time. Series D powders were fabricated by adding chloroauric acid, $HAuCl_4$ to optimized TiO_2 powder.

3.2.2.1 Materials

Series D TiO_2-Au nanocomposite powder were synthesised using titanium isopropoxide, triethanolamine, polyvinylpyrrolidone, chloroauric acid, deionized water and ethanol by hydrothermal process and sol-gel method.

3.2.2.2 Synthesis of TiO_2-Au Powder by Hydrothermal Process

Sample D1 titanium oxide-gold powder was prepared by mixing 11.2 ml of TTIP with 5 ml TEA to produce Ti^{4+} solution. Then 13 ml Ti^{4+} solution was added dropwise to a solution of deionized water:ethanol (1:14) mixture. 3 mg of $HAuCl_4$ was diluted with 3 ml of deionized water and added to the mixture. The mixture was stirred continuously at room temperature for 24 hours and then heated at 180 °C for 24 hours in a Teflon-lined autoclave. The obtained slurry was centrifuged and washed several times with ethanol. The slurry was dried at 60 °C for overnight. The dried slurry was then ground in a mortar and sintered at 450 °C for 2 hours. The volume of TTIP was changed to 22.4 ml for sample D2. Figure 3.4 shows the fabrication scheme of TiO_2-Au powder by hydrothermal process.

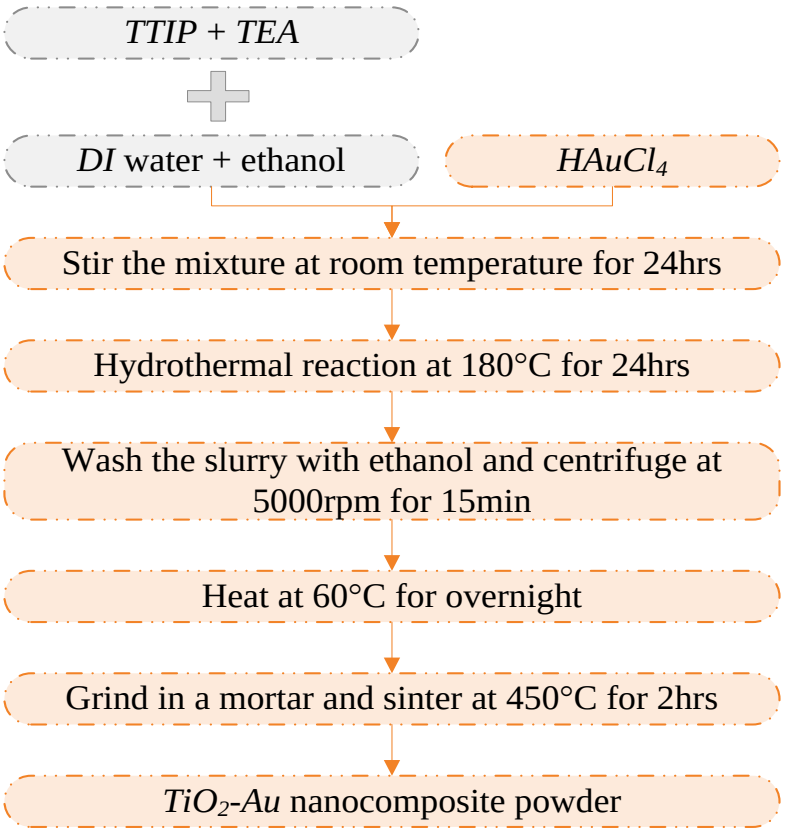

Figure 3.4: Fabrication Scheme of TiO_2-Au Powder by Hydrothermal Process

3.2.2.3 Synthesis of TiO_2-Au Powder by Sol-Gel Method

Sample D3 titanium oxide-gold, TiO_2-Au powder was prepared by mixing 11.2 ml of TTIP with PVP (1g:10g of 10% solution in absolute ethanol). Then the solution was added dropwise to a solution of deionized water:ethanol (5:3) mixture. 3 mg of $HAuCl_4$ was diluted with 3 ml of deionized water and added to the mixture. The mixture was then stirred overnight to form gel and dried at 60 °C. Next, the dried slurry was ground in a mortar and sintered at 450 °C for 2 hours. Figure 3.5 show the fabrication scheme of TiO_2-Au powder by sol-gel method.

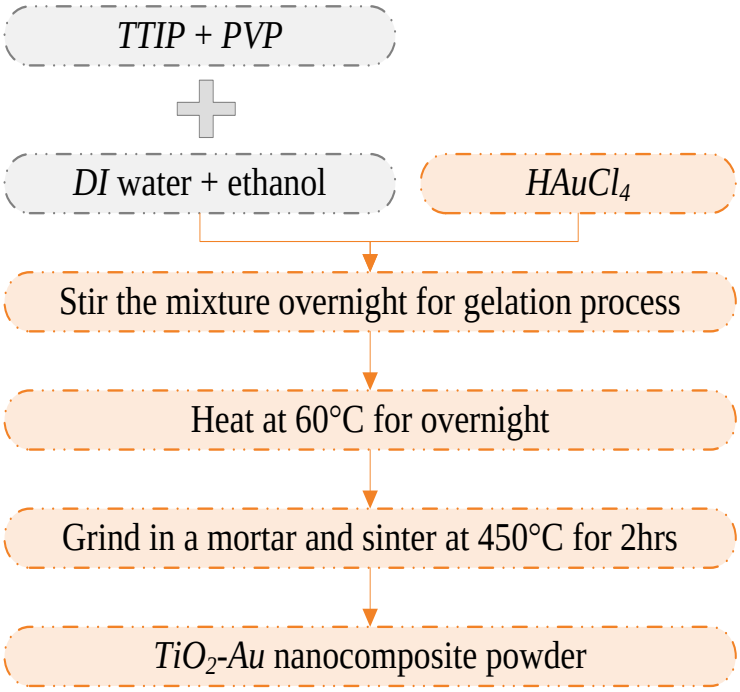

Figure 3.5: Fabrication Scheme of TiO_2-Au Powder by Sol-Gel Method

3.3 Fabrication of Semiconductor Oxide Paste

Two categories of semiconductor oxide paste were fabricated to investigate the effect of gold nanoparticles on dye-sensitized solar cell power conversion efficiency.

3.3.1 Materials

Titanium oxide paste and titanium oxide-gold paste were synthesised by mixing TiO_2 powder, TiO_2-Au powder, terpinol, ethyl cellulose, acetic acid, deionized water and absolute ethanol.

3.3.2 Fabrication of TiO_2 Paste and TiO_2-Au Paste

The pastes for doctor blade technique were prepared by grinding 1.5 g of TiO_2 powder with 0.25 ml of acetic acid in an alumina mortar for 5 minutes. Then 0.25 ml of deionized water was added and ground for 5 minutes. Next, 3.75 ml of absolute ethanol was added and ground for 5 minutes. 3.75 ml of absolute ethanol was then added to the mixture and ground for 15 minutes. The mixture was transferred to a beaker with 20 ml of absolute ethanol and stirred with magnetic tip for 1 minute at 300 rpm and sonicated using ultrasonic bath for 4 minutes. 5 g of terpinol was added into the mixture and then stirred for 1 minute and sonicated for 4 minutes. Then a mixture solution of ethyl cellulose and ethanol (0.75g:7.5g of 10% solution in absolute ethanol) was added, stirred and sonicated. Lastly, the dispersion was concentrated by stirred overnight at room temperature to evaporate excess ethanol. At each step, the solution was added drop by drop into the mortar (Ito et al., 2007). Figure 3.6 shows the fabrication scheme of TiO_2 paste.

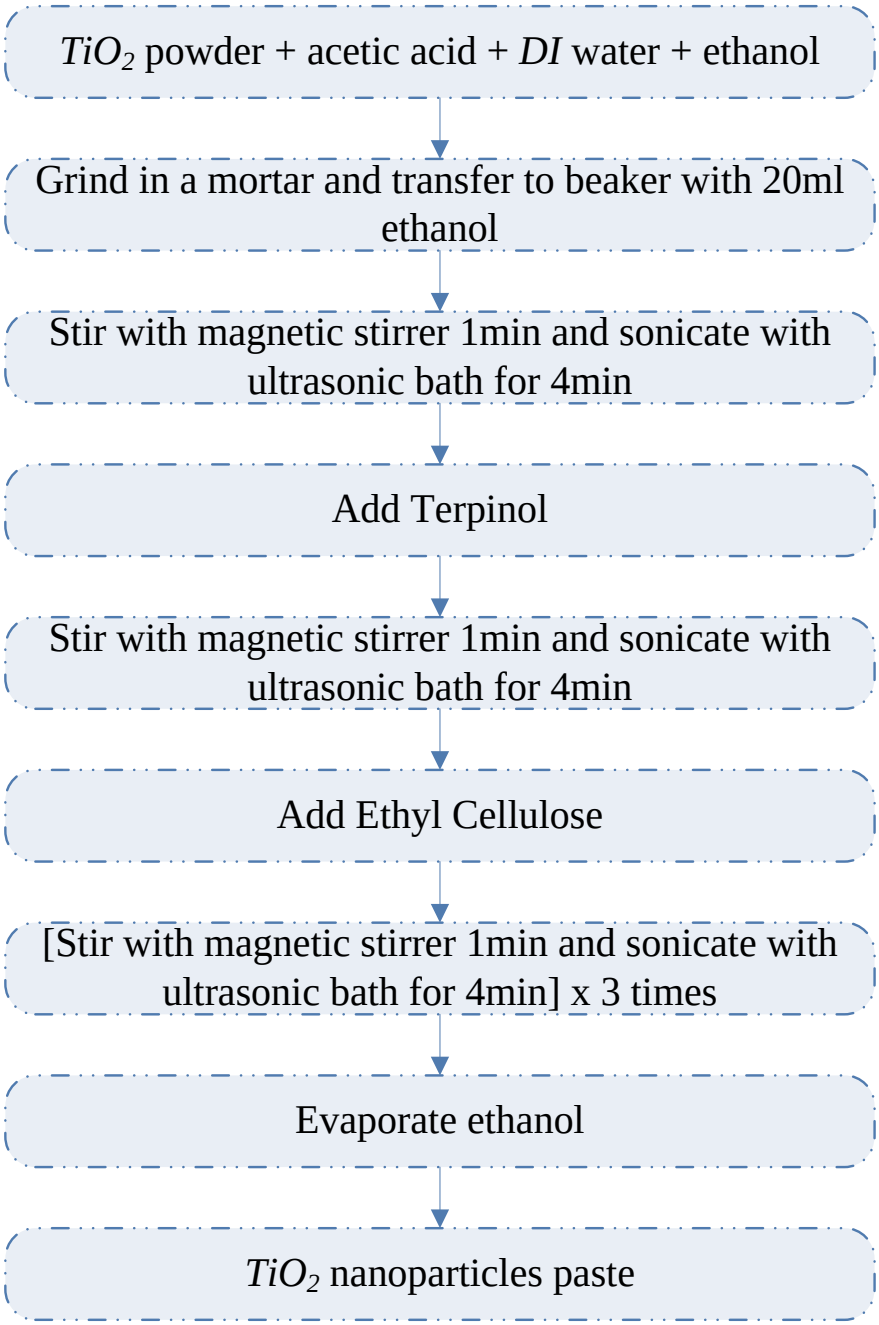

Figure 3.6: Fabrication Scheme of TiO_2 Paste

TiO_2-Au pastes were produced following the same procedures except the TiO_2 powder was replaced with TiO_2-Au powder. The fabrication scheme of TiO_2-Au nanocomposite paste is shown in Figure 3.7.

Figure 3.7: Fabrication Scheme of TiO_2-Au Nanocomposite Paste

3.4 Dye-Sensitized Solar Cell Fabrication

3.4.1 Materials

Fluorine-doped tin oxide glass substrate was used as substrate for photo-electrode and counter electrode. 0.3 mM of ruthenium, Ru-II complex (N719) and iodide / triiodide, I^-/I_3^- redox mediator was used as sensitizer and electrolyte. 30 μm thermoplastic film was used as sealant to seal the solar cell.

3.4.2 DSSC Preparation and Assembly

The dye-sensitized solar cell fabrication process is presented in Figure 3.8. FTO glass substrates were cut by diamond cutter. Then the substrates were washed with mild detergent and rinsed with water. The substrates were cleaned with distilled water, deionized water, acetone and absolute ethanol by ultrasonic bath. The substrates were then heated at 400 °C for 15 minutes to remove contaminants and organic solvent. For counter electrode glass substrate, a hole was drilled on the FTO glass after cutting.

Photo-electrode was fabricated by depositing TiO_2 paste on FTO coated glass substrate by doctor blade technique and sintered at 500 °C for 30 minutes. Then, the TiO_2 electrode was soaked in N719 dye solution for 24 hours to allow for complete sensitizer uptake.

Counter electrode was fabricated by depositing platinum, Pt paste on perforated FTO glass and sintered at 400 °C for 15 minutes.

Photoanode and counter electrode were constructed into a sandwich-type cell. The cell was sealed using thermoplastic ionomer as sealant at 135 °C for 5 minutes. The electrolyte was injected into the cell via vacuum

backfilling through the hole on the counter electrode. Lastly, the hole was sealed by thermoplastic sealant and covering glass.

Titanium oxide-gold dye-sensitized solar cell (TiO_2-Au DSSC) was fabricated following above procedures by replacing TiO_2 paste with TiO_2-Au paste.

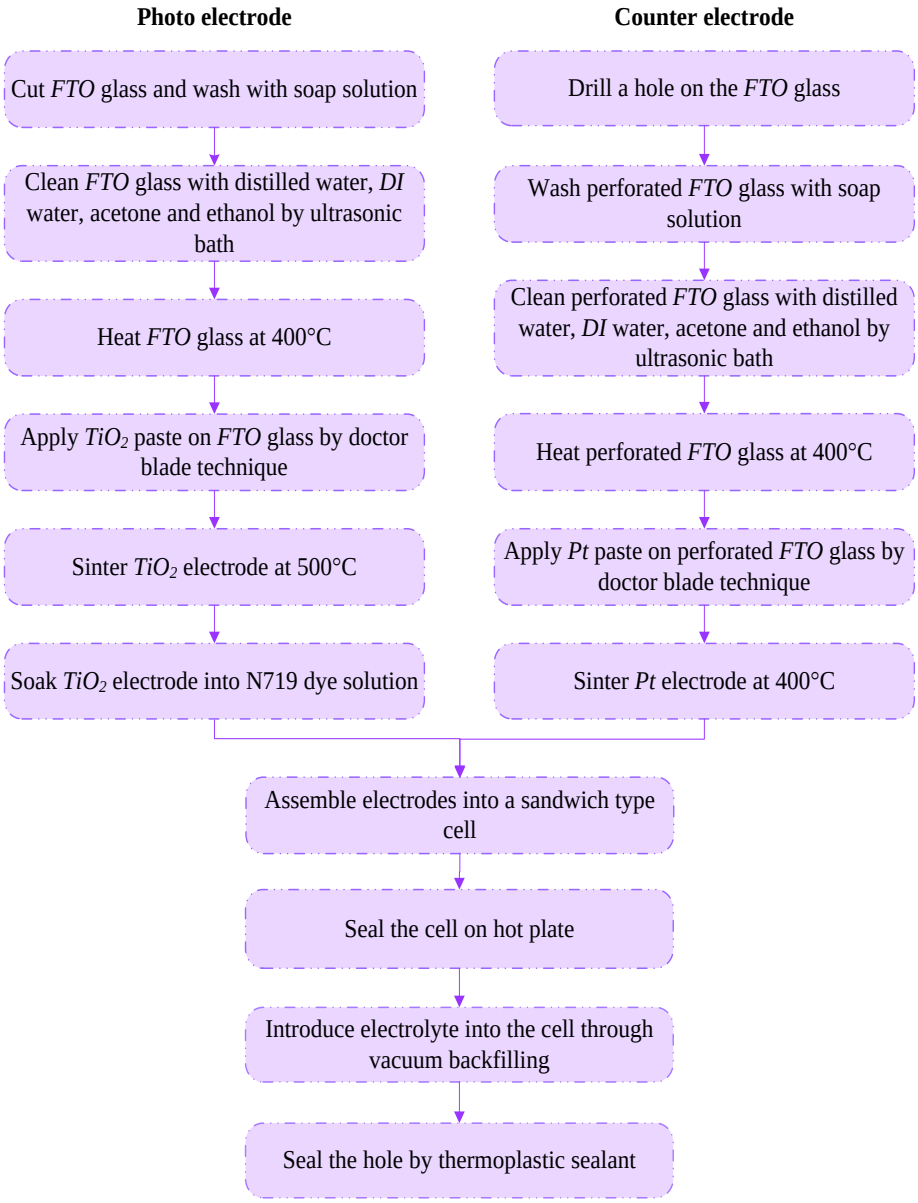

Figure 3.8: Fabrication Scheme of Dye-Sensitized Solar Cell (DSSC)

3.5 Characterisation Techniques

3.5.1 I-V Testing

Photocurrent density-voltage (J-V) curve measurement is one of the essential characterisation techniques for solar cell. I-V tester was utilised to measure the cell parameters, for example, short circuit current density, fill factor and light conversion efficiency of dye-sensitized solar cell. The cell performance was measured using Keithley 2400 Source Meter with the light intensity of 1000 W/m^2 under an AM1.5 light source. A standard silicon photodiode was used to calibrate the light intensity of the illumination source. PVIV 1.2 was used to compute the cell performance.

The overall DSSC power conversion efficiency, η can be obtained from the current density-voltage (J-V) curve. Figure 3.9 shows the typical I-V curve of a DSSC. The cell efficiency, η is a function of J_{sc}, V_{oc}, and FF of the cell. It can be calculated using Equation 3.1.

$$\eta = \frac{J_{sc}\, V_{oc}\, FF}{\Phi} \tag{3.1}$$

where

η = power conversion efficiency

J_{sc} = short circuit current density, mA/cm^2

V_{oc} = open circuit voltage, V

FF = fill factor

Φ = intensity of the incident light, W/m^2

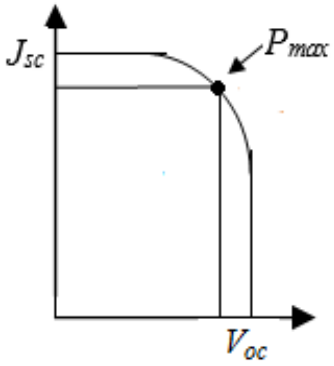

Figure 3.9: J-V Curve

The J_{sc} is the photocurrent density at zero volt and V_{oc} is the voltage when the current density in the cell is zero. The maximum power, P_{max} corresponds visually to the largest rectangle area which can fit inside the current-voltage curve. The *FF* measure the squareness of the I-V curve. *FF* is defined as the ratio of maximum power, P_{max} to open circuit voltage and short circuit current density. It can be calculated using the Equation 3.2.

$$FF = \frac{V_{\max} J_{\max}}{V_{oc} J_{sc}} = \frac{P_{\max}}{V_{oc} J_{sc}} \tag{3.2}$$

where

FF = fill factor

V_{max} = voltage at maximum power, V

J_{max} = current at maximum power, mA/cm^2

V_{oc} = open circuit voltage, V

J_{sc} = short circuit current density, mA/cm^2

P_{max} = maximum power, W

3.5.2 Field-Emission Scanning Electron Microscopy (FE-SEM) Analysis

Field-emission scanning electron microscope was used to study the morphology and the surface structure of the synthesised semiconductor oxide powders. It provides information on surface appearance or topography of the samples and allows the study of the microstructure (particle size) of these samples. Cross-sectional studies on titanium oxide, TiO_2 layers were done to investigate the thickness of those films.

The energy-dispersion x-ray spectroscopy (EDX) detector attached to the FE-SEM was utilised to identify the composition of the titanium oxide-gold, TiO_2-Au nanocomposite powders. The element mapping feature provides the qualitative image of the gold, Au distribution. The SEM-EDX analysis was carried out using JEOL JSM-6701F.

3.5.3 X-Ray Diffractometer (XRD) Analysis

X-ray diffractometer analysis is a rapid analytical method mainly utilised for phase identification of crystalline material. The sample is scanned by a high intensity monochromated Cu-Kα radiation. Lab X XRD-6000 by Shimadzu was utilised to study the sample x-ray diffraction patterns. The incident wavelength was λ=1.5406 Å and the scanning speed was 2 deg/min in 2θ range from 20° to 80°.

3.5.4 UV-Visible Spectroscopy Analysis

UV-Visible spectrophotometer is an instrument used to analyse compound in the ultraviolet and visible region of electromagnetic spectrum. It allows determination of wavelength and maximum absorbance of the compound.

Usually, the scanned region is in the range between 200 nm and 400 nm for ultraviolet and the visible region is between 400 nm and 800 nm.

Cary 100 UV-Vis spectrophotometer was utilised to investigate dye loading capacity of the oxide film. The test was prepared by desorbing the dye in a 10mM mixture solution of sodium hydroxide, NaOH and ethanol.

CHAPTER 4

RESULTS AND DISCUSSIONS

4.1 Introduction

The efficiency performance of dye-sensitized solar cell is affected by the semiconductor oxide layer properties. This chapter discusses the results obtained from several techniques such as I-V testing, XRD, FE-SEM, EDX and UV-Vis analyses. Table 4.1 shows the types of semiconductor oxide layer used in this project.

Table 4.1: Types of Semiconductor Oxide Layer

Series	Type of Semiconductor Oxide layer
A	TiO_2 nanoparticle active transparent layer
B	TiO_2 nanoparticle active opaque layer
C	TiO_2 nanoparticle scattering layer
D	TiO_2-Au nanocomposite active and scattering layer

4.2 Preparation of TiO_2 Powders by Hydrothermal Process and Sol-Gel Method

Titanium oxide nanoparticles powder was prepared by hydrothermal process and sol-gel method. As described in Section 2.2, hydrothermal process is commonly utilised for small particle TiO_2 powder fabrication while sol-gel method is usually for large particle fabrication.

The volume of surfactant may affect the properties of TiO_2 nanoparticles powder, consequently influence the power conversion efficiency, η of a DSSC. Series A TiO_2 powder was prepared by hydrothermal process with various triethanolamine volume. Table 4.2 shows the list of series A TiO_2 powder.

Table 4.2: List of TiO_2 Powders Fabricated with Various TEA Volume by Hydrothermal Process (Series A)

Sample	TEA Volume (ml)
A1	1
A2	3
A3	4
A4	5
A5	6
A6	7
A7	8
A8	9
A9	10

Two series of TiO_2 powder with various titanium tetraisopropoxide volume were prepared by hydrothermal process (series B) and sol-gel method (series C). Table 4.3 and 4.4 show the list of fabricated TiO_2 powders for series B and series C.

Table 4.3: List of TiO_2 Powders Fabricated with Various TTIP Volume by Hydrothermal Process (Series B)

Sample	TTIP Volume (ml)
B1	14.0
B2	16.8
B3	19.6
B4	22.4
B5	25.2

Table 4.4: List of TiO_2 Powders Fabricated with Various TTIP Volume by Sol-Gel Method (Series C)

Sample	TTIP Volume (ml)
C1	8.4
C2	11.2
C3	14.0
C4	16.8
C5	19.6
C6	22.4

4.2.1 Characterisation of TiO_2 Powders

4.2.1.1 XRD Analysis

Figure 4.1 – 4.3 show the XRD patterns for series A, series B and series C TiO_2 powders. The structural refinement and lattice parameter were determined by *Chekcell* program.

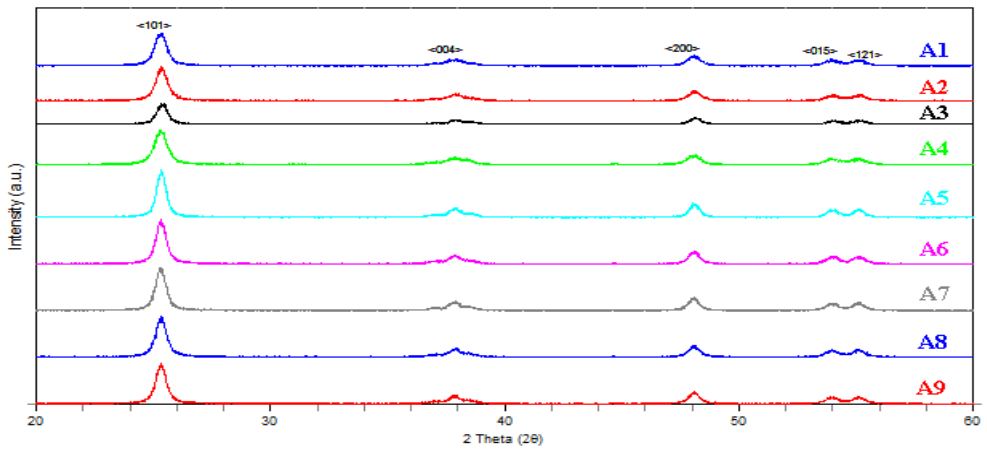

Figure 4.1: XRD Patterns of Series A TiO_2 Powders

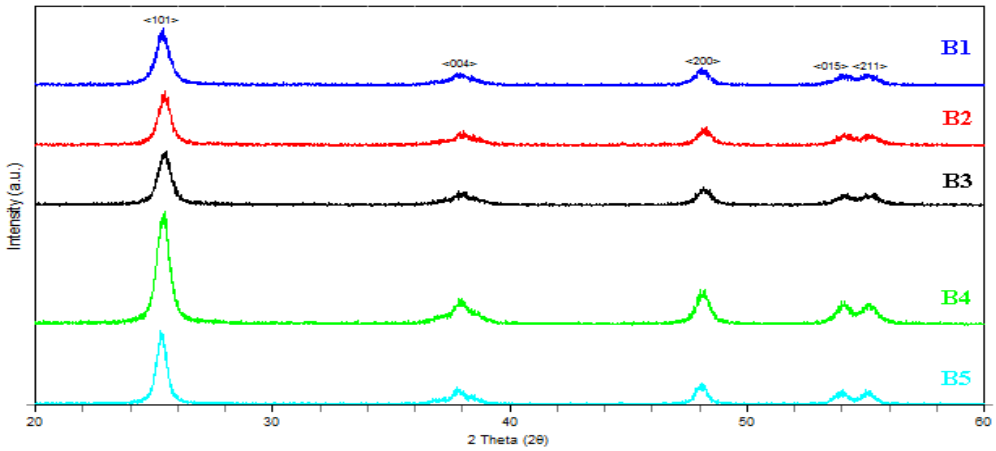

Figure 4.2: XRD Patterns of Series B TiO_2 Powders

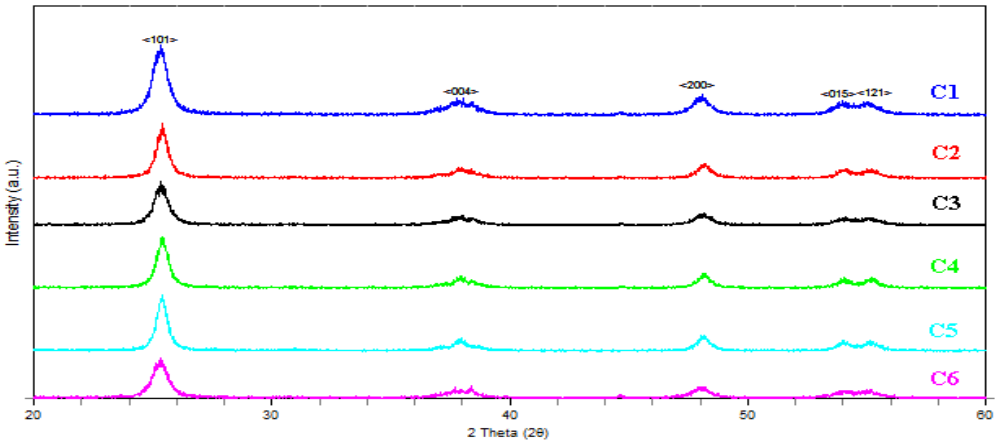

Figure 4.3: XRD Patterns of Series C TiO_2 Powders

The X-ray diffraction patterns show similar trends for all TiO_2 powders which imply that the volume of precursor and surfactant has no synergy impact on the formation of TiO_2 crystal phase. The highest intensity of signal at the value of 2 Theta falls around 25.3 <101> (JCPDS-021-1272) indicates the TiO_2 nanoparticles exhibit high fraction of anatase phase without any impurities.

Anatase TiO_2 nanoparticles possess better performance than rutile and brookite due to it crystal structure shape. Anatase TiO_2 appears as pyramid-like crystals which have a high surface area for optimum dye absorption. Besides, the band-gaps for anatase TiO_2 is 3.2 eV which is slightly higher than rutile 3.0 eV (Lee et al., 2009).

4.2.1.2 Current-Voltage Characterisation of TiO_2 DSSC

The dye-sensitized solar cell performance is affected by the characteristics of TiO_2 nanoparticles. The solar cell performance was tested by I-V test station to analyse the DSSC parameters.

Series A TiO_2 nanoparticles serve as active layer with the aim to boost the DSSC conversion efficiency, η by high dye loading. Series A was fabricated by varying the surfactant volume. The efficiency, η versus triethanolamine volume graph shown in Figure 4.4 indicates that the conversion efficiency of DSSC increased as the surfactant volume is increased from 1 ml to 5 ml and further increase on surfactant volume diminishes the solar cell performance.

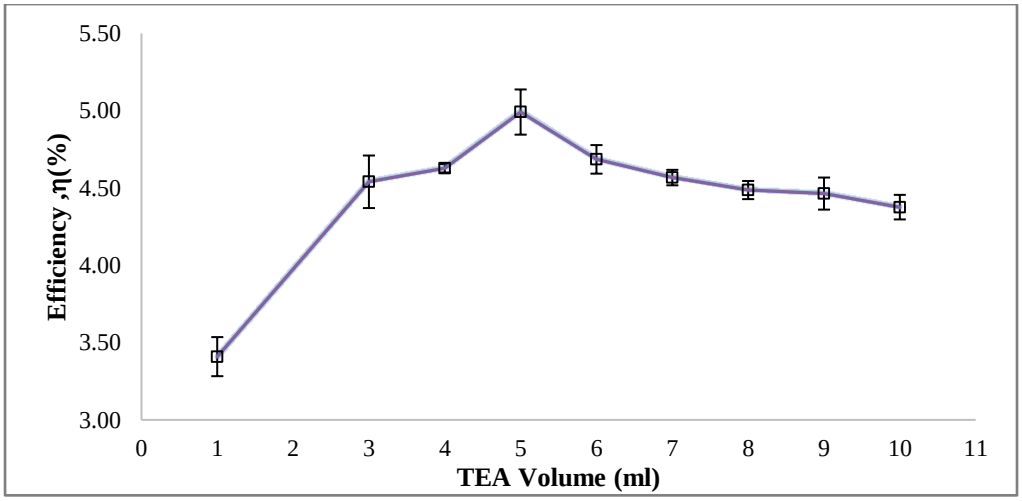

Sample	TEA (ml)	η (%)
A1	1	3.409±0.126
A2	3	4.540±0.170
A3	4	4.627±0.027
A4	**5**	**4.991±0.146**
A5	6	4.685±0.092
A6	7	4.567±0.051
A7	8	4.486±0.059
A8	9	4.464±0.104
A9	10	4.376±0.079

Figure 4.4: DSSC Efficiency Performance of Series A

The intention of series B is to produce TiO_2 nanoparticles powder with larger particle size that possesses some haze effect with sufficient dye loading capacity. Figure 4.5 shows the better light conversion efficiency of DSSC as the amount of titanium tetraisopropoxide was increased from 11.2 ml to 25.2 ml and further increased on TTIP volume caused lower efficiency. The result shows that the suitable TTIP volume is 22.4 ml.

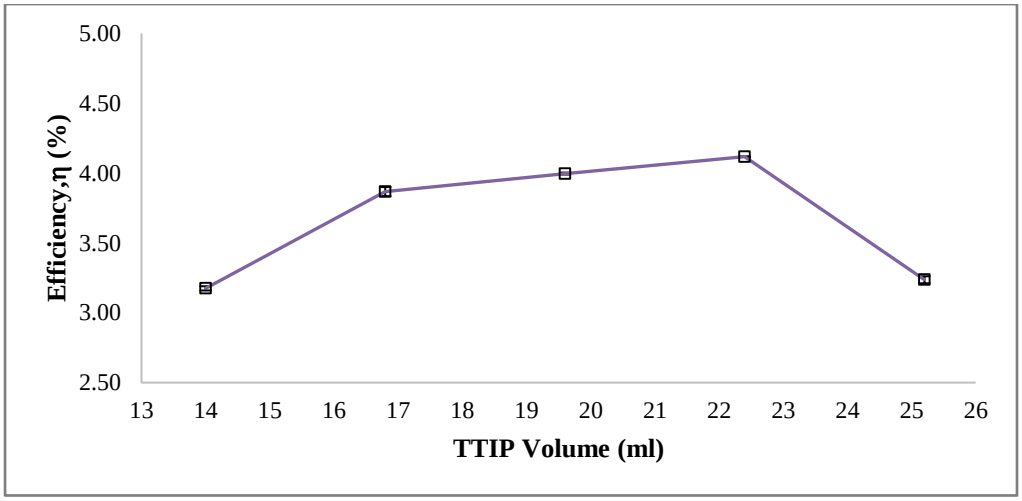

Sample	TTIP (ml)	η (%)
B1	14	3.175±0.015
B2	16.8	3.867±0.033
B3	19.6	3.996±0.007
B4	**22.4**	**4.118±0.002**
B5	25.2	3.236±0.025

Figure 4.5: DSSC Efficiency Performance of Series B

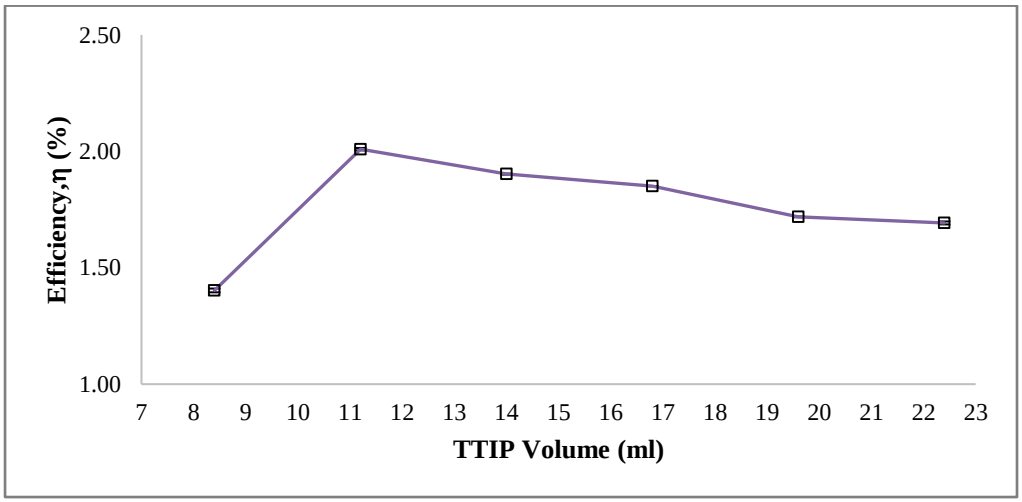

Sample	TTIP (ml)	η (%)
C1	8.4	1.402±0.008
C2	**11.2**	**2.009±0.005**
C3	14	1.902±0.002
C4	16.8	1.850±0.001
C5	19.6	1.718±0.002
C6	22.4	1.692±0.006

Figure 4.6: DSSC Efficiency Performance for Series C

Series C TiO_2 nanoparticles powder were fabricated by sol-gel method. The aim of series C is to facilitate light scattering effect. The result shown in Figure 4.6 indicates that the highest efficiency of 2.01% is obtained with optimum TTIP volume of 11.2 ml.

The reason for this phenomenon is that the excessive surfactant increases the viscosity of the reaction mixture and leads to difficulty in controlling the particle size distribution of TiO_2 powder. It is worth highlighting that there is also a negative impact on the efficiency of DSSC if too little amount of triethanolamine is used (TEA) might not be sufficient to coat the TiO_2 powder which consequently causes aggregation that affects the dye loading. (Huang et al., 2014) Both the phenomena cannot lead to a favourable outcome as TiO_2 powder with narrow size distribution is produced only under optimal conditions. TiO_2 powder with narrow size distribution is essential to yield good dye loading quality. TiO_2 powder with wide size distribution leads to unsatisfactory control of the dye loading as small particles have higher surface area which capable of adsorbing more dye molecules while large particles adsorb less dye molecule due to lower surface area. In addition, the narrow particle size distributed TiO_2 nanoparticles in DSSC is known to enhance the charge transfer properties, and thus improving the conversion efficiency of DSSC (Kang et al., 2008).

In this study titanium tetraisopropoxide (TTIP) is used as precursor to form the TiO_2 powder and the volume of TTIP is not the primary interest of study in this research project. TTIP is one of the chemical required to produce the TiO_2 powder. The TTIP volume is varied to search for optimum volume that produces TiO_2 powder with better DSSC efficiency.

4.2.1.3 UV-Visible Spectroscopy Analysis

The amount of N719 dye absorbs on surface of TiO_2 nanoparticles is greatly influenced by the characteristics of TiO_2 nanoparticles. UV-visible spectrometer was used to study the TiO_2 layer dye loading capability.

N719 dye molecules are attached to the TiO_2 nanoparticles through the carboxyl group interaction. Figure 4.7 shows that N719 dye consists of dual bipyridyl ligands with dual carboxyl groups at the 4 and 4' position of the bipyridyl. N719 dye has better interaction with titanium oxide, TiO_2 compared to other dye owing to the two carboxyl groups. (Hwang et al., 2010)

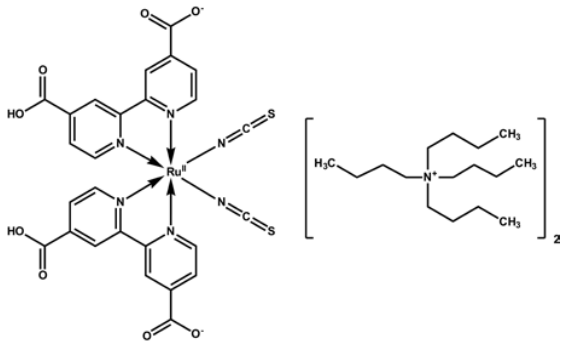

Figure 4.7: Molecular Structure of N719 Dye

N719 is a hydrophilic dye that soluble in alkaline water solution thus the sample was diluted in a mixture solution of 10 mM sodium hydroxide and ethanol (1:1) to remove all dye molecules from the TiO_2 nanoparticle surface. The amount of dye molecule adsorbed was determined by acquiring an absorption spectrum of the dilute solution.

The absorption peaks of N719 dye are at 309 nm, 368 nm and 505 nm based on the UV-vis spectroscopy data. The peak position of 309 nm is due to bipyridine intra ligand ($\pi - \pi^*$) charge transition. On the other hand, the peaks position of 368 nm and around 505 nm are attributed to metal-to-ligand charge transfer (MLCT) with the same contribution of an intra ligand ($\pi - \pi^*$) transition for higher energy MLCT. (Kisserwan and Ghaddar, 2010) The peak around 505 nm is slightly shifted toward longer wavelengths as the concentration of N719 dye is increased implying that the intermolecular interaction between the dye molecules have influence on the peak position in the visible region. (Katoh et al., 2010) The scanning analysis report for optimum TiO_2 nanoparticles photo-electrode is shown in Appendix A.

The dye loading capacity of the photo-electrode is greatly determined by the internal surface area of the titanium oxide film which is depended on the TiO_2 layer thickness and the TiO_2 particle size. Both the parameters must be optimized to improve the light harvesting efficiency. UV-Visible spectrum shown in Figure 4.8 demonstrates that sample A4 yield higher dye loading than sample B4 and sample C2. Therefore, sample A4 yield higher efficiency than sample B4 and sample C2 as sample A4 obtains higher dye absorption due to larger surface area. Higher dye loading is one of the factors leading to higher efficiency.

Thicker TiO_2 layer is supposed to yield higher dye loading but the UV-Visible spectroscopy result shows otherwise. Even though the TiO_2 layer for sample B4 is thicker than sample A4, however Figure 4.8 shows that the dye loading capacity for sample B4 is lower than sample A4 as sample B4 has lower surface area for dye molecules to attach on it. Sample C2 has the lowest dye absorption as it has the lowest film thickness (refer to Table 4.5) and smallest surface area.

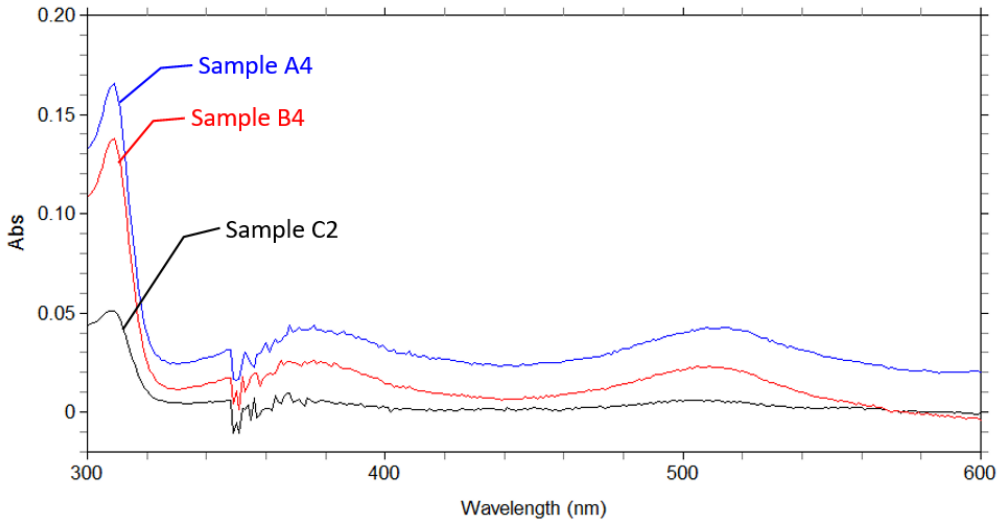

Figure 4.8: UV-visible Spectrum for Various TiO_2 Nanoparticles Samples

Besides, DSSC photoanode for sample A4 shows typical red wine colour while sample B4 is pink and sample C2 is light pink further imply that the dye

loading is much lower for large particle. Figure 4.9 presents the images of TiO_2 layer on FTO glass after dye loading.

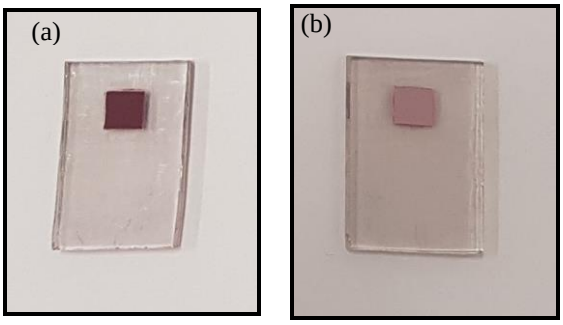

Figure 4.9: Images of TiO_2 Photo-electrode for (a) Sample A4 (b) Sample C2

The photoanode soaking time was fixed to 24 hours as longer soaking time caused a reduction in fill factor, *FF*. Although, studies have shown that longer soaking time increases the amount of dye adsorbed and higher dye absorption results in better performance due to low charge transfer resistance. However, the dye molecules tend to agglomerate when the soaking time exceeds the critical soaking time. Agglomeration of dye molecules inhibited electrolyte diffusion through the TiO_2 pores as dye molecules tend to block the opening of the pores thereby higher charge transfer resistance (Hwang et al., 2010).

4.2.2 Characterisation of Optimized TiO_2 Layer

4.2.2.1 FE-SEM Analysis of TiO_2 Powder

4.2.2.1.1 Microstructure of TiO_2 Powder

The microstructure of TiO_2 particles affects the dye-sensitized solar cell performance. The particle size distribution was analysed by *Image J* software and the histogram of particle size distribution together with Gaussian profile was plotted for analysis.

The SEM micrograph of sample A4 TiO_2 powder synthesised by hydrothermal process is shown in Figure 4.10. The image implies that sample A4 exhibits TiO_2 particles with homogeneous spherical shape with average particle size of 13.11 ± 3.25 nm (Figure 4.11). Homogeneous spherical TiO_2 particles are favourable as it have large surface to volume ratio which facilitates high dye loading and greater light conversion efficiency (Ito et al., 2005; Xin et al., 2011). Sample A4 with approximately 15 nm TiO_2 particles is used to produce an active transparent TiO_2 film (Wang et al., 2004). As discussed, small particles possess high surface area that promotes better dye loading thus improving the solar cell performance.

Figure 4.12 shows the micrograph of sample B4 TiO_2 powder synthesised by hydrothermal process, which suggests that the powder consists of spherical structures. The histogram presented in Figure 4.13 indicates that the average particle size of sample B4 is 29.40 ± 10.82 nm. Sample B4 is utilised to formulate an active opaque TiO_2 layer that possesses some haze effect with adequate dye loading (Hore et al., 2006).

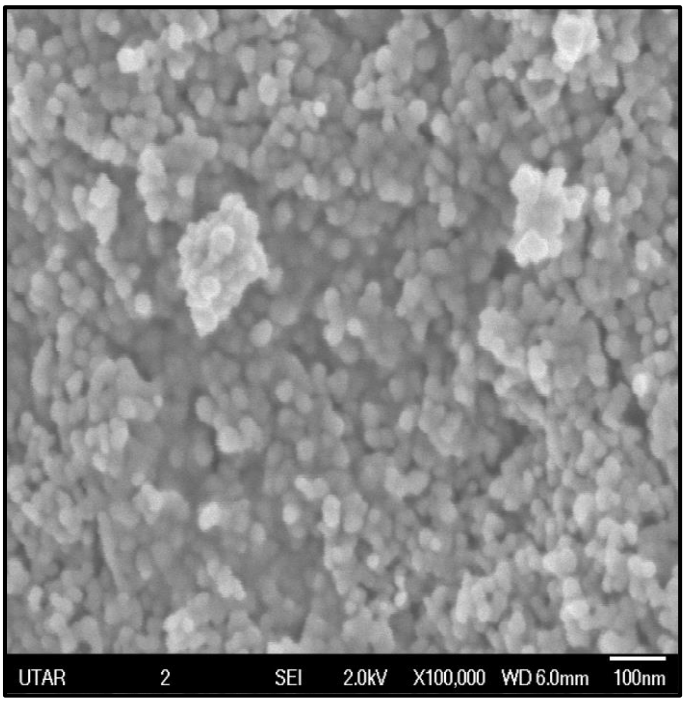

Figure 4.10: SEM Micrograph of Sample A4 TiO_2 Powder

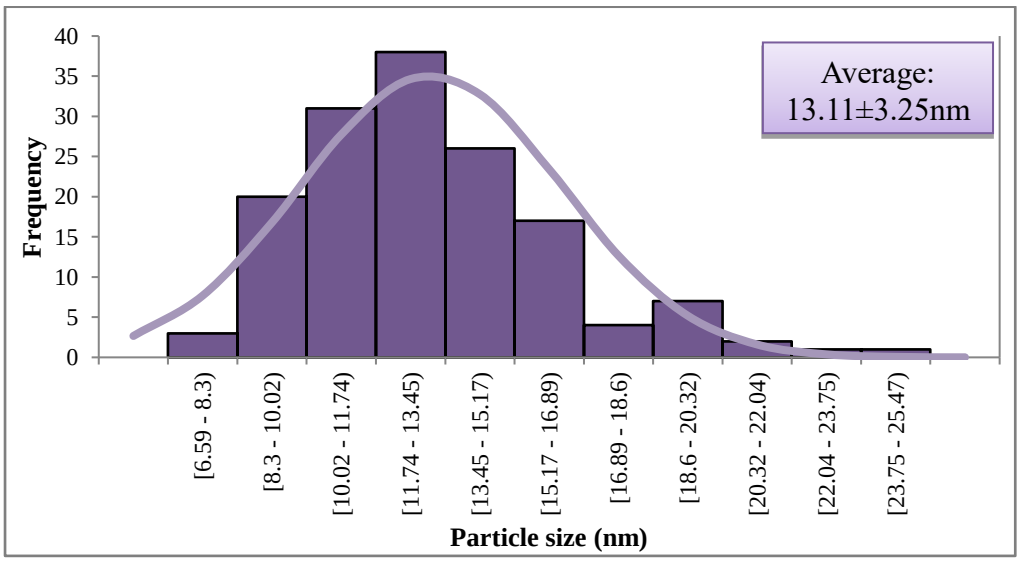

Figure 4.11: Histogram of Particle Size Distribution for Sample A4

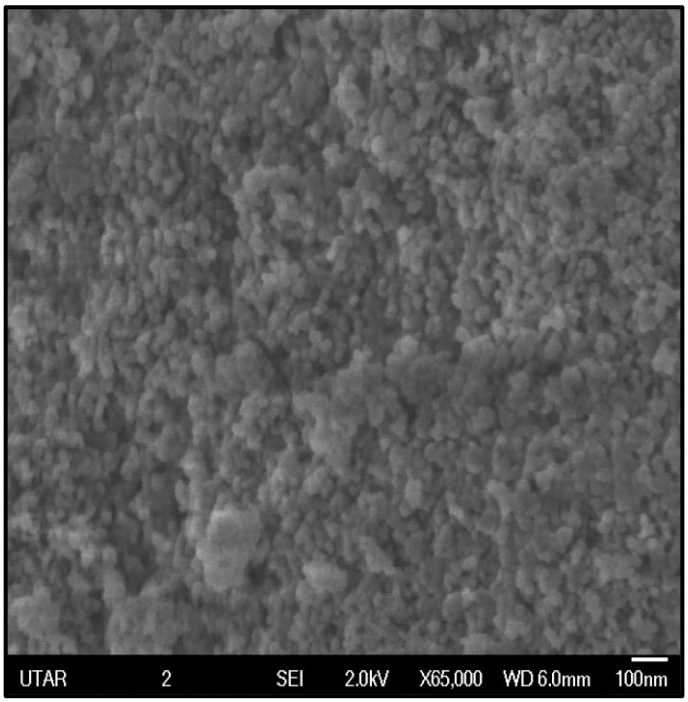

Figure 4.12: SEM Micrograph of Sample B4 TiO_2 Powder

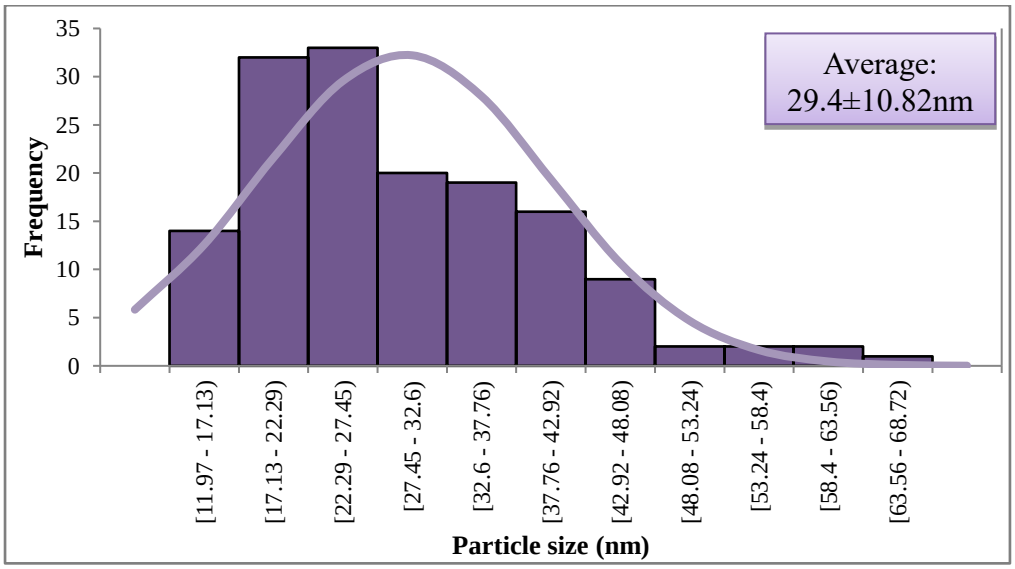

Figure 4.13: Histogram of Particle Size Distribution for Sample B4

The FE-SEM image of sample C2 fabricated by sol-gel method is shown in Figure 4.14. The figure demonstrates that the TiO_2 powder consists of dispersed TiO_2 spheres with an average size of 152.96 ± 50.01 nm (Figure 4.15).

The sample is employed to prepare a white TiO_2 layer that promotes high light scattering effect (Bi-Tao et al., 2008).

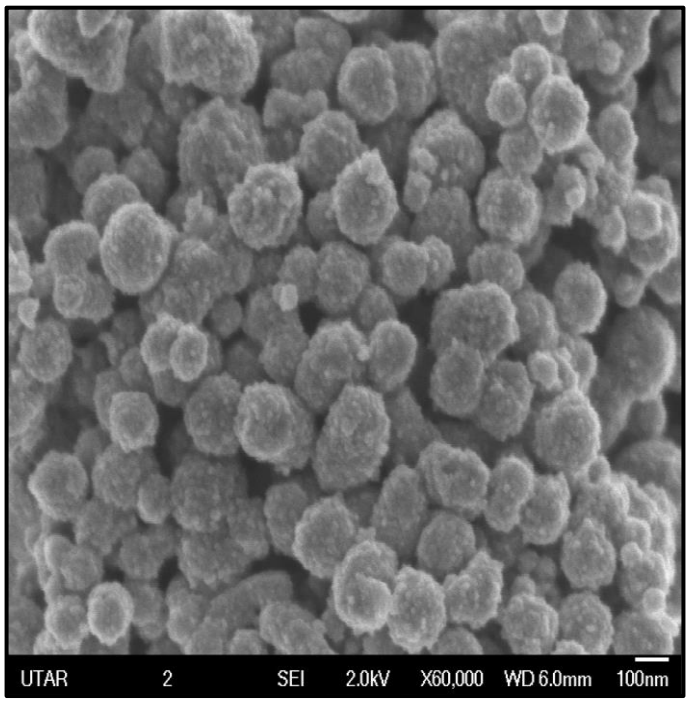

Figure 4.14: SEM Micrograph of Sample C2 TiO_2 Powder

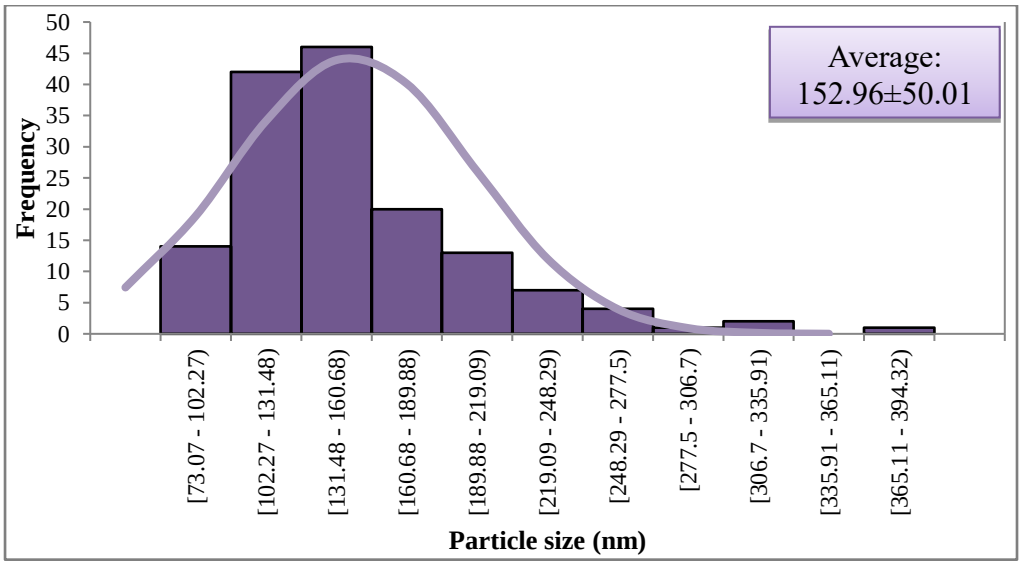

Figure 4.15: Histogram of Particle Size Distribution for Sample C2

4.2.2.1.2 Cross-Sectional Analysis of TiO_2 Film

The thickness of titanium oxide film has strong impacts on the dye absorption capacity. The amount of dye uptake is higher as the TiO_2 film thickness increased. The TiO_2 layer thickness was obtained by cross-sectional image using scanning electron microscopy. All the TiO_2 films were prepared by doctor blade technique and those photoelectrodes were cut vertically into half using diamond cutter for cross-sectional analyses..

Paste A4 is an anatase TiO_2 nanoparticles paste that produces an active transparent TiO_2 film with small particle size. This TiO_2 layer aims to promote dye loading capacity. Figure 4.16 indicates that the double-layer A4 sample film thickness is 10.4 μm. Figure 4.19(a) shows the appearance of paste A4 after sintering.

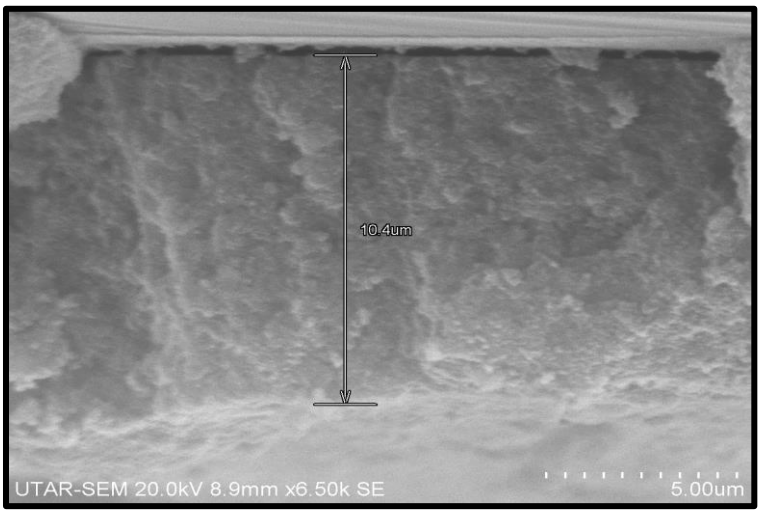

Figure 4.16: Cross-sectional Image of Double-layer A4 Sample

Paste B4 is an anatase TiO_2 nanoparticles paste formulated for active opaque TiO_2 film with larger particle size. The active opaque film intends to provide some haze effect with adequate dye loading abilities. The cross-sectional image shown in Figure 4.17 illustrates that the TiO_2 film thickness for double-layer B4 sample is 13.3 μm. The appearance of paste B4 after sintering is shown in Figure 4.19(b).

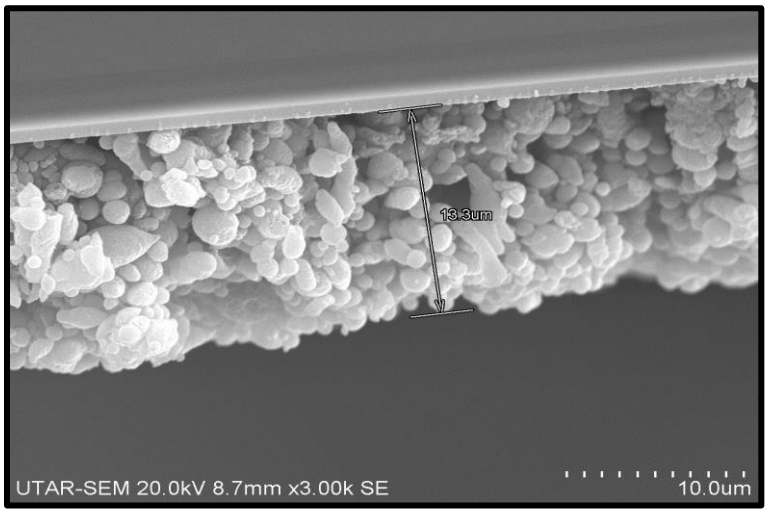

Figure 4.17: Cross-sectional Image of Double-layer B4 Sample

Paste C2 is an anatase TiO_2 paste that offer a white scattering layer. The film thickness for double-layer paste C2 sample is shown in Figure 4.18. The figure shows that the TiO_2 layer thickness is 9.96 μm. Figure 4.19(c) shows the appearance of paste C2 after sintering.

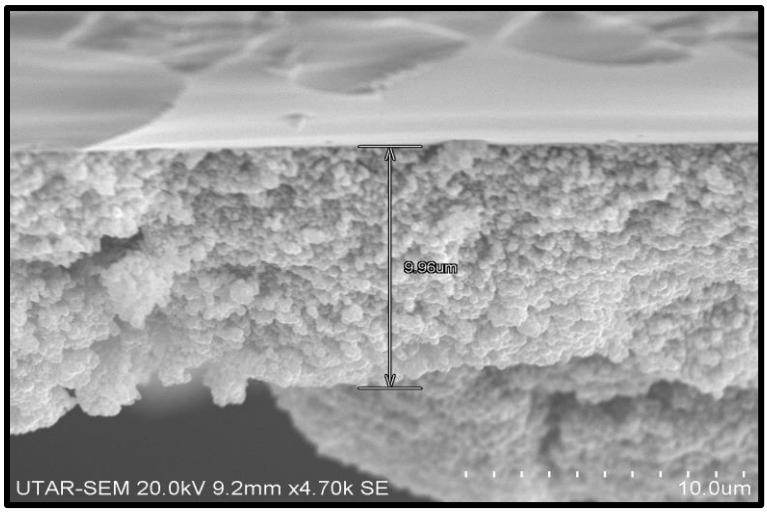

Figure 4.18: Cross-sectional Image of Double-layer C2 Sample

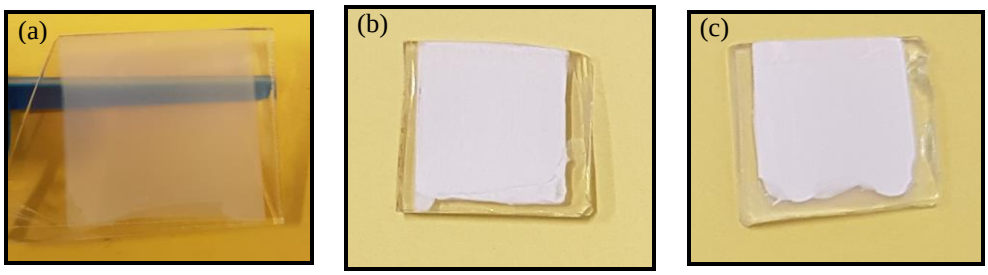

Figure 4.19: Images of TiO_2 Photo-electrode (a) Paste A4 (b) Paste B4 and (c) Paste C2

Figure 4.20 and Figure 4.21 show the cross-sectional images for sample A4 + B4 and sample A4 + C2. The samples were prepared by depositing paste A4 as the first layer followed by paste B4 or paste C2 as second layer. Figure 4.20 presents the total film thickness for sample A4 + B4 is 15.2 μm with the thickness for first layer (paste A4) is 5.27 μm and second layer (paste B4) is 9.86 μm. The total thickness for sample A4 + C2 is shown in Figure 4.21. The image indicates that the film thickness for first layer (paste A4) is 5.53 μm and second layer (paste C2) is 6.39 μm, therefore the total TiO_2 film thickness is 12.0 μm.

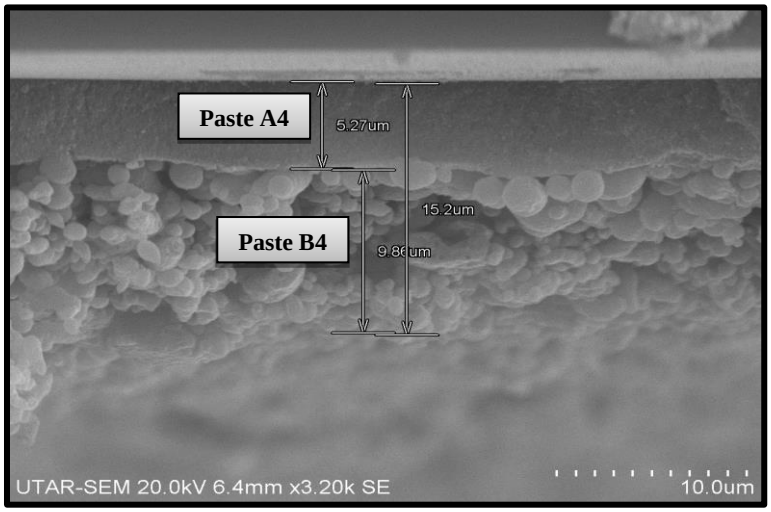

Figure 4.20: Cross-sectional Image of Sample A4 + B4

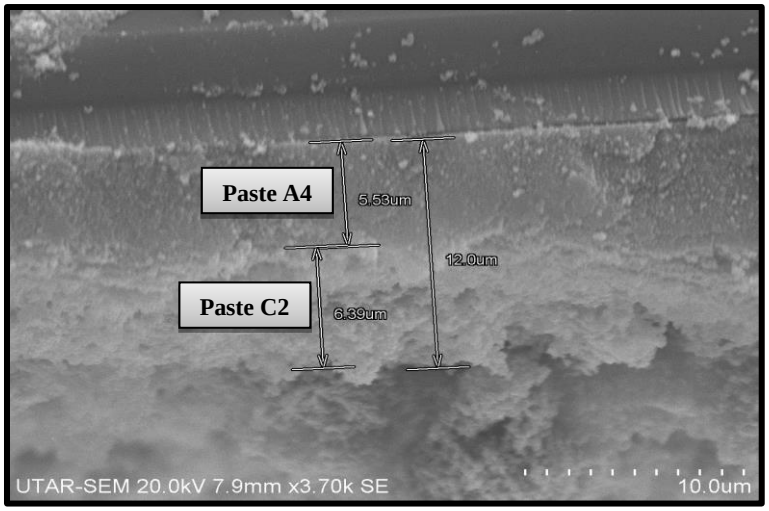

Figure 4.21: Cross-sectional Image of Sample A4 + C2

The triple layer photoanode was fabricated by applied paste A4 as the first layer followed by paste B4 as second layer and paste C2 as third layer. The TiO_2 film thickness for sample A4 + B4 + C2 is shown in Figure 4.22. The thickness for paste A4 is 5.43 μm, paste B4 is 6.42 μm and paste C2 is 6.10 μm. Hence, the total TiO_2 film thickness for sample A4 + B4 + C2 is about 20.5 μm.

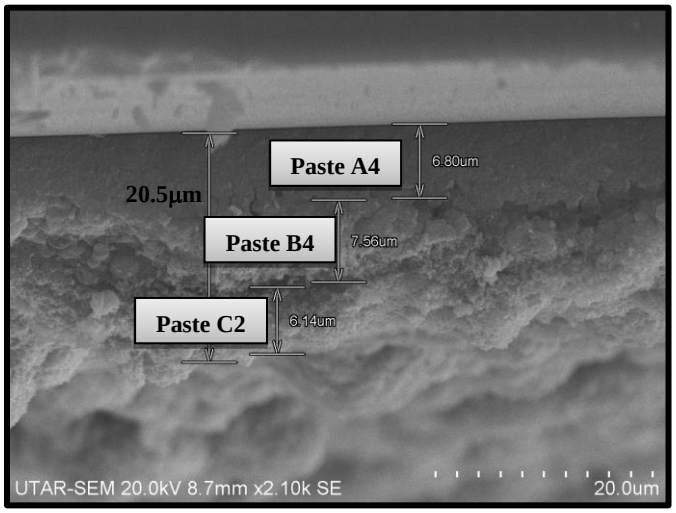

Figure 4.22: Cross-sectional Image of Sample A4 + B4 + C2

The weight ratio of elements in the TiO_2 powder is determined by EDX analysis. The EDX analysis data reports that all the TiO_2 powders contain approximately 88 wt% of titanium and 11 wt% of oxygen. The minor trace of carbon element is attributed to the carbon tape used to hold the sample on the sample holder. Figure 4.23 shows the EDX analysis of sample B4 (Refer to Appendix B for sample B4 and sample C2).

Element	Weight (%)
C K	1.04
O K	11.95
Ti K	87.01
Total	100.00

Figure 4.23: EDX Analysis of Sample A4

4.2.2.2 Current-Voltage Characterisation of DSSC with Optimized TiO_2 Layer

Dye-sensitized solar cell performance for a combination of optimized TiO_2 layer was analysed by I-V test station. The current density-voltage curves shown in Figure 4.24 indicate that TiO_2 film with smaller TiO_2 nanoparticles (double-layer A4 sample) lead to greater short circuit current density, J_{sc}. The improvement is attributed to the high dye loading capacity as small particles possess higher surface area for dye molecule absorption, as mentioned in Section 4.2.1.3. This can be correlated to higher light harvesting efficiency as more dye molecules are available to react with the light entering the cell.

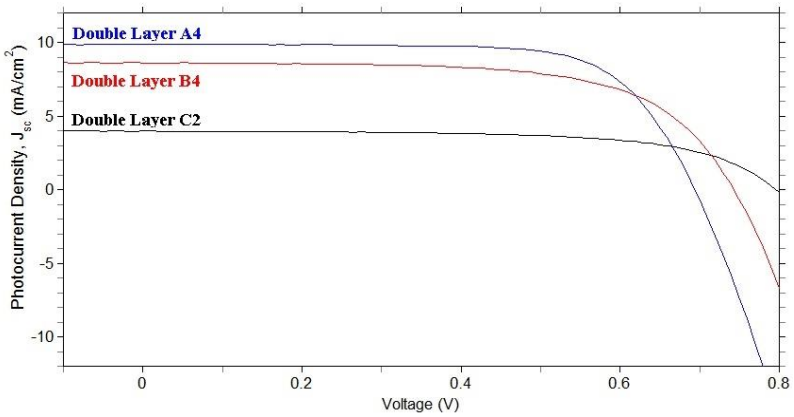

Figure 4.24: Current Density-Voltage Curves of TiO_2 Nanoparticles DSSC for Sample Double-layer A4, B4 and C2

The current density-voltage curves for dual-layer photo-electrode with optimized TiO_2 layer is shown in Figure 4.25. The dual-layer DSSC was prepared by coating a layer of transparent active TiO_2 (paste A4) as first layer followed by an opaque active TiO_2 (paste B4) layer or a scattering TiO_2 (paste C2) as second layer. The J-V curve illustrates that combining two different types of TiO_2 layer increases the short circuit current density, J_{sc} of the DSSC, subsequently enhances the solar cell performance. Figure 4.25 reveals that short circuit current density, J_{sc} for DSSC fabricated with sample A4 + B4 is higher than double-layer A4 sample and sample A4 + C2 is higher than double-layer C2 sample. The increment in photocurrent density is ascribed from the first active TiO_2 layer that promotes high dye loading and the second scattering TiO_2 layer that imposes light scattering effect (Zhu et al., 2012). Sample A4 + B4 shows power conversion efficiency of 5% which is about 3% higher in efficiency compared to double-layer A4 sample. It is agreed with Lee et al. (2009) and Liu et al. (2012) studies which demonstrated that TiO_2 layer of large particle had a tendency to scatter light within the DSSC, thereby resulted in an increase of the photocurrent density, J_{sc} and light conversion efficiency. Lee et al. (2009) reported the power conversion efficiency was improved when TiO_2 layer with particle size of 20 nm or 123 nm were deposited on top of TiO_2 layer with particle size of 9 nm. Liu et al. (2012) reported efficiency of 4.45% was obtained when light scattering layer of 200 nm TiO_2 particles was layered on top of P25 nanocrystalline layer.

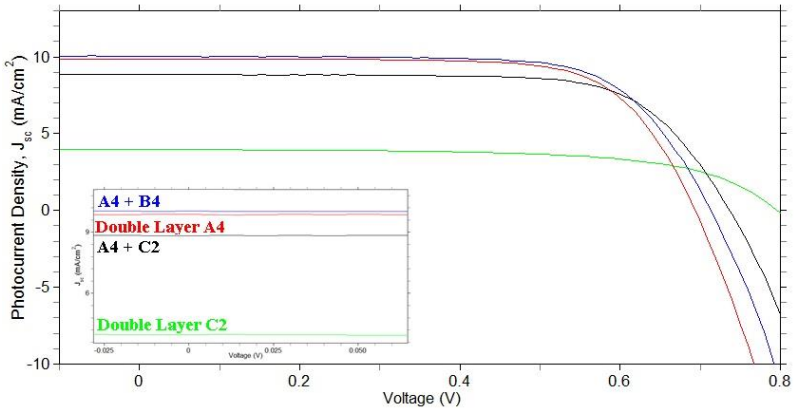

Figure 4.25: Current Density-Voltage Curve of TiO_2 Nanoparticles DSSC for Sample A4 + B4, A4 + C2, Double-layer A4 and Double-layer C2

Besides, the transparent active TiO_2 layer (paste A4) provides greater light transmission, therefore improves the photocurrent generation as more light reacts with dye molecules. On the other hand, the light loss due to back scattering is high for the transparent paste A4 since it has no light scattering effect. Therefore, larger TiO_2 nanoparticles (paste B4 and paste C2) are incorporated to retrieve the light loss by introducing light scattering. The light scattering layer has a tendency to capture incident light within the dye-sensitized solar cell thereby improves the solar cell performance. Figure 4.26 presents the mechanism of light scattering.

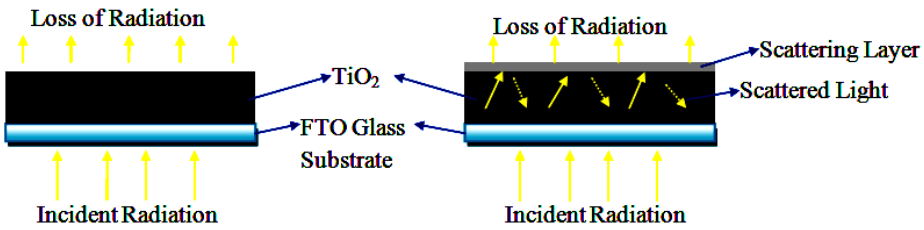

Figure 4.26: Mechanism of Scattering Layer

Dye uptake for large titanium oxide, TiO_2 nanoparticles is found to have reduced due to low surface area. However, large TiO_2 nanoparticles facilitate the light scattering and increase the light absorption in the red region consequently enhanced the light conversion efficiency of DSSC (Grätzel, 2005).

The conversion efficiency of DSSC was improved by about 4% when paste B4 was deposited on top of paste A4 layer.

In addition, study reported the TiO_2 film thickness greatly influences the amount of dye loading (Shin et al., 2010). Thicker TiO_2 film thickness results in higher dye uptake which subsequently improves the light harvesting efficiency of photo-electrode. Supposedly, double-layer B4 sample with thicker oxide film yields higher efficiency than double-layer A4 sample but the result presented in Table 4.5 shows otherwise. This is due to small particle size of TiO_2 in double-layer A4 sample increases internal surface area for dye uptake, as discussed in Section 4.2.1.3.

Table 4.5: TiO_2 Nanoparticles Film Thickness and Photovoltaic Characteristic of DSSC

Sample	Thickness (μm)	J_{sc} (mA/cm^2)	V_{oc} (V)	Fill Factor *FF*	η (%)
Double-layer A4	10.4	9.86	0.69	70.88	4.84
Double-layer B4	13.3	8.60	0.74	64.46	4.12
Double-layer C2	9.96	3.97	0.80	63.86	2.01
A4+B4	**15.2**	**10.03**	**0.71**	**69.95**	**5.00**
A4+C2	12.0	8.84	0.74	70.83	4.61
A4+B4+C2	20.5	9.97	0.70	70.77	4.94

Conversely, sample with TiO_2 film that is too thick will reduce cell performance. Table 4.5 reports that the conversion efficiency of triple layer TiO_2 nanoparticles DSSC (sample A4 + B4 + C2) is lower as the TiO_2 film thickness exceeds the optimum thickness. The thick TiO_2 film tends to crack due to shrinkage of the TiO_2 film. Evaporation and decomposition of organic substances and volume change due to crystallization induces significant stress in the film give rise to cracking of thick film. The cracking film reduces electron transport efficiency, therefore lowering the DSSC performance (Ito et al., 2003).

Moreover, the recombination rate is higher and charge collection efficiency is lower for thick TiO_2 layer, thereby decreases the photovoltaic performance. The electron travelling distance is increased as the TiO_2 film thickness increase thus increased the recombination rate. The high electron loss rate results in lower short circuit current density, therefore reduces the cell performance.

As was in earlier discussion, double-layer A4 sample with small TiO_2 nanoparticles has higher dye loading and is expected to yield higher conversion efficiency than sample A4 + B4 but the result shows otherwise. This is due to the haze effect of paste B4 where higher haze contributes to higher diffused transmittance (Chiba et al., 2006). The haze effect is beneficial in improving the short circuit current density, J_{sc} and the solar cell conversion efficiency. Sample A4 + B4 obtained short circuit current density, J_{sc} of 10.03 mA/cm^2, slightly higher than double-layer A4 sample which is 9.86 mA/cm^2. This complied with Chiba et al. study that the short circuit current density, J_{sc} was improved when employing TiO_2 electrodes with haze degree and greater haze degree lead to higher short circuit current density, J_{sc}.

4.3 Effects of Gold Nanoparticles on DSSC Performance

The application of noble metal such as gold to enhance the power conversion efficiency of dye-sensitized solar cell is well recognized. The addition of Au nanoparticles to nanocrystalline TiO_2 layer facilitates the light absorption and photocurrent generation of the DSSC.

In order to simplify the fabrication process, the TiO_2-Au nanocomposite powder was synthesised by adding chloroauric acid during TiO_2 powder fabrication. The TiO_2 nanoparticles powder with the optimum performance in each series (series A, series B and series C) were selected for further study with the addition of gold nanoparticles. Table 4.6 lists the types of titanium oxide-gold nanocomposite layer (series D).

Table 4.6: Types of TiO_2-Au Nanocomposite Layer (Series D)

Sample	Types of TiO_2-Au Layer
A4 + $HAuCl_4$ → D1	TiO_2-Au active layer
B4 + $HAuCl_4$ → D2	TiO_2-Au active layer
C2 + $HAuCl_4$ → D3	TiO_2-Au scattering layer

4.3.1 Characterisation of TiO_2-Au Powder

4.3.1.1 X-ray Diffraction (XRD) Analysis

Figure 4.27 shows the XRD patterns for TiO_2-Au nanocomposite powders. The structural refinement and lattice parameter were determined by *Chekcell* program.

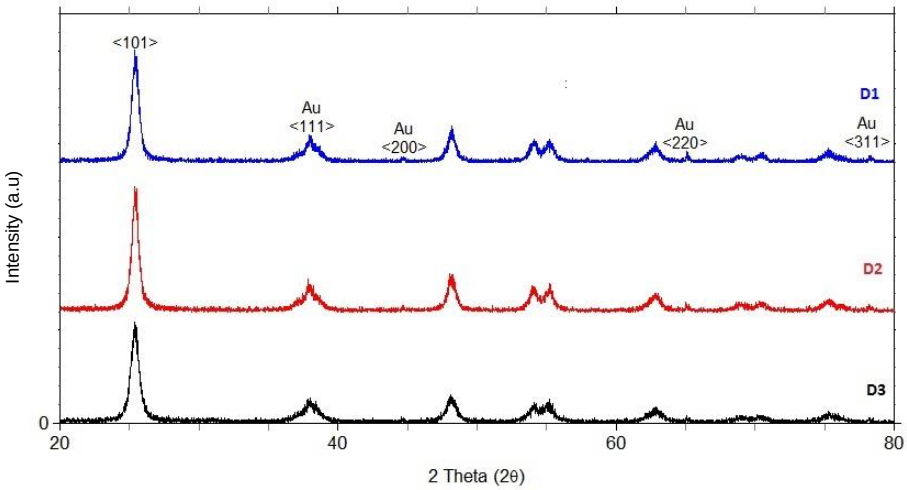

Figure 4.27: XRD Patterns of TiO_2-Au Nanocomposite Powders (Series D)

The XRD patterns shown in Figure 4.27 reports that the highest intensity signal falls around 25.3 <101> demonstrates that all the powders are anatase titania with tiny peaks at 38.4 <111>, 44.6 <200>, 65.1 <220> and 78.2 <311> (JCPDS-04-0784) confirms the presence of metallic gold in TiO_2-Au nanocomposite powders.

4.3.1.2 FE-SEM Analysis of TiO_2-Au Powders

4.3.1.2.1 Microstructure of TiO_2-Au Powder

The photovoltaic performance of TiO_2-Au DSSC is influenced by the microstructure of TiO_2-Au powder. The particle size distribution was analysed by *Image J* software and the histogram of particle size distribution together with Gaussian profile was plotted.

The SEM micrographs of TiO_2-Au nanocomposite powders show similar trend as that of TiO_2 powders. All the TiO_2-Au powders appeared as homogeneous spherical shape which possess effective surface area for dye absorption. The microstructure and particle size distribution of sample D1 are shown in Figure 4.28 and Figure 4.29. The microstructure and particle size distribution of sample D2 and sample D3 are shown in Appendix C.

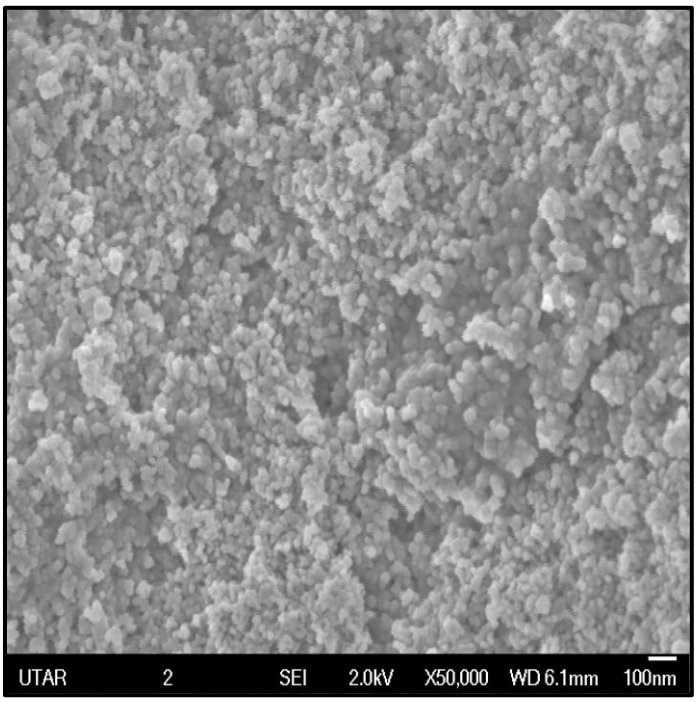

Figure 4.28: SEM Micrograph of Sample D1 TiO_2-Au Powder

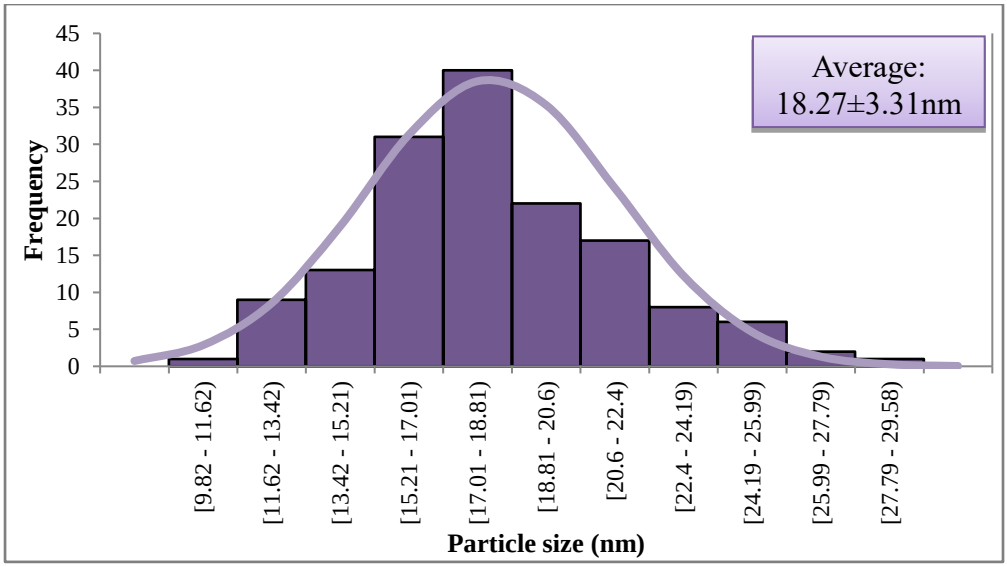

Figure 4.29: Histogram of Particle Size Distribution for Sample D1

4.3.1.2.2 Cross-Sectional Analysis of TiO_2-Au Film

The thickness of TiO_2-Au nanocomposite film has strong influences on the dye loading ability. Thicker film results in higher dye loading thereby improving the conversion efficiency of the DSSC. The film thickness was examined by scanning electron microscopy.

Paste D1 is an anatase active TiO_2-Au nanocomposite paste aims to facilitate dye absorption. This small particle size with high surface area is capable of supporting more dye molecules. Figure 4.30 illustrated that the double-layer D1 sample film thickness is 9.71μm.

The intention of paste D2 is to provide TiO_2-Au layer that possesses some haze effect with satisfactory dye absorption level. Figure 4.31 demonstrates that the TiO_2-Au film thickness for double-layer D2 sample is 12.8 μm.

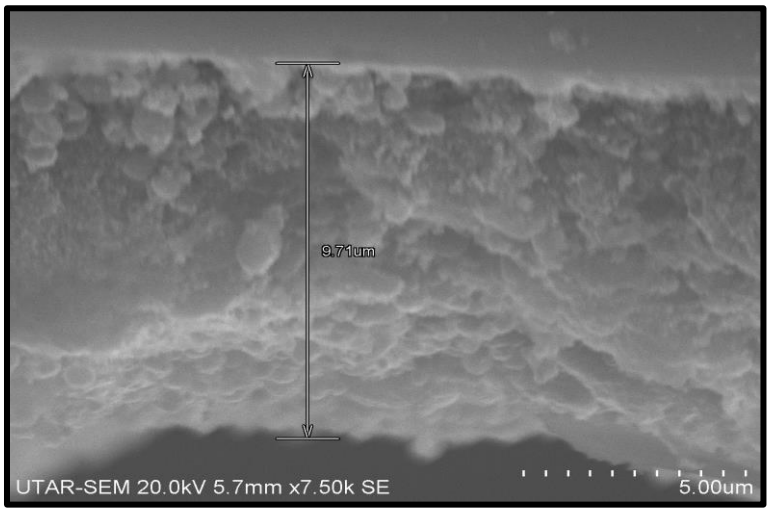

Figure 4.30: Cross-sectional Image of Double-layer D1 Sample

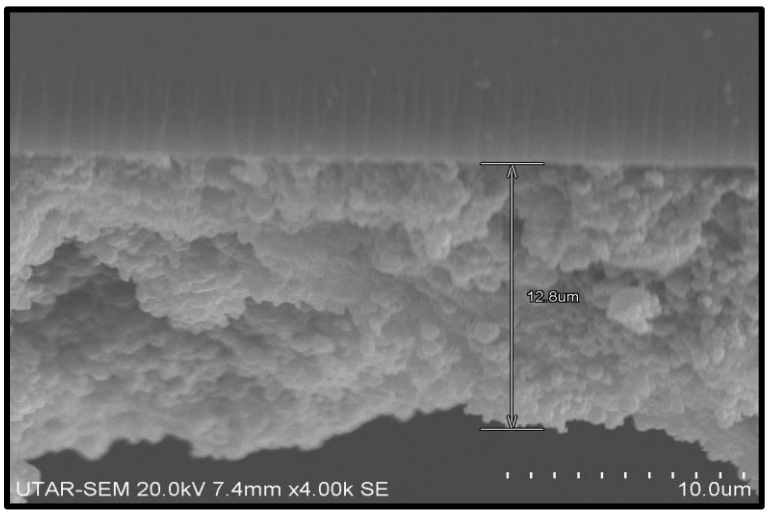

Figure 4.31: Cross-sectional Image of Double-layer D2 Sample

The purpose of paste D3 is to reduce the light loss by imposing light scattering effect. The film thickness for double-layer D3 sample is presented in Figure 4.32 displays that the TiO_2-Au layer thickness is 10.4 μm.

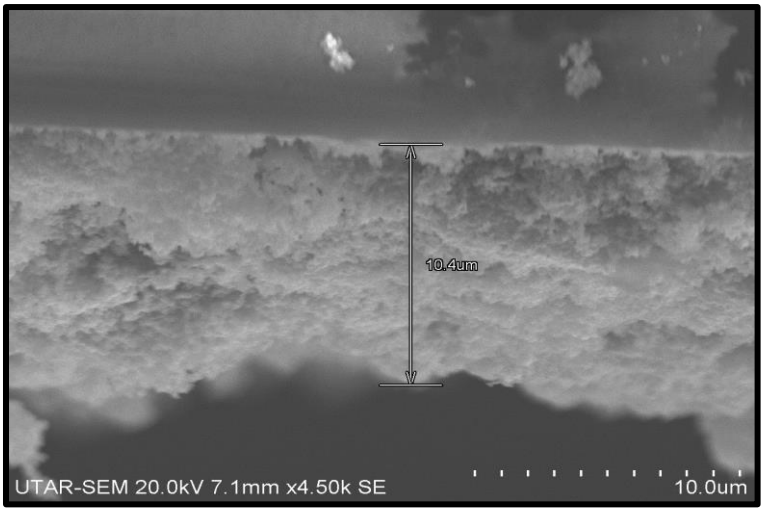

Figure 4.32: Cross-sectional Image of Double-layer D3 Sample

The cross-sectional images for dual-layer photoanode with two types of paste are shown in Figure 4.33 and Figure 4.34. sample D1 + D2 and sample D1 + D3 were produced by applying paste D1 as first layer then paste D2 or paste D3 as second layer. The total TiO_2-Au film thickness for sample D1 + D2 is 11.5 μm while sample D1 + D3 is 11.5 μm.

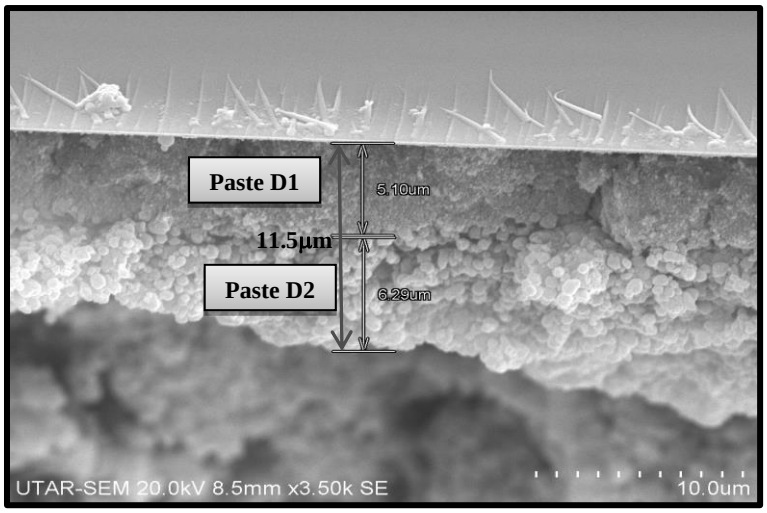

Figure 4.33: Cross-sectional Image of Sample D1 + D2

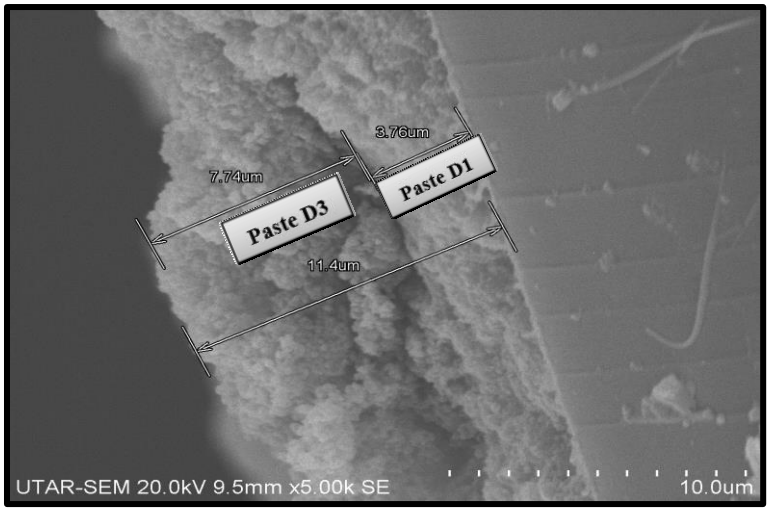

Figure 4.34: Cross-sectional Image of Sample D1 + D3

The total TiO_2-Au nanocomposite layer thickness for triple layer sample (sample D1 + D2 + D3) is 19.84 μm. The triple layer photoanode was made by deposited paste D1 as first layer, followed by paste D2 as second layer and paste D3 as third layer. The thickness for each TiO_2-Au layer are shown in Figure 4.35.

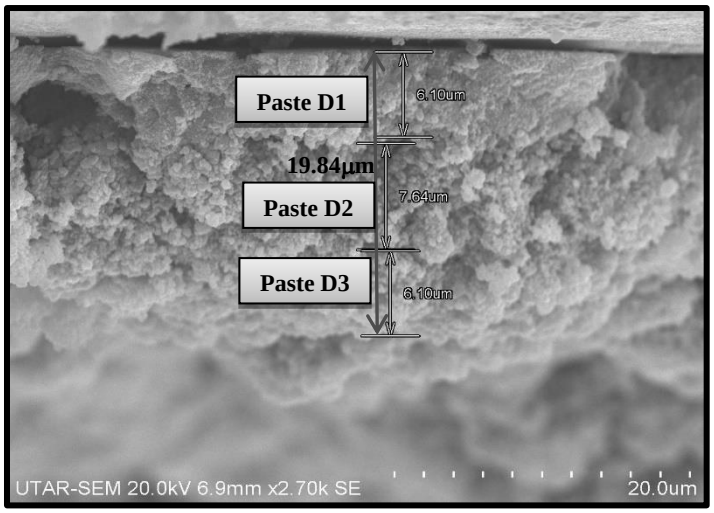

Figure 4.35: Cross-sectional Image of Sample D1 + D3

The sectional-images show that the film thickness for TiO_2-Au layer is lower than that of TiO_2 layer. According to Atwater and Polman (2010), plasmonic structure can reduce the physical thickness of the semiconductor

oxide layer while keeping their optical thickness constant. This can be achieved by three methods. In the first method, Au nanoparticles can be used as subwavelength scattering elements to couple and trap freely propagating plane waves from the Sun into TiO_2 layer, by folding the light into TiO_2 layer. For second method, Au nanoparticles can be used as subwavelength antennas in which the plasmonic near -field is coupled to the TiO_2, increasing its effective absorption cross-section. The third method uses a corrugated Au film on the back surface of TiO_2 layer can couple sunlight into surface plasmon polariton modes supported at the Au/TiO_2 interface as well as guided modes in the TiO_2 slab, whereupon the light is converted to photocarriers in the TiO_2.

The concentration and distribution of gold, Au nanoparticles greatly influence the enhancement of photovoltaic performance. The EDX analysis shows the gold, Au nanoparticles are evenly distributed and there is ~ 0.83 wt% of gold in each sample. The presence of carbon element was attributed to the carbon tape used to secure the sample to the holder and serves as electron collector. The EDX analysis and element mapping for sample D1 are shown in Figure 4.36. (refer to Appendix D for sample D2 and sample D3)

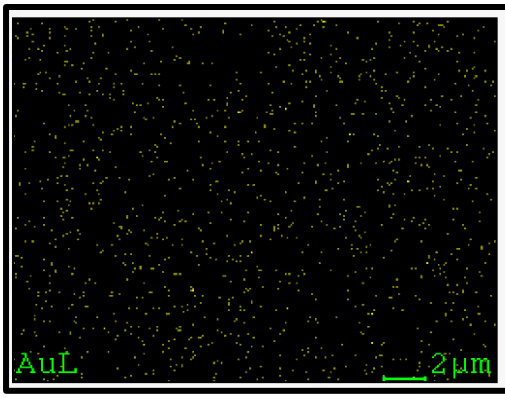

Element	Weight (%)
C K	0.62
O K	9.56
Ti K	88.99
Au L	0.83
Total	100.00

Figure 4.36: EDX Analysis and Element Mapping for Gold Nanoparticles of Sample D1

4.3.1.3 Current-Voltage Characterisation of TiO_2-Au DSSC

The performances of titanium oxide-gold nanocomposite dye-sensitized solar cell was analysed by I-V tester. The characteristics of the titanium oxide-gold, TiO_2-Au nanocomposite have synergy effect on the solar cell parameters.

The current density-voltage curves shown in Figure 4.37 indicate that TiO_2-Au film with small particle size (paste D1) produces higher short circuit current density, J_{sc} due to higher dye absorption. This agreed with the appearances of photo-electrode after dye soaking process. Figure 4.38 displays that photo-electrode with paste D1 presents a typical red wine colour while photo-electrode with paste D3 is light pink indicate that the particle size of the TiO_2-Au layer is affecting the dye uptake. Small particles possess higher surface area for greater dye loading, therefore achieve higher light harvesting efficiency and generate greater photocurrent density.

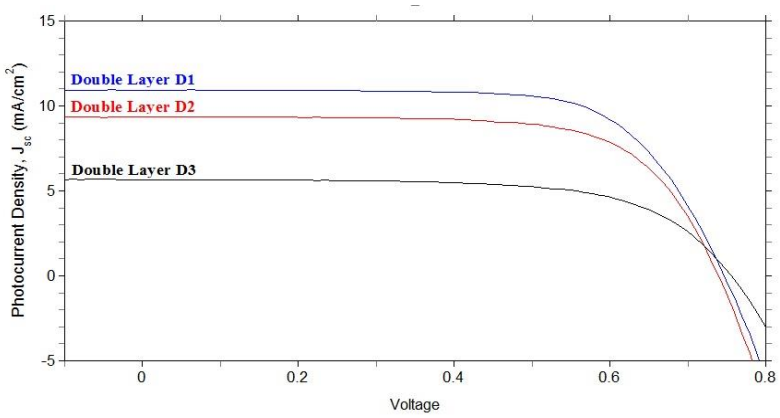

Figure 4.37: Current Density-Voltage Curves of TiO_2-Au Nanocomposite DSSC for Sample D1, D2 and D3

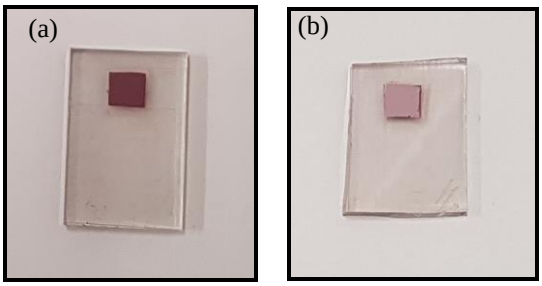

Figure 4.38: Images of TiO_2-Au Nanocomposite Photo-electrode for (a) Paste D1 (b) Paste D3

Figure 4.39 shows the current density-voltage curve for dual-layer TiO_2-Au nanocomposite DSSC. The dual-layer TiO_2-Au DSSC was fabricated by applying paste D1 as first layer followed by paste D2 or paste D3 as second layer. Paste D1 acts as an active layer that maximises dye absorption, paste D2 aims to provide some haze effect with a satisfactory amount of dye loading and paste C3 intends to facilitate light scattering effect. The results demonstrate that applying two different types of TiO_2-Au layer improve the photocurrent density and power conversion efficiency of the solar cell. The J-V graph demonstrates that photocurrent density for sample D1 + D2 is higher than double-layer D1 sample and sample D1 + D3 is higher than double-layer D3 sample. The TiO_2-Au DSSC with combination of two TiO_2-Au layers possess better dye loading and light scattering effect leads to better performance.

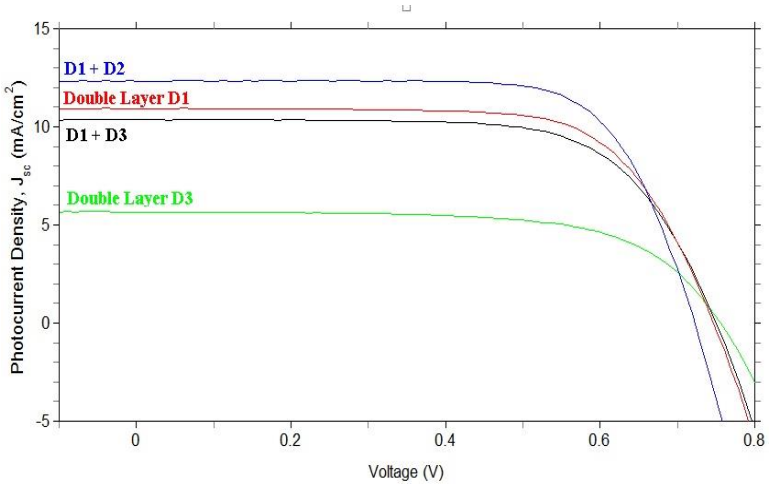

Figure 4.39: Current Density-Voltage Curves of TiO_2-Au Nanocomposite DSSC for Sample D1 + D2, D1 + D3, Double-layer D1 and Double-layer D3

Table 4.7 shows that sample D1+D2 has the best performance with the film thickness of 11.5 μm which falls within the optimum thickness (12 μm – 14 μm) (Ito et al., 2008). Sample D1+D2 records a power conversion efficiency of 6.40% and short circuit current density, J_{sc} of 12.33 mA/cm^2.

Table 4.7: TiO_2-Au Nanocomposite Film Thickness and Photovoltaic Characteristic of DSSC

Sample	Thickness (μm)	J_{sc} (mA/cm^2)	V_{oc} (V)	Fill Factor *FF*	η (%)
Double-layer D1	9.71	10.92	0.75	69.95	5.64
Double-layer D2	12.8	9.35	0.74	70.83	4.75
Double-layer D3	10.4	5.66	0.70	70.77	2.79
D1+D2	**11.5**	**12.33**	**0.72**	**71.85**	**6.40**
D1+D3	11.4	10.37	0.75	67.75	5.27
D1+D2+D3	19.84	11.2	0.68	67.96	5.18

As discussed previously, thicker TO_2-Au film leads to higher dye absorption thus improving the DSSC performance. However, Table 4.7 shows that the conversion efficiency for double-layer D2 sample is lower than double-layer D1 sample even though it has the thickest TiO_2-Au film among the entire double-layer samples. The low efficiency is caused by the low dye absorption as large particle has lower surface area for dye uptake. Besides, the performance for triple-layer TiO_2-Au DSSC (sample D1 + D2 +D3) is limited due to cracking of thick film. The cracked film causes higher electron transport resistance hence reduced the power conversion efficiency. Moreover, the electron travelling distance is increased as the film thickness increase, consequently increased the recombination rate and reduced the charge collection efficiency (Chander et al., 2014).

The J-V curves shown in Figure 4.40 and Appendix E indicate that adding gold nanoparticle improves the short circuit current density and fill factor of the solar cell consequently enhances the power conversion efficiency of the DSSC. The primary role of gold in DSSC is to accept electrons from the photo-excited TiO_2, thereby improves the photocurrent density of the DSSC.

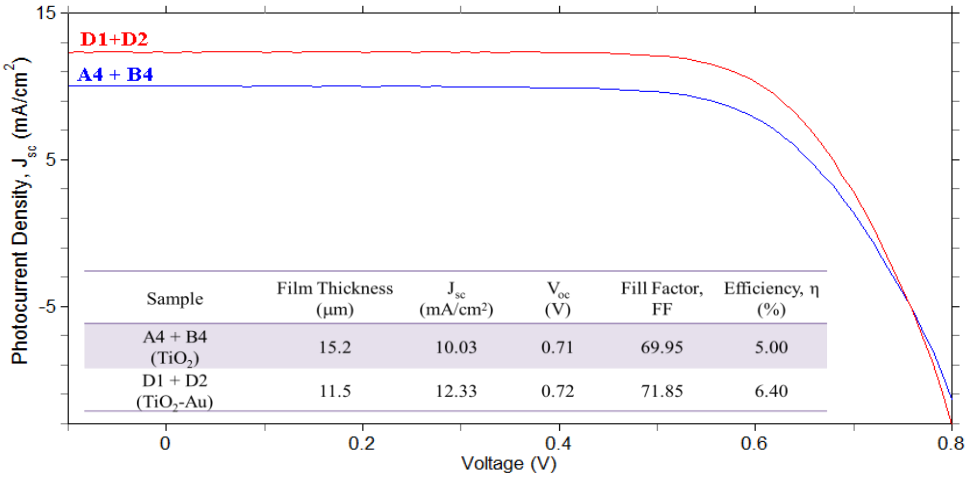

Sample	Film Thickness (μm)	J_{sc} (mA/cm²)	V_{oc} (V)	Fill Factor, FF	Efficiency, η (%)
A4 + B4 (TiO_2)	15.2	10.03	0.71	69.95	5.00
D1 + D2 (TiO_2-Au)	11.5	12.33	0.72	71.85	6.40

Figure 4.40: Current Density-Voltage Curves for Sample D1 + D2 and Sample A4 + B4

The improvement of photocurrent generation on titanium oxide-gold nanocomposite dye-sensitized solar cell can be attributed to the plasmon induce charge transfer from Au nanoparticles to TiO_2 nanoparticles (Du et al., 2009). The fill factor, *FF* and open circuit voltage, V_{oc} of TiO_2-Au film is higher than TiO_2 nanoparticles film are associated with decrease electron-hole recombination (Law et al., 2006). The Au nanoparticles in TiO_2-Au film acts as Schottky barrier to reduce the charge recombination (Chou et al., 2009).

Besides, the performance of TiO_2-Au nanocomposite DSSCs are better than TiO_2 nanoparticles DSSCs can be correlated to the reduction of charge transfer resistance at TiO_2-dye-electrolyte interface (Muduli et al., 2012). The interfacial charge transfer process and stability of interfaces have a big impact on the ability of TiO_2-Au nanocomposite to sustain charge separation.

Generally, the main purpose of adding gold nanoparticles are to improve the light harvesting efficiency of the DSSC. This is obtained through three mechanisms. The first mechanism is through the excitation of localised surface plasmon resonances of Au nanoparticles. It utilises the benefit of strong local field enhancement around Au nanoparticles to increase the absorption in surrounding TiO_2 layer. The strong energy surrounding TiO_2 particles separates the electron-hole thus lowers the charge carrier recombination. This works

exclusively with small particles (paste D1) in the range of 5 nm to 20 nm (Atwater and Polman, 2010). Figure 4.41 illustrates the light concentration mechanism of gold nanoparticles.

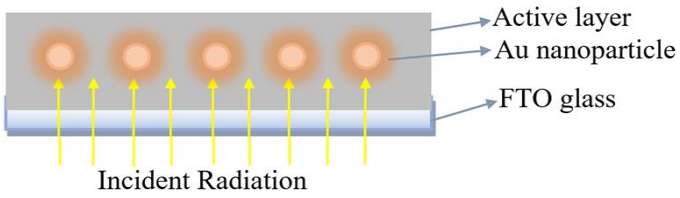

Figure 4.41: Light Concentration by Gold Nanoparticles

The second mechanism is through the light trapping geometry by Au nanoparticles. The light is converted into surface plasmon polarity which is the magnetic waves that travel along the surface of gold nanoparticles. The SPP excitation can efficiently trap and guide the light in the oxide film (Atwater and Polman, 2010). Figure 4.42 illustrates the light trapping mechanism of gold nanoparticles.

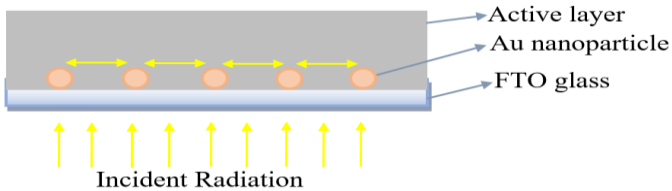

Figure 4.42: Light Trapping by Gold Nanoparticles

The third mechanism is through the scattering effect of Au nanoparticles. It works particularly with large particle (paste D3). The Au nanoparticles act as subwavelength scattering element to couple and trap freely propagating incident light in the oxide layer. As a result, it reduces loss of radiation as well as lowering the oxide layer thickness (Atwater and Polman, 2010). Figure 4.43 illustrates the light scattering effect of gold nanoparticles.

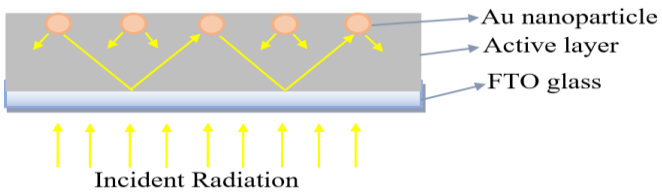

Figure 4.43: Light Scattering by Gold Nanoparticles

Thicker TiO_2 film supposedly yields higher conversion efficiency as the amount of the dye absorbed by the film is increased. However, the results obtained in this study show otherwise; the conversion efficiency of TiO_2-Au DSSC samples are higher compared to TiO_2 DSSC even though the TiO_2-Au film thickness is lower than those TiO_2 film (Figure 4.40 and Appendix E). The improvement in conversion performance of TiO_2-Au DSSC further implies that the gold nanoparticles play an important role in improving the conversion efficiency.

Moreover, UV-visible spectroscopy results (refer to Appendix A) show that the absorption peak in the visible region for TiO_2-Au samples was slightly shifted toward longer wavelength which corresponded well with the surface plasmon resonance absorption band of gold nanoparticles. This indicated the presence of metallic gold nanoparticles as plasmon nanoparticles in enhancing the DSSC performance.

In addition, reducing the film thickness by plamonic light trapping, reduces the dark current density, I_{dark} subsequently increases the open circuit voltage, V_{oc} of the DSSC. According to Equation 4.1, the performance of TiO_2-Au DSSC is increased in logarithmic proportion to the reduction in film thickness and is limited by the charge recombination.

As film thickness decreased, the electron diffusion length is reduced thus lowering the electron recombination rate as well. Therefore, lowering the film thickness is not only reducing the material cost but also enhancing the electrical properties of the solar cell.

$$V_{oc} = \frac{k_B T}{q} \ln\left(\frac{I_{photo}}{I_{dark}} + 1\right) \quad (4.1)$$

where

V_{oc} = open circuit voltage, V

k_B = Boltzmann constant

T = temperature

q = charge

I_{photo} = photocurrent

I_{dark} = dark current

The improvement of overall conversion efficiency of gold-incorporated DSSC was demonstrated by Muduli et al. (2012), Chen et al. (2015) and Choi et al. (2012) studies. Muduli et al. synthesised TiO_2-Au powder through hydrothermal process by mixing $HAuCl_4$ with TTIP, urea, ethanol and deionized water. The study reported that the TiO_2-Au DSSC power conversion efficiency was improved by 20% compared to the TiO_2 DSSC. Chen et al. fabricated gold nanoparticles inlaid mesoporous titania nanoparticles, Au@MTN using sol-gel reaction by mixing $HAuCl_4$ with TTIP, sodium borohydride, $NaBH_4$ and ethanol. The preparation steps for TiO_2-Au DSSC in both studies are similar to this research project in which gold nanoparticles were added during the TiO_2 powder fabrication. The power conversion efficiency of TiO_2-Au DSSC in this study achieved better performance compared to both studies. This might be due to the inclusion of multilayers TiO_2-Au compared to single layer used by both studies. Multilayers TiO_2-Au have effective dye absorption and light harvesting, therefore higher photocurrent density and photovoltaic performance.

Nevertheless, it is worth highlighting that Choi et al. (2012) achieves better photovoltaic efficiency (~10%) than the TiO_2-Au DSSC fabricated in this research project. The method used to prepare TiO_2-Au DSSC by Choi et. al. was coupling the semiconductor nanostructure (TiO_2 and SiO_2) with gold

nanoparticles in a core-shell geometry. The gold core-oxide shell structures were prepared separately and then added to commercial TiO_2 paste for TiO_2-Au DSSC fabrication. This fabrication method involves more chemicals and synthesis steps compared to the method used in this research project. The conversion efficiency of TiO_2-Au DSSC is summarised in Table 4.8.

Table 4.8: List of TiO_2-Au DSSC Performance

Sample	Au (wt%)	J_{sc} (mA/cm^2)	V_{oc} (V)	*FF*	η (%)
TiO_2 + Au@SiO_2 (Choi et al.)	0.7	20.31	0.73	69.1	10.21
Au@MTNs (Chen et al.)	0.8	12.53	0.67	67.0	5.62
D1 + D2	0.8	12.33	0.72	71.9	6.40
TiO_2-Au (Muduli et al.)	1.65	13.2	0.74	61.0	6.00

Even though the preparation methods used in the studies were different, but all the studies confirmed that the improvement of DSSC performance is correlated to the plasmonic effect of gold nanoparticles in the TiO_2 layer. The power conversion efficiency of TiO_2-Au DSSC (sample D1 + D2) in this study is improved by ~ 28% compared to TiO_2 DSSC (sample A4 + B4).

CHAPTER 5

CONCLUSION AND RECOMMENDATIONS

5.1 Conclusion

DSSC is the third generation solar cell that promises low manufacturing cost, non-toxic and abundant materials and simple fabrication method. A basic DSSC consists of a photoanode, counter electrode, sensitizer and electrolyte. The characteristic of oxide layer greatly influences the solar cell performance as the crystallite size and film thickness affects the dye loading, pore volume and transport of redox couple. Therefore, the performance of DSSC was examined by I-V tester, XRD, FE-SEM and UV-Visible spectrophotometer.

The goal of this study is to analyse the effect of gold nanoparticles on the conversion efficiency of DSSC with optimized TiO_2 layers. Thus, three series of TiO_2 powders with average particle sizes of 15 nm, 30 nm and 150 nm were fabricated and then converted to TiO_2 films by doctor blade technique for DSSC fabrication. The DSSC with the optimum performance within each series were chosen for further studies with the addition of gold nanoparticles.

In summary, TiO_2 nanoparticles powder and TiO_2-Au nanocomposite powders with high proportion of anatase phase were successfully synthesised and were converted to oxide pastes. Small nanoparticles paste serves as an active transparent layer that promotes high dye loading while medium particles paste formulate an active opaque layer that possesses some haze effect with

sufficient dye uptake and larger particles paste produces a white scattering layer that enhances light scattering effect.

The results showed that the particle size and film thickness strongly affect the amount of dye absorbed. High dye absorption is one of the factors leading to high solar cell performance. As the oxide film thickness increased, the dye loading increased, consequently improving the photocurrent generation and the cell efficiency. However, thick oxide layer diminishes the solar cell performance due to higher charge transport resistance caused by cracking film. Besides, small particle has higher adherence of dye molecules then large particle.

The conversion efficiency,η of DSSC is improved by ~ 28% and the short circuit current density, J_{sc} is ~ 23% higher compared to the reference DSSC (without gold). This indicates that the gold nanoparticles are able to improve the performance of DSSC by increasing the photocurrent generation due to the improvement of incident light harvesting efficiency and the improvement of open circuit voltage, V_{oc} owing to lower film thickness, thereby increased the fill factor, *FF* of the cell. The ideal combination is found to be of 15 nm + 30 nm with highest conversion efficiency,η of 6.40%.

5.2 Recommendations and Future Improvements

The optimization of dye-sensitized solar cell in this study considered few parameters and there are some other important parameters that require further research.

The materials and fabrication method of titanium oxide powder could be further study. The synthesis temperature and condition greatly influence the TiO_2 powder morphology and properties. Additional measurement methods on titania properties such as surface roughness, effective surface area and porosity

of oxide layer have to be introduced as SEM analysis just provide a brief perception on these parameters.

Currently, the deposition of titania pastes and platinum layer was performed using Doctor Blade method. This method results in low consistency as the applied force may vary from one photo-electrode to another. Screen printing or automated machine system such as spin coating may be implemented to have better control and higher consistency of the film thickness.

Next, the concentration and shape of noble metal such as Ag and Au in TiO_2 film affects the light conversion efficiency of the DSSC. Thus, the effect of types, concentration and shape of noble metal could be included in future study as these parameters were fixed for this study.

Other minor improvements such as adding anti-reflective coating and surface treatment, utilising flexible and low sheet resistance substrate should be considered.

REFERENCES

Abdel-Azim, S.M., Aboul-Gheit, A.K., Ahmed, S.M., El-Desouki, D.S. and Abdel-Mottaleb, M.S.A., 2014. Preparation and application of mesoporous nanotitania photocatalysts using different templates and ph media. *International Journal of Photoenergy*, 2014.

Al-Azawi, M.A., Bidin, N., Bououdina, M. and Mohammad, S.M., 2016. Preparation of gold and gold-silver alloy nanoparticles for enhancement of plasmonic dye-sensitized solar cells performance. *Solar Energy*, 126(2016), pp.93–104.

Atwater, H.A. and Polman, A., 2010. Plasmonics for improved photovoltaic devices. *Nature Materials*, 9(3), pp.205–213.

Banerjee, S., Kumar Ojha, Y., Vikas, K. and Kumar, A., 2016. High Efficient CIGS based Thin Film Solar Cell Performance Optimization using PC1D. *International Research Journal of Engineering and Technology*, pp.2395–56.

Barbe, C.J., Arendse, F., Comte, P., Jirousek, M., Lenzmann, F., Shklover, V. and Gratzel, M., 1997. Nanocrystalline titanium oxide electrodes for photovoltaic applications. *Journal of the Americn Ceramic Society*, 80(12), pp.3157–3171.

Benk, G., Skrman, B., Wallenberg, R., Hagfeldt, A., Sundstrm, V. and Yartsev, A.P., 2003. Particle Size and Crystallinity Dependent Electron Injection in Fluorescein 27-Sensitized TiO_2 Films. *The Journal of Physical Chemistry B*, 107(6), pp.1370–1375.

Bi-Tao, X., Bao-Xue, Z., Jing, B., Qing, Z., Yan-Biao, L., Wei-Min, C. and Jun, C., 2008. Light scattering of nanocrystalline TiO_2 film used in dye-sensitized solar cells. *Chinese Physics B*, 17(10), pp.3713–3719.

Bischoff, B.L. and Anderson, M.A., 1995. Peptization Process in the Sol-Gel Preparation of Porous Anatase (TiO_2). *Chemistry of Materials*, 7(10), pp.1772–1778.

Byrappa, K. and Yoshimura, M., 2001. *Handbook of Hydrothermal Technology, A Technology for Crystal Growth and Materials Processing*. Norwich: Noyes Publication / William Andrew Publishing. LLC.

Cao, F., Oskam, G., Meyer, G.J. and Searson, P.C., 1996. Electron Transport in Porous Nanocrystalline TiO_2 Photoelectrochemical Cells. *The Journal of Physical Chemistry*, 100(42), pp.17021–17027.

Chae, S.Y., Park, M.K., Lee, S.K., Kim, T.Y., Kim, S.K. and Lee, W.I., 2003. Preparation of size-controlled TiO_2 nanoparticles and derivation of optically transparent photocatalytic films. *Chemistry of Materials*, 15(17), pp.3326–3331.

Chander, N., Khan, A.F., Thouti, E., Sardana, S.K., Chandrasekhar, P.S., Dutta, V. and Komarala, V.K., 2014. Size and concentration effects of gold nanoparticles on optical and electrical properties of plasmonic dye sensitized solar cells. *Solar Energy*, 109(2014), pp.11–23.

Chang, B.Y.S., Huang, N.M., An'amt, M.N., Marlinda, A.R., Norazriena, Y., Muhamad, M.R., Harrison, I., Lim, H.N. and Chia, C.H., 2012. Facile hydrothermal preparation of titanium dioxide decorated reduced graphene oxide nanocomposite. *International Journal of Nanomedicine*, 7, pp.3379–3387.

Chen, H.W., Hong, C.Y., Kung, C.W., Mou, C.Y., Wu, K.C.W. and Ho, K.C., 2015. A gold surface plasmon enhanced mesoporous titanium dioxide photoelectrode for the plastic-based flexible dye-sensitized solar cells. *Journal of Power Sources*, 288, pp.221–228.

Chen, X. and Mao, S.S., 2007. Titanium dioxide nanomaterials: Synthesis, properties, modifications and applications. *Chemical Reviews*, 107, pp. 2891–2859.

Chiba, Y., Islam, A., Watanabe, Y., Komiya, R., Koide, N. and Han, L., 2006. Dye-sensitized solar cells with conversion efficiency of 11.1%. *Japanese Journal of Applied Physics*, 45(25), pp.638–640.

Choi, H., Chen, W.T. and Kamat, P. V., 2012. Know thy nano neighbor. Plasmonic versus electron charging effects of metal nanoparticles in dye-sensitized solar cells. *ACS Nano*, 6(5), pp.4418–4427.

Chou, C.-S., Yang, R.-Y., Yeh, C.-K. and Lin, Y.-J., 2009. Preparation of TiO_2/Nano-metal composite particles and their applications in dye-sensitized solar cells. *Powder Technology*, 194(2009), pp.95–105.

Cleveland, C.J. and Morris, C., 2014. *Handbook of Energy. Volume II_ Chronologies, Top Ten Lists, and Word Clouds*. Oxford: Elsevier Science.

Dang, X., Qi, J., Klug, M.T., Chen, P.-Y., Yun, D.S., Fang, N.X., Hammond, P.T. and Belcher, A.M., 2013. Tunable Localized Surface Plasmon-Enabled Broadband Light-Harvesting Enhancement for High-Efficiency Panchromatic Dye-Sensitized Solar Cells. *Nano Letters*, 13(2), pp.637–642.

Ding, X.-Z., Qi, Z.-Z. and He, Y.-Z., 1995. Effect of hydrolysis water on the preparation of nano-crystalline titania powders via a sol-gel process. *Journal of Materials Science Letters*, 14(1), pp.21–22.

Dloczik, L., Ileperuma, O., Lauermann, I., Peter, L.M., Ponomarev, E.A., Redmond, G., Shaw, N.J. and Uhlendorf, I., 1997. Dynamic Response of Dye-Sensitized Nanocrystalline Solar Cells: Characterization by Intensity-Modulated Photocurrent Spectroscopy. *The Journal of Physical Chemistry B*, 101(49), pp.10281–10289.

Du, L., Furube, A., Yamamoto, K., Hara, K., Katoh, R. and Tachiya, M., 2009. Plasmon-Induced Charge Separation and Recombination Dynamics in Gold−TiO_2 Nanoparticle Systems: Dependence on TiO_2 Particle Size. *The Journal of Physical Chemistry C*, 113(16), pp.6454–6462.

Ferekides, C.S., Balasubramanian, U., Mamazza, R., Viswanathan, V., Zhao, H. and Morel, D.L., 2004. CdTe thin film solar cells: Device and technology issues. *Solar Energy*, 77(6), pp.823–830.

Gong, J., Sumathy, K., Qiao, Q. and Zhou, Z., 2017. Review on dye-sensitized solar cells (DSSCs): Advanced techniques and research trends. *Renewable and Sustainable Energy Reviews*, 68 (2017), pp.234–246.

Grätzel, M., 2005. Solar Energy Conversion by Dye-Sensitized Photovoltaic Cells. *Inorganic Chemistry*, 44(20), pp.6841–6851.

Green, M.A., Hishikawa, Y., Warta, W., Dunlop, E.D., Levi, D.H., Hohl-Ebinger, J. and Ho-Baillie, A.W.H., 2017. Solar cell efficiency tables (version 50). *Progress in Photovoltaics: Research and Applications*, 25(7), pp.668–676.

Hagfeldt, A. and Graetzel, M., 1995. Light-Induced Redox Reactions in Nanocrystalline Systems. *Chemical Reviews*, 95(1), pp.49–68.

Hersch, P., Office, S.E.R.I.T.I. and Zweibel, K., 1982. *Basic Photovoltaic Principles and Methods*. Colorado: Technical Information Office Solare Energy Research Institute.

Hore, S., Vetter, C., Kern, R., Smit, H. and Hinsch, A., 2006. Influence of scattering layers on efficiency of dye-sensitized solar cells. *Solar Energy Materials and Solar Cells*, 90(9), pp.1176–1188.

Huang, G.Y., Xu, S.M., Li, L.Y. and Wang, X.J., 2014. Effect of surfactants on dispersion property and morphology of nano-sized nickel powders. *Transactions of Nonferrous Metals Society of China*, 24(2014), pp.3739–3746.

Hwang, K., Jung, S., Park, D., Yoo, S. and Lee, J., 2010. Heterogeneous ruthenium dye adsorption on nano-structured TiO_2 films for dye-sensitized solar cells. *Current Applied Physics*, 10(2), pp.S184–S187.

Ito, S., Liska, P., Comte, P., Charvet, R., Péchy, P., Bach, U., Schmidt-Mende, L., Zakeeruddin, S.M., Kay, A., Nazeeruddin, M.K. and Grätzel, M., 2005. Control of dark current in photoelectrochemical ($TiO_2/I^-–I_3^-$) and dye-sensitized solar cells. *Chemical Communications*, 87(34), pp.4351–4353.

Ito, S., Chen, P., Comte, P., Nazeeruddin, M.K., Liska, P., Péchy, P. and Grätzel, M., 2007. Fabrication of screen-printing pastes from TiO2 powders for dye-sensitised solar cells. Progress in Photovoltaics: Research and Applications, 15(7), pp.603–612.

Ito, S., Murakami, T.N., Comte, P., Liska, P., Grätzel, C., Nazeeruddin, M.K. and Grätzel, M., 2008. Fabrication of thin film dye sensitized solar cells with solar to electric power conversion efficiency over 10%. *Thin Solid Films*, 516(14), pp.4613–4619.

Ito Takayuki; Wada, Yuji; Yanagida, Shozo, S.K., 2003. Facile fabrication of mesoporous TiO_2 electrodes for dye solar cells: chemical modification and repetitive coating. *Solar Energy Materials and Solar Cells*, 76(1), pp.3–13.

Jeng, M.-J., Wung, Y.-L., Chang, L.-B. and Chow, L., 2013a. Dye-Sensitized Solar Cells with Anatase TiO_2 Nanorods Prepared by Hydrothermal Method. *International Journal of Photoenergy*, 2013, pp.1–8.

Jeng, M.-J., Wung, Y.-L., Chang, L.-B. and Chow, L., 2013b. Particle Size Effects of TiO_2 Layers on the Solar Efficiency of Dye-Sensitized Solar Cells. *International Journal of Photoenergy*, 2013, pp.1–9.

Jun, Y.W., Casula, M.F., Sim, J.H., Kim, S.Y., Cheon, J. and Alivisatos, A.P., 2003. Surfactant-Assisted Elimination of a High Energy Facet as a Means of Controlling the Shapes of TiO_2 Nanocrystals. *Journal of the American Chemical Society*, 125(51), pp.15981–15985.

Kajihara, K. and Yao, T., 2000. Macroporous Morphology of the Titania Films Prepared by a Sol-Gel Dip-Coating Method from the System Containing Poly(ethylene glycol). IV. General Principle of Morphology Formation and Effect of Heat Treatment. *Journal of Sol-Gel Science and Technology*, 17(2), pp.173–184.

Kang, S.H., Choi, S.-H., Kang, M.-S., Kim, J.-Y., Kim, H.-S., Hyeon, T. and Sung, Y.-E., 2008. Nanorod-Based Dye-Sensitized Solar Cells with Improved Charge Collection Efficiency. *Advanced Materials*, 20(1), pp.54–58.

Katoh, R., Fuke, N., Furube, A. and Koide, N., 2010. Effect of dye coverage on photo-induced electron injection efficiency in N719-sensitized nanocrystalline TiO_2 films. *Chemical Physics Letters*, 489(2010), pp.202–206.

Kawawaki, T., Takahashi, Y. and Tatsuma, T., 2013. Enhancement of Dye-Sensitized Photocurrents by Gold Nanoparticles: Effects of Plasmon Coupling. *The Journal of Physical Chemistry C*, 117(11), pp.5901–5907.

Kisserwan, H. and Ghaddar, T.H., 2010. Enhancement of photovoltaic performance of a novel dye, ‘T18’, with ketene thioacetal groups as electron donors for high efficiency dye-sensitized solar cells. *Inorganica Chimica Acta*, 363(11), pp.2409–2415.

Lai, W.H., Su, Y.H., Teoh, L.G. and Hon, M.H., 2008. Commercial and natural dyes as photosensitizers for a water-based dye-sensitized solar cell loaded with gold nanoparticles. *Journal of Photochemistry and Photobiology A: Chemistry*, 195(2008), pp.307–313.

Law, M., Greene, L.E., Radenovic, A., Kuykendall, T., Liphardt, J. and Yang, P., 2006. ZnO-Al_2O_3 and ZnO-TiO_2 core-shell nanowire dye-sensitized solar cells. *Journal of Physical Chemistry B*, 110(45), pp.22652–22663.

Lee, J.-K.K., Jeong, B.-H.H., Jang, S. il, Kim, Y.-G.G., Jang, Y.-W.W., Lee, S.-B. Bin and Kim, M.-R.R., 2009. Preparations of TiO_2 pastes and its application to light-scattering layer for dye-sensitized solar cells. *Journal of Industrial and Engineering Chemistry*, 15(5), pp.724–729.

Lee, J. and Yang, M., 2011. Progress in light harvesting and charge injection of dye-sensitized solar cells. *Materials Science and Engineering: B*, 176(15), pp.1142–1160.

Liao, D.L. and Liao, B.Q., 2007. Shape, size and photocatalytic activity control of TiO_2 nanoparticles with surfactants. *Journal of Photochemistry and Photobiology A: Chemistry*, 187(2007), pp.363–369.

Lin, S.J., Lee, K.C., Wu, J.L. and Wu, J.Y., 2012. Plasmon-enhanced photocurrent in dye-sensitized solar cells. *Solar Energy*, 86(9), pp.2600–2605.

Liu, Z.H., Su, X.J., Hou, G.L., Bi, S., Xiao, Z. and Jia, H.P., 2012. Enhanced performance for dye-sensitized solar cells based on spherical TiO_2 nanorod-aggregate light-scattering layer. *Journal of Power Sources*, 218(2012), pp.280–285.

Mahshid, S., Askari, M. and Ghamsari, M.S., 2007. Synthesis of TiO_2 nanoparticles by hydrolysis and peptization of titanium isopropoxide solution. *Journal of Materials Processing Technology*, 189(2007), pp.296–300.

Maldonado-Valdivia, A.I., Galindo, E.G., Ariza, M.J. and García-Salinas, M.J., 2013. Surfactant influence in the performance of titanium dioxide photoelectrodes for dye-sensitized solar cells. *Solar Energy*, 91, pp.263–272.

Mathew, S., Yella, A., Gao, P., Humphry-Baker, R., Curchod, B.F.E., Ashari-Astani, N., Tavernelli, I., Rothlisberger, U., Nazeeruddin, M.K. and Grätzel, M., 2014. Dye-sensitized solar cells with 13% efficiency achieved through the molecular engineering of porphyrin sensitizers. *Nature Chemistry*, 6(3), pp.242–247.

McEvoy, A.J., Castañer, L. and Markvart, T., 2013. *Solar cells : materials, manufacture and operation*. 2nd ed. Oxford: Academic Press.

Movla, H., 2014. Optimization of the CIGS based thin film solar cells: Numerical simulation and analysis. *Optik*, 125(1), pp.67–70.

Muduli, S., Game, O., Dhas, V., Vijayamohanan, K., Bogle, K.A., Valanoor, N. and Ogale, S.B., 2012. TiO_2-Au plasmonic nanocomposite for enhanced dye-sensitized solar cell (DSSC) performance. *Solar Energy*, 86(5), pp.1428–1434.

Nakade, S., Saito, Y., Kubo, W., Kitamura, T., Wada, Y. and Yanagida, S., 2003. Influence of TiO_2 Nanoparticle Size on Electron Diffusion and Recombination in Dye-Sensitized TiO_2 Solar Cells. *The Journal of Physical Chemistry B*, 107(33), pp.8607–8611.

Nakada, T., 2012. Invited Paper: CIGS-based thin film solar cells and modules: Unique material properties. *Electronic Materials Letters*, 8(2), pp.179–185.

Ngamsinlapasathian, S., Sreethawong, T., Suzuki, Y. and Yoshikawa, S., 2005. Single- and double-layered mesoporous TiO_2/P25 TiO2 electrode for dye-sensitized solar cell. *Solar Energy Materials and Solar Cells*, 86(2), pp.269–282.

Oguri, Y., Riman, R.E. and Bowen, H.K., 1988. Processing of anatase prepared from hydrothermally treated alkoxy-derived hydrous titania. *Journal of Materials Science*, 23(8), pp.2897–2904.

Qi, L., Gao, Y. and Ma, J., 1999. Synthesis of ribbons of silver nanoparticles in lamellar liquid crystals. *Colloids and Surfaces A: Physicochemical and Engineering Aspects*, 157(1999), pp.285–294.

Ray, S.C. and Mallick, K., 2013. Cadmium Telluride (CdTe) Thin Film for Photovoltaic Applications. *International Journal of Chemical Engineering and Applications*, 4(4), pp.183–186.

Reyes-Coronado, D., Rodríguez-Gattorno, G., Espinosa-Pesqueira, M.E., Cab, C., de Coss, R. and Oskam, G., 2008. Phase-pure TiO_2 nanoparticles: anatase, brookite and rutile. *Nanotechnology*, 19(14), pp.145605–155615.

Romeo, N., Bosio, A., Menossi, D., Romeo, A. and Aramini, M., 2014. Last progress in CdTe/CdS thin film solar cell fabrication process. In: *Energy Procedia*, 57(2014), pp.65–72.

Soga, T., 2006. *Nanostructured materials for solar energy conversion*. Oxford:Elsevier Science.

Shin, I., Seo, H., Son, M.-K., Kim, J.-K., Prabakar, K. and Kim, H.-J., 2010. Analysis of TiO_2 thickness effect on characteristic of a dye-sensitized solar cell by using electrochemical impedance spectroscopy. *Current Applied Physics*, 10(3), pp.S422–S424.

Sima, C., Grigoriu, C. and Antohe, S., 2010. Comparison of the dye-sensitized solar cells performances based on transparent conductive ITO and FTO. *Thin Solid Films*, 519(2), pp.595–597.

Su, Y.H., Lai, W.H., Teoh, L.G., Hon, M.H. and Huang, J.L., 2007. Layer-by-layer Au nanoparticles as a Schottky barrier in a water-based dye-sensitized solar cell. *Applied Physics A*, 88(1), pp.173–178.

Subramanian, V., Wolf, E. and Kamat, P. V., 2001. Semiconductor-metal composite nanostructures. To what extent do metal nanoparticles improve the photocatalytic activity of TiO_2 films?. *Journal of Physical Chemistry B*, 105(46), pp.11439–11446.

Tiwari, A., Boukherroub, R. and Sharon, M., 2013. *Solar cell nanotechnology*. Beverly: Scrivener.

Vorkapic, D. and Matsoukas, T., 1998. Effect of Temperature and Alcohols in the Preparation of Titania Nanoparticles from Alkoxides. *Journal of the American Ceramic Society*, 81(11), pp.2815–2820.

Wang, Z.-S., Kawauchi, H., Kashima, T. and Arakawa, H., 2004. Significant influence of TiO_2 photoelectrode morphology on the energy conversion efficiency of N719 dye-sensitized solar cell. *Coordination Chemistry Reviews*, 248(2004), pp.1381–1389.

Wood, A., Giersig, M. and Mulvaney, P., 2001. Fermi level equilibration in quantum dot-metal nanojunctions. *Journal of Physical Chemistry B*, 105(37), pp.8810–8815.

Wu, M., Lin, G., Chen, D., Wang, G., He, D., Feng, S. and Xu, R., 2002. Sol-hydrothermal synthesis and hydrothermally structural evolution of nanocrystal titanium dioxide. *Chemistry of Materials*, 14(5), pp.1974–1980.

Wu, X., 2004. High-efficiency polycrystalline CdTe thin-film solar cells. *Solar Energy*, 77(6), pp.803–814.

Xie, Y., Ye, R. and Liu, H., 2006. Synthesis of silver nanoparticles in reverse micelles stabilized by natural biosurfactant. *Colloids and Surfaces A: Physicochemical and Engineering Aspects*, 279(1–3), pp.175–178.

Xin, X., Scheiner, M., Ye, M. and Lin, Z., 2011. Surface-Treated TiO_2 Nanoparticles for Dye-Sensitized Solar Cells with Remarkably Enhanced Performance. *Langmuir*, 27(23), pp.14594–14598.

Yang, J., Mei, S. and Ferreira, J.M.F., 2000. Hydrothermal Synthesis of Nanosized Titania Powders: Influence of Peptization and Peptizing Agents on the Crystalline Phases and Phase Transitions. *Journal of the American Ceramic Society*, 83(6), pp.1361–1368.

You, Y.F., Xu, C.H., Xu, S.S., Cao, S., Wang, J.P., Huang, Y.B. and Shi, S.Q., 2014. Structural characterization and optical property of TiO_2 powders prepared by the sol-gel method. *Ceramics International*, 40(6), pp.8659–8666.

Yu, I.G., Kim, Y.J., Kim, H.J., Lee, C., Lee, W.I., Huo, Y., Li, H., Lu, Y., Kim, M.-R., Shklover, V., Spiccia, L., Deacon, G.B., Bignozzi, C.A. and Grätzel, M., 2011. Size-dependent light-scattering effects of nanoporous TiO2 spheres in dye-sensitized solar cells. *J. Mater. Chem.*, 21(2), pp.532–538.

Yu, S., You, J.S., Yang, I.S., Kang, P., Rawal, S.B., Sung, S. Do and Lee, W.I., 2016. Tailoring of nanoporous TiO_2 spheres with 100-200 nm sizes for efficient dye-sensitized solar cells. *Journal of Power Sources*, 325, pp.7–14.

Zhu, F., Wu, D., Li, Q., Dong, H., Li, J., Jiang, K. and Xu, D., 2012. Hierarchical TiO_2 microspheres: synthesis, structural control and their applications in dye-sensitized solar cells. *RSC Advances*, 2(31), p.11629–11637.

APPENDICES

APPENDIX A: UV-Visible Spectrometer Scan Analysis Report

Scan Analysis Report

Report Time : Fri 03 Mar 11:49:16 AM 2017
Method:
Batch: C:\Users\DMBE\Desktop\LCC\20170228 UV-Vis\20170222_10mMNaOH_after filter_stirring_complete_repeat 8d_11.DSW
Software version: 3.00(339)
Operator:

Sample Name: Double-layer Paste A4

Peak Table
Peak Style Peaks
Peak Threshold 0.0100
Range 800.00nm to 200.00nm

Wavelength (nm)	Abs
508.00	0.043
376.00	0.044
309.00	0.166

Sample Name: Double-layer Paste B4

Peak Table
Peak Style Peaks
Peak Threshold 0.0100
Range 800.00nm to 200.00nm

Wavelength (nm)	Abs
505.00	0.023
376.00	0.026
309.00	0.138

Sample Name: Double-layer Paste C2

Peak Table
Peak Style Peaks
Peak Threshold 0.0100
Range 800.00nm to 200.00nm

Wavelength (nm)	Abs
368.00	0.010
356.00	0.007
307.00	0.051

Sample Name: Paste A4 + B4

Peak Table
Peak Style: Peaks
Peak Threshold: 0.0100
Range: 800.00nm to 200.00nm

Wavelength (nm)	Abs
511.00	0.109
353.00	0.068
348.00	0.058
309.00	0.187

Sample Name: Paste A4 + C2

Peak Table
Peak Style: Peaks
Peak Threshold: 0.0100
Range: 800.00nm to 200.00nm

Wavelength (nm)	Abs
503.00	0.016
368.00	0.028
309.00	0.125

Sample Name: Paste A4 + B4 + C2

Peak Table
Peak Style: Peaks
Peak Threshold: 0.0100
Range: 800.00nm to 200.00nm

Wavelength (nm)	Abs
504.00	0.072
375.00	0.068
309.00	0.202

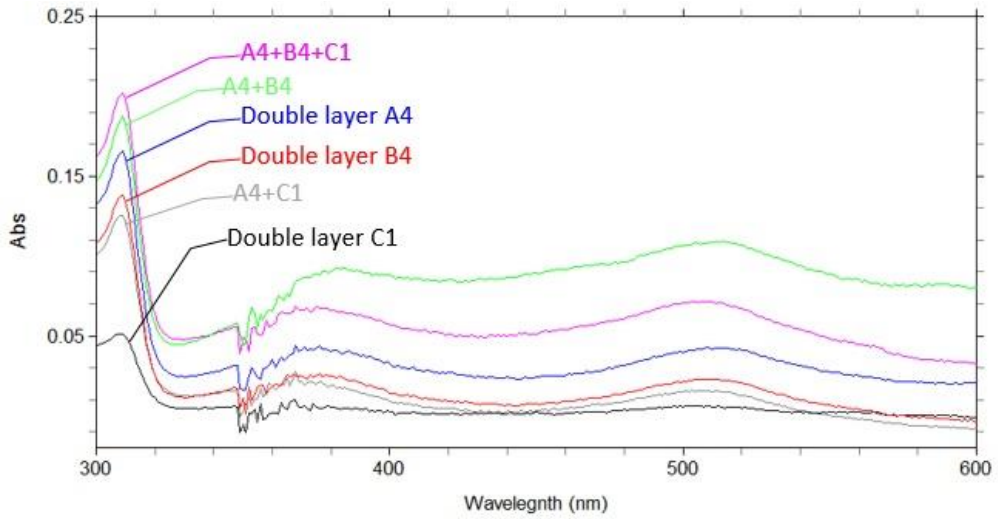

Figure A.1: UV-visible Spectrum for Various TiO_2 Nanoparticles Samples

Sample Name: Double-layer D1

Peak Table
Peak Style: Peaks
Peak Threshold: 0.0100
Range: 800.00nm to 200.00nm

Wavelength (nm)	Abs
510.00	0.023
368.00	0.023
309.00	0.108

Sample Name: Double-layer D2

Peak Table
Peak Style: Peaks
Peak Threshold: 0.0100
Range: 800.00nm to 200.00nm

Wavelength (nm)	Abs
510.00	0.012
368.00	0.018
309.00	0.102

Sample Name: Double-layer D3

Peak Table
Peak Style: Peaks
Peak Threshold: 0.0100
Range: 800.00nm to 200.00nm

Wavelength (nm)	Abs
368.00	-0.001
307.00	0.028

Sample Name: Paste D1 + D2

Peak Table
Peak Style: Peaks
Peak Threshold: 0.0100
Range: 800.00nm to 200.00nm

Wavelength (nm)	Abs
513.00	0.040
368.00	0.041
309.00	0.130

Sample Name: Paste D1 + D3

Peak Table
Peak Style: Peaks
Peak Threshold: 0.0100
Range: 800.00nm to 200.00nm

Wavelength (nm)	Abs
506.00	0.007
368.00	0.011
350.00	0.007
308.00	0.076

Sample Name: Paste D1 + D2 + D3

Collection Time	2/22/2017 12:08:05 PM

Peak Table	
Peak Style	Peaks
Peak Threshold	0.0100
Range	800.00nm to 200.00nm

Wavelength (nm)	Abs
508.00	0.086
380.00	0.076
309.00	0.181

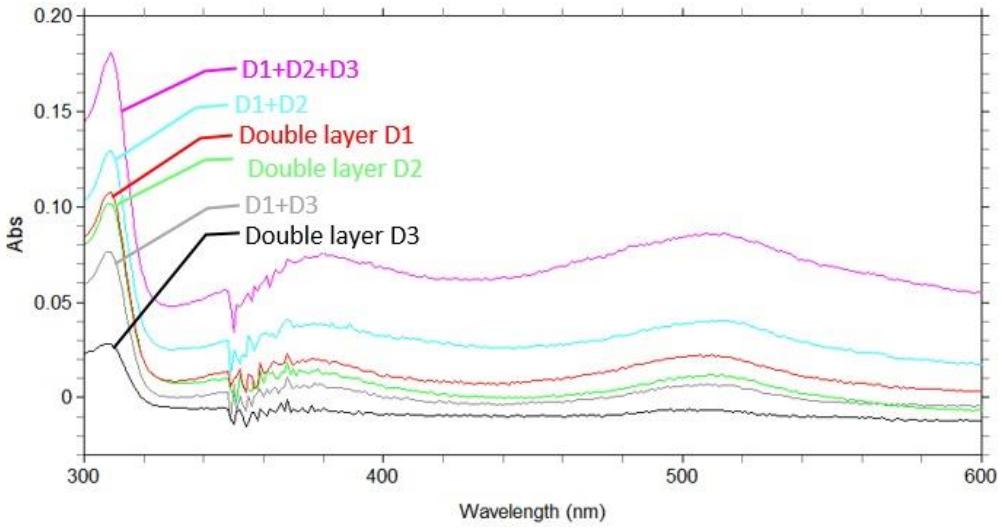

Figure A.2: UV-visible Spectrum for Various TiO_2-Au Nanocomposite Samples

APPENDIX B: EDX Analysis for TiO_2 Powder

Element	Weight (%)
C K	1.89
O K	10.51
Ti K	87.60
Total	100.00

Figure B.1: EDX Analysis of Sample B4

Element	Weight (%)
C K	0.95
O K	11.00
Ti K	88.05
Total	100.00

Figure B.2: EDX Analysis of Sample C2

APPENDIX C: SEM micrograph and Histogram of Particles Size Distribution of TiO_2-Au powder

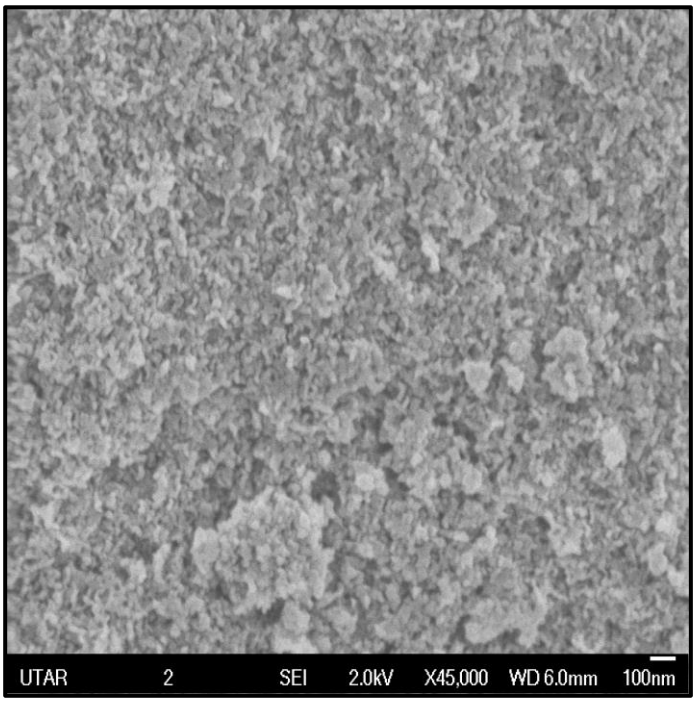

Figure C.1: SEM Micrograph of Sample D2 TiO_2-Au Powder

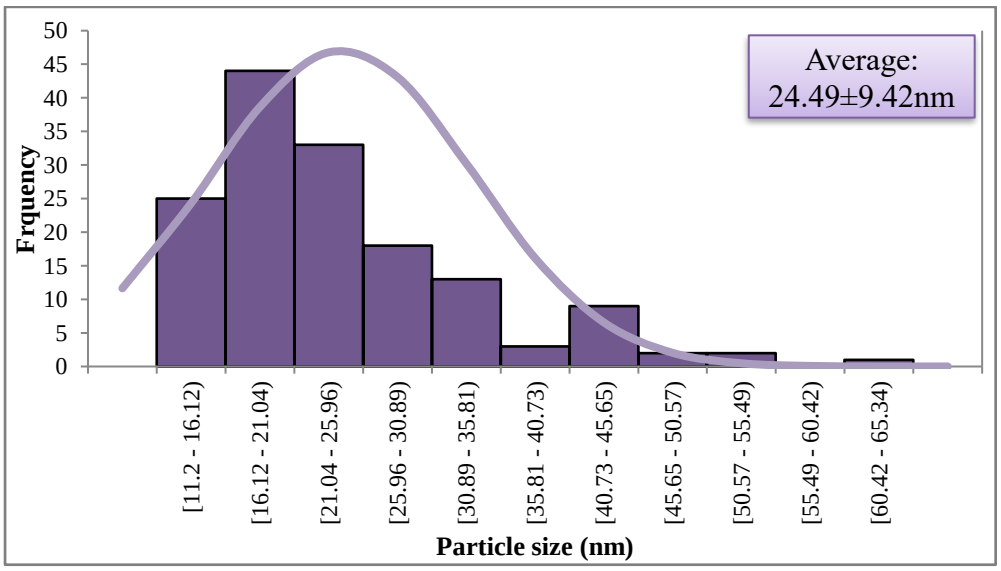

Figure C.2: Histogram of Particle Size Distribution for Sample D2

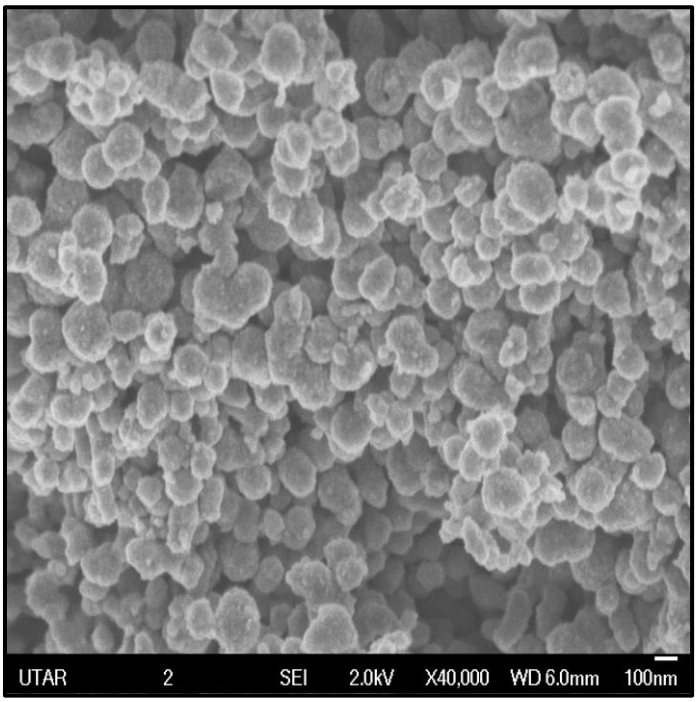

Figure C.3: SEM Micrograph of Sample D3 TiO_2-Au Powder

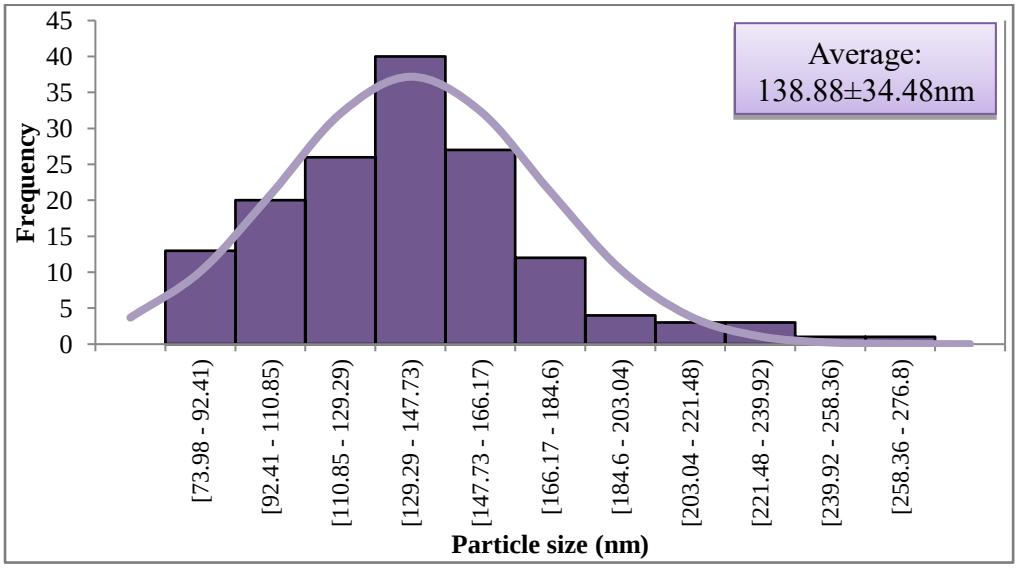

Figure C.4: Histogram of Particle Size Distribution for Sample D3

APPENDIX D: EDX Analysis for TiO_2-Au Powder

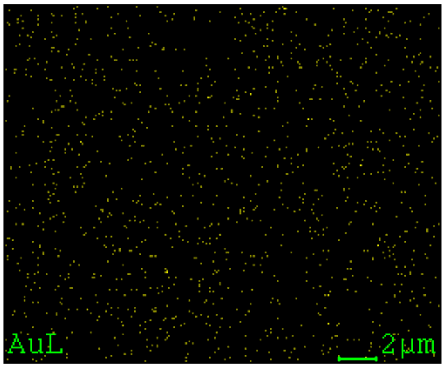

Element	Weight (%)
C K	0.48
O K	9.25
Ti K	89.48
Au K	0.80
Total	100.00

Figure D.1: EDX Analysis and Element Mapping for Gold of Sample D2

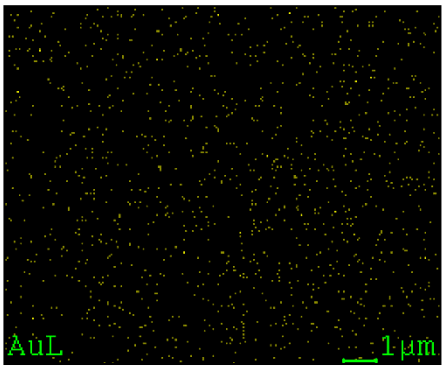

Element	Weight (%)
C K	0.48
O K	7.72
Ti K	90.93
Au K	0.87
Total	100.00

Figure D.2: EDX Analysis and Element Mapping for Gold of Sample D3

APPENDIX E: I-V Curve for TiO_2-Au DSSC vs. TiO_2 DSSC

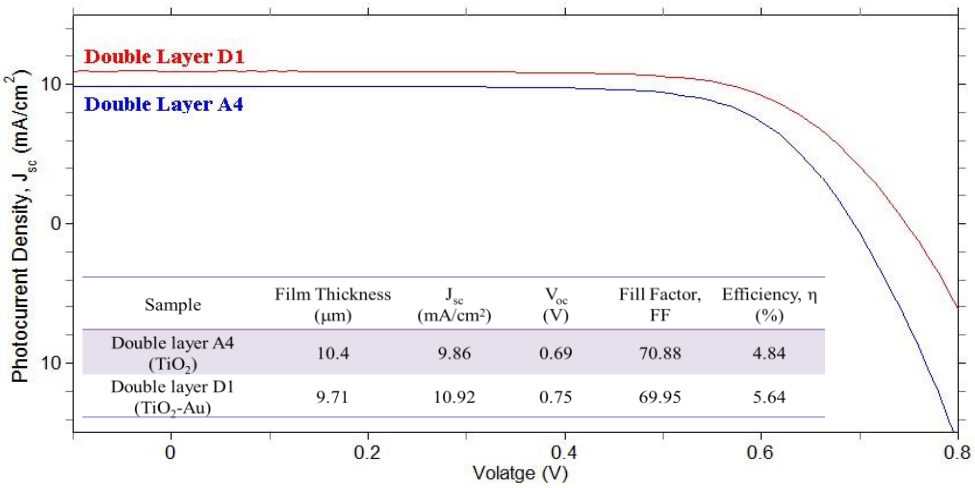

Sample	Film Thickness (μm)	J_{sc} (mA/cm²)	V_{oc} (V)	Fill Factor, FF	Efficiency, η (%)
Double layer A4 (TiO_2)	10.4	9.86	0.69	70.88	4.84
Double layer D1 (TiO_2-Au)	9.71	10.92	0.75	69.95	5.64

Figure E.1: Current-Voltage Curve for Double-layer D1 Sample and Double-layer A4 Sample

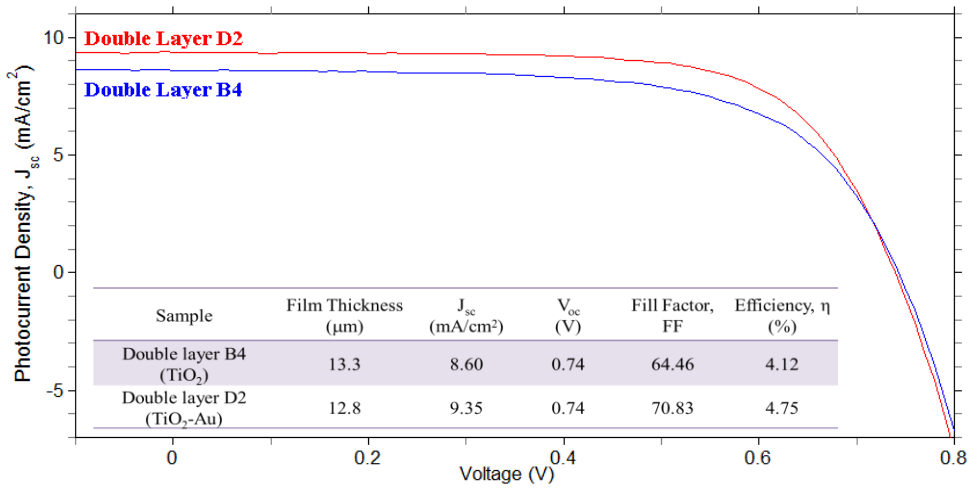

Sample	Film Thickness (μm)	J_{sc} (mA/cm²)	V_{oc} (V)	Fill Factor, FF	Efficiency, η (%)
Double layer B4 (TiO_2)	13.3	8.60	0.74	64.46	4.12
Double layer D2 (TiO_2-Au)	12.8	9.35	0.74	70.83	4.75

Figure E.2: Current-Voltage Curve for Double-layer D2 Sample and Double-layer B4 Sample

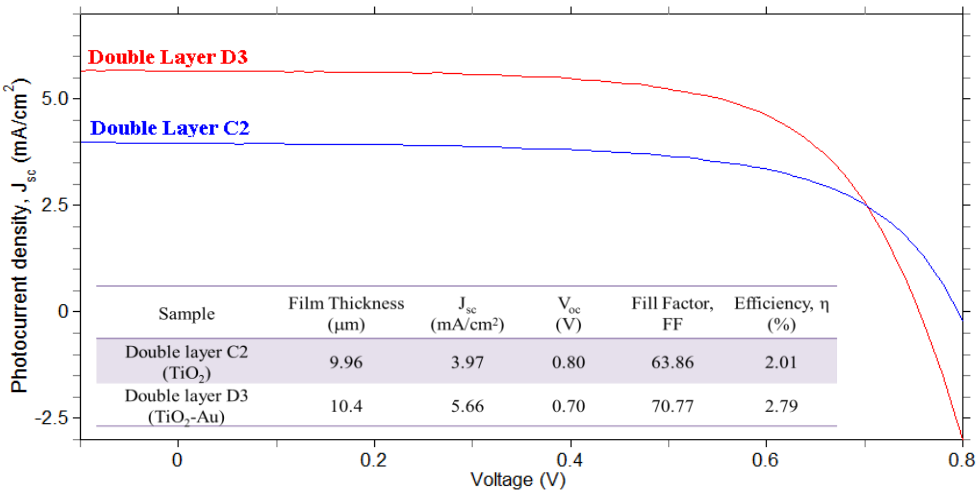

Sample	Film Thickness (μm)	J_{sc} (mA/cm²)	V_{oc} (V)	Fill Factor, FF	Efficiency, η (%)
Double layer C2 (TiO_2)	9.96	3.97	0.80	63.86	2.01
Double layer D3 (TiO_2-Au)	10.4	5.66	0.70	70.77	2.79

Figure E.3: Current-Voltage Curve for Double-layer D3 Sample and Double-layer C2 Sample

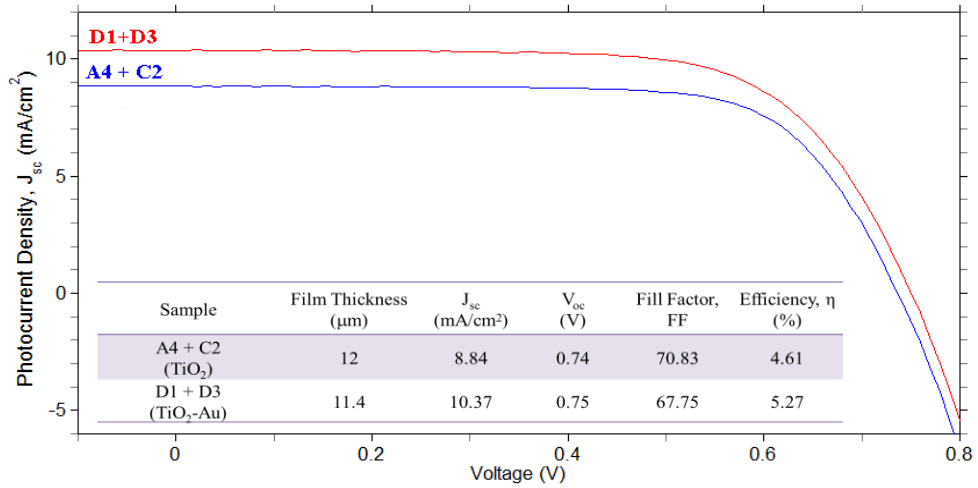

Sample	Film Thickness (μm)	J_{sc} (mA/cm²)	V_{oc} (V)	Fill Factor, FF	Efficiency, η (%)
A4 + C2 (TiO_2)	12	8.84	0.74	70.83	4.61
D1 + D3 (TiO_2-Au)	11.4	10.37	0.75	67.75	5.27

Figure E.4: Current-Voltage Curve for Sample D1 + D3 and Sample A4 + C2

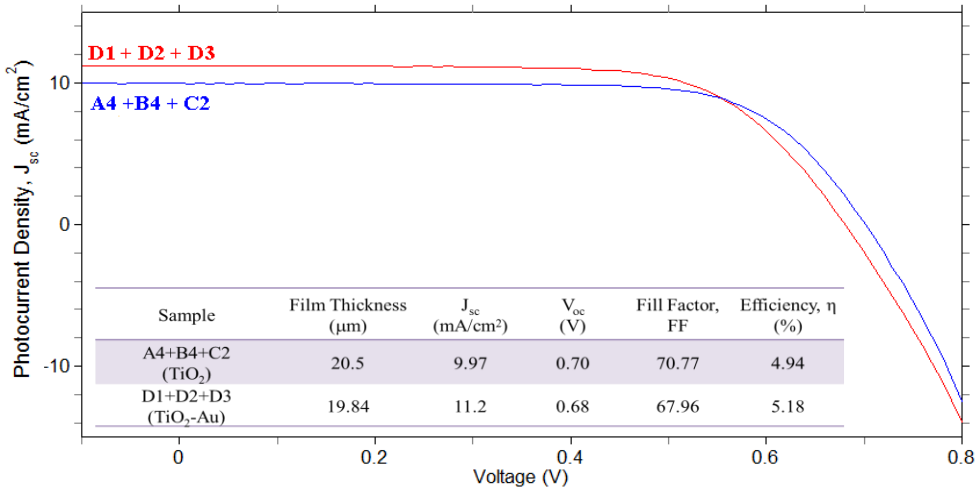

Sample	Film Thickness (μm)	J_{sc} (mA/cm²)	V_{oc} (V)	Fill Factor, FF	Efficiency, η (%)
A4+B4+C2 (TiO_2)	20.5	9.97	0.70	70.77	4.94
D1+D2+D3 (TiO_2-Au)	19.84	11.2	0.68	67.96	5.18

Figure E.5: Current-Voltage Curve for Sample D1+D2+D3 and Sample A4+B4+C2